Alma Mater Studiorum · University of Bologna

School of Science
Department of Physics and Astronomy
Master Degree in Physics

Explicit inflationary models for the enhancement of primordial fluctuations

Supervisor:

Prof. Roberto Casadio

Co-supervisor:

Dr. Alessandro Tronconi

Submitted by:

Federico Alessandrini

Academic Year 2022/2023

Abstract

The nature of dark matter remains one of the fundamental quests of modern physics. One of its simplest explanations is based on the assumption that a large amount of DM is made of black holes of primordial origin (PBHs). Such an explanation is compelling since it does not rely on the existence of new particles or some modification of the gravitational interaction. PBHs can form from the collapse of large density perturbations in the early universe, that could have formed from the inflaton fluctuations. An amplification of these fluctuations of several orders of magnitude with respect to those probed by Cosmic Microwave Background (CMB) radiation is necessary to trigger the collapse. In this work, two different scenarios of amplification are studied. First, we analyze the case of a minimally coupled inflaton. The reconstruction of a class of potentials leading to an amplification is discussed and then we study the resulting spectrum and the dynamical features of the amplification for different potentials. The same study is then employed for the more general scenario of a non-minimally coupled inflaton, restricting the analysis, for simplicity, to the induced gravity case. In this context, we used the superpotential method to reconstruct the form of a potential leading to a spectrum amplification. In both cases, we build complete models of inflation that account for the constraints of CMB observations at larger scales and the requirements for PBH production at smaller scales. Finally, we compared the models analyzed to some of the recent PTA data sets analysis and we obtained that some inflationary models are mildly favoured w.r.t. others in fitting the constraints for the production of SIGW.

Contents

Introduction

One of the key ideas of modern cosmology is inflation, an epoch of accelerated expansion in the very early stages of the universe, when some scalar field potential, or vacuum, energy dominated other forms of energy, such as matter or radiation. This phase has important consequences for being able to address many unsolved puzzles of the Hot Big Bang model, *e.g.* the "flatness" and the "horizon" problems. Moreover, it was soon realized that this epoch of quasi-exponential expansion provides also an explanation for the quantum mechanical origin of structures such as galaxies and the anisotropies in the Cosmic Microwave Background (CMB) radiation. In the last two decades, the advances in observational cosmology and, in particular, the observations of the CMB and the large-scale structures (LSS) of our universe have so far confirmed the predictions of inflation [1]. For these reasons, the inflationary scenario is arguably established as the main theoretical framework describing the very early universe.

However, our knowledge of inflation is restricted to observations of the largest cosmological scales today ($10^{-4} - 10^{-1}\,\mathrm{Mpc}^{-1}$), corresponding only to a small fraction of the early evolution of the universe. Hence, while inflation provides us with a consistent, testable framework for understanding the initial conditions in the universe, we do not have direct access to most of the inflationary dynamics, and to the universe's evolution in the early post-inflationary era. Nevertheless, these stages could be a crucial environment for several interesting phenomena, including the production of stable relics such as dark matter (DM) that is essential for understanding the universe we observe today and possibly connects to new physics. In particular, the existence of some form of non-luminous, cold dark matter (CDM) that constitutes a quarter of the total energy budget of the universe [1] seems one of the most indisputable piece of evidence beyond the Standard Model physics. Despite the acknowledged relevance of this topic, we are still far from understanding the physical processes at the heart of dark matter formation and direct signatures from experimental searches are still missing.

In this thesis, we give some introductory notions about one of the most straightforward and simple explanations of this topic, illustrating a possible scenario in which DM is composed of compact objects, such as primordial black holes (PBHs). The idea that black holes could have formed in the early universe dates back to the late 1960's by the pioneer works of Y. Zel'dovic and I. Novikov [2] and to the early 1970's in a paper by S. Hawking [3]. The first ideas in this direction began suggesting that PBHs could be formed by the gravitational collapse of over-dense inhomogeneities that originated in the early universe. In the mid-'70s, it was later realized by the works of B. Carr [4] and G. Chapline [5] that PBHs could contribute to DM density and provide the seeds for the supermassive BHs populating our universe. Following this theoretical progress, the

first formation scenarios in the context of inflation were proposed in the 1990's, but usually led to evaporating PBHs, with very small masses. The interest of the scientific community in PBHs has risen by the reported detection of micro-lensing events from MACHO collaboration [6], suggesting the possibility that a significant fraction of mass density in our galaxy could be composed of sub-solar mass PBHs. However, this hypothesis was later found invalid by the results of EROS [7] and OGLE [8, 9] collaborations, concluding that only a small fraction of masses in the Milky Way could be in the form of PBHs.

Since the first detection of gravitational waves from merging BHs by the LIGO/VIRGO collaborations [10], a second surge of interest in PBHs was ignited. Different groups suggested that merging of PBHs could be responsible for some of the observed GW signals while constituting a fraction of DM density in our universe.

The general assumption, not clashing with present cosmological data is that PBHs formed well before the end of the radiation-dominated era (*i.e.* before the so-called matter-radiation equality), and behave like cold and collision-less matter. In particular, they constitute viable DM candidate if they are massive enough $M_{\rm pbh} \gtrsim 10^{-15}\,{\rm g} \simeq 10^{-18} M_\odot$, to have a lifetime similar with that of our universe. A particularly compelling feature of PBH dark matter is its "economical" origin, in the sense that this scenario does not require any additional physics beyond the Standard Model, apart from a mechanism for the production of large energy density fluctuations.

Similarly to the generation of CMB anisotropies, a "natural" source of these large perturbations in the early universe could be the quantum fluctuations of the inflaton field that are stretched outside the horizon during inflation. However, to generate such over-dense regions that can collapse to form PBHs in the post-inflationary universe, one needs a particular phase of the inflationary evolution which enhances by several orders of magnitude the inflationary perturbations at small length scales, $k \gg k_{\rm CMB}$, far below the scales imprinted in the CMB. The microscopic physics that originates such a mechanism of amplification is still debated. For example, the amplification needed can be generated by a phase of ultra slow-roll (USR) in the presence of an inflection point of the inflaton potential [11]. This USR phase is a transient period of the inflationary evolution, when slow-roll conditions are violated, and the inflaton relaxes towards a de Sitter attractor. In contrast to the evolution of the fluctuations imprinted in the CMB, the perturbations which exit the horizon during an USR phase (see References in [12]) do not freeze due to the presence of a growing solution of the Mukhanov-Sasaki (MS) equation. Such a growing solution may then be responsible for the amplification of the perturbations. Many other possibilities have been considered in the literature. In particular, for single-field models of inflation, a blue-tilted spectrum with a large amplification can also be obtained without the presence of the growing solution (*e.g.* [13, 14]).

Another interesting fact, related to the production of PBH, is the emission of the so-called scalar-induced gravitational waves (SGIWs). The detection of gravitational waves (GWs) represents a unique opportunity to study the physics of large-scale structures and non-linear gravity regimes. Recently some progress has been made in detecting the stochastic background of gravitational waves in the range of 10 nHz. Such a background has been observed by four pulsar timing array (PTA) collaborations, namely NANOGrav [15, 16], PPTA [17, 18], EPTA [19, 20], and CPTA [21]. These data provide valuable insights into the astrophysical origins of GWs, such as the merging of binary

black holes. However, this signal can be also evidence of the emission of scalar-induced gravitational waves (SIGW), which can be originated by the collapse of PBHs.

In this work, we principally analyze two different mechanisms to generate a sufficient enhancement of the inflationary spectrum in single-field inflationary models. The content of this master thesis is organized into four Chapters:

- **Chapter 1**: We first recall the basic properties of the Friedmann-Robertson-Walker spacetime, and the standard Hot Big Bang model. We then discuss the principal shortcomings of the theory, which motivate the introduction of inflation. We then illustrate the theory of cosmological perturbations and show how quantum fluctuations in the early stages of inflation can be generated and described by an appropriate quantization scheme.

- **Chapter 2**: We first present a concise review of the present knowledge about PBHs and we conclude by discussing their formation in the inflationary universe, giving some approximate estimate for the required conditions to produce PBHs from the perspective of inflationary dynamics and as DM candidates.

- **Chapter 3**: We first illustrate the general features of the amplification mechanisms in the scenario of single-field inflation. We initially introduce a model-independent description of the dynamics of inflationary perturbations in generic gravity models. Then, we illustrate how to reconstruct an inflaton potential from a given evolution of the Hubble parameter, leading to an amplification of the inflationary perturbations. Then we perform a stability analysis of the analytical solutions found and we build complete models of inflation, exploiting the previously determined potential, which lead to significant PBH production. We compared the results obtained from our inflationary models to a recent analysis, constraining the shape of the primordial spectrum using the PTAs dataset.

- **Chapter 4**: In the last part we consider a different framework, the case in which inflation takes place in a modified gravity model, in which the inflaton is non-minimally coupled to gravity. For simplicity, we consider the Induced Gravity case which is particularly relevant due to its connection with both Higgs and Starobinsky inflationary models. Since, the discovery of the Higgs boson in 2012 [22], the possibility that inflation may be driven by a non-minimally coupled Higgs field has been investigated in detail and the model proposed by [23] is among those that best fit the latest Planck data [24]. We then study the amplification of perturbations in the IG inflation model, focusing on several peculiar features related to the evolution of cosmological perturbations. With the help of the superpotential method and in analogy with the previous Chapter, we finally reconstruct a class of viable inflaton potentials for the amplification of the power spectrum. Finally, we analyse the amplified scalar power spectrum with the PTAs dataset as we did for the minimally coupled case.

Chapter 1

Theory of Inflation

1.1 Homogeneous and isotropic universe

The modern theory of cosmology is based upon the

Copernican Principle. *The reference system composed by the Earth does not represent a preferred system in the universe.*

In other words, it is reasonable to assume that the universe would appear to any other observers identically as it looks for us. This kind of statement alone does not entail any practical consequences. However, cosmologists usually rely on a simplifying assumption known as the

Cosmological Principle. *The universe is spatially homogeneous and isotropic.*

Isotropy is taken as an observational statement, while homogeneity derives from assuming this property is independent of the observation point, according to the Copernican Principle. Results from redshift surveys of the distribution of relatively nearby galaxies seem to imply that the universe isn't homogeneous and isotropic. However, when we study the most distant objects we can find at much larger distances from Earth, the structure appears to smooth out and become more homogeneous on the largest scales. For example, the all-sky map of the locations of objects detected by radio telescopes reveals a much more uniform appearance. These objects are mostly expected to lie at higher redshifts, suggesting that when we consider the largest distance scales, the universe appears to be homogeneous and isotropic. Thus, we currently find support for the Cosmological Principle in the distribution of galaxies in the universe.

From a more technical standpoint, the Cosmological Principle implies that there exists a slicing of space-time with spatial slices Σ_t that are maximally symmetric spaces, *i.e.* they have the maximum number of Killing vectors [25]: 3 generating spatial translations and 3 generating rotations. Therefore, we are uniquely led to the Friedmann-Lemaitre-Robertson-Walker (FLRW) line element

$$\mathrm{d}s^2 = \mathrm{d}t^2 - a^2(t)\left[\frac{\mathrm{d}r^2}{1-kr^2} + r^2\left(\mathrm{d}\theta^2 - \sin^2\theta\,\mathrm{d}\varphi^2\right)\right], \tag{1.1.1}$$

where $a(t)$ is the cosmic-scale factor of the universe and k is the curvature signature, that determines the inherent geometry of space. The coordinates r, θ and φ are usually referred as comoving

coordinates, since an observer at rest at a given point in space (r, θ, φ) will remain there if there are no external forces, while t is generally called cosmic time, and it is the proper time of such observer.

We can always rescale our radius-like coordinate r in order to have the constant k equal to -1, 0 or $+1$, corresponding to an open, flat and closed universe, respectively. Physical and comoving distances are then connected through the scale factor a, which determines the time evolution of the universe, hence

$$\text{Physical distance} = a(t) \times \text{ comoving distance}\,. \tag{1.1.2}$$

In order to understand how $a(t)$ evolves, we need to solve the equations that control the dynamics of the metric. The evolution of the scale factor $a(t)$ is governed by the Einstein field equations [25]

$$R_{\mu\nu} - \frac{1}{2} R g_{\mu\nu} \equiv G_{\mu\nu} = 8\pi G\, T_{\mu\nu}\,, \tag{1.1.3}$$

where $R_{\mu\nu}$ is the Ricci tensor, R is the Ricci scalar and $T_{\mu\nu}$ is the energy-momentum tensor. In particular, working with the homogeneity and isotropy assumptions, we can approximate the matter content of the universe (*i.e.* anything except the gravitational field) with a perfect fluid filling up the entire space. Hence, we assume that a perfect fluid is described by

$$T^{\mu}{}_{\nu} = \text{diag}(\rho, -p, -p, -p)\,, \tag{1.1.4}$$

where $\rho = \rho(t)$ is its energy density and $p = p(t)$ is its pressure. The Einstein equations (1.1.3) then reduce to the Friedmann equations

$$H^2 \equiv \left(\frac{\dot{a}}{a}\right)^2 = \frac{1}{3\,M_{\rm p}^2}\rho - \frac{k}{a^2}\,, \tag{1.1.5}$$

$$\dot{H} + H^2 = \frac{\ddot{a}}{a} = -\frac{1}{6\,M_{\rm p}^2}(\rho + 3p)\,, \tag{1.1.6}$$

where $M_{\rm P}^2 = (8\pi \mathrm{G})^{-1}$ is the Planck mass, H is called Hubble parameter and determines the rate of expansion of our universe, and the dot stands for a derivative in the cosmic time t. In addition to these two equations, we shall also include the continuity equation for our cosmic fluid, that is the energy conservation equation for our source. This follows from the Bianchi identity $\nabla_\mu G^{\mu}{}_{\nu} = \nabla_\mu T^{\mu}{}_{\nu} = 0$:

$$\frac{\mathrm{d}\rho}{\mathrm{d}t} + 3\,H(\rho + p) = 0\,. \tag{1.1.7}$$

Indeed, the term $3H\rho$ reproduces the reduction in density due to the increase in volume, and the term $3Hp$ is the reduction in energy caused by the thermodynamic work done by the pressure when this expansion occurs. By defining the equation of state of the fluid as

$$p = \omega\rho\,, \tag{1.1.8}$$

the energy conservation equation (1.1.7) becomes

$$\frac{\dot{\rho}}{\rho} = -3(1+\omega)\frac{\dot{a}}{a} \quad \Longrightarrow \quad \rho \propto a^{-3(1+\omega)}\,, \tag{1.1.9}$$

provided ω is constant. The most relevant types of cosmological fluids are:

- **Dust:** Non-relativistic particles that are only subjected to gravity. Without any other force being active, the net pressure density of the fluid is null, leading to $\omega = 0$. Then, the energy density falls off as

$$\rho_D \propto a^{-3}\,, \tag{1.1.10}$$

  which is related to the decrease in the number density of particles due to the expansion of the universe.

- **Radiation:** In this case, the fluid satisfies the relation $p = 1/3\,\rho$, that is in general valid for any gas composed of relativistic particles. Setting $\omega = 1/3$ in (1.1.9) simply gives

$$\rho_R \propto a^{-4}\,. \tag{1.1.11}$$

  The result is the joint consequence of two effects, indeed, we have the dilution due to the expansion of the universe $V \propto a^{-3}$, but also the redshift of the energy of the particles, $E \propto a^{-1}$.

- **Dark energy (Λ):** The universe is dominated today by an exotic form of energy, with a negative pressure, $p = -\rho$, and a constant energy density ($\omega = -1$) scaling as

$$\rho_\Lambda \propto a^0\,. \tag{1.1.12}$$

  Since dark energy does not dilute, there should exist some process of creation of energy as the universe expands. This process does not violate energy conservation, as long as equation (1.1.7) is satisfied.

  One of the possible origins of this kind of exotic fluid is the vacuum energy of the empty space itself. As the universe expands, more space is being created and this energy therefore increases in proportion to the volume. In quantum field theory, such a "vacuum energy" is actually predicted and is described by an energy-momentum tensor of the form

$$T^{\mu\nu}_{\text{vac}} = -\rho_{\text{vac}}\, g^{\mu\nu}\,. \tag{1.1.13}$$

  Unfortunately, quantum field theory also predicts the value of vacuum energy ρ_{vac} to be much larger than that inferred from cosmological observations. However, the origin of the dark energy can also be associated with the old concept of "cosmological constant", originally introduced by Einstein to make the universe static. This term is usually understood as a contribution to the energy tensor proportional to the space-time metric, hence

$$T^{\mu\nu}_{\Lambda} = -\frac{\Lambda}{8\pi G}\, g^{\mu\nu} \equiv -\rho_\Lambda\, g^{\mu\nu}\,, \tag{1.1.14}$$

  which has the same form of (1.1.13). What we call "dark energy" identifies a more general fluid whose equation of state may not be exactly that of a cosmological constant, $\omega \approx -1$,

or may even change in time. Whatever dark matter really is, it plays a crucial role in the standard cosmological model, the ΛCDM model.

We can use the Friedmann equation to relate the curvature of the universe to total energy density and expansion rate:

$$\Omega - 1 = \frac{k}{a^2 H^2}\,, \quad \Omega = \frac{\rho}{\rho_{\rm crit}}\,, \tag{1.1.15}$$

and define the critical density $\rho_{\rm crit} \equiv 3H^2/8\pi G$. Such a critical density today is $\rho_{\rm crit}^{\rm (today)} = 1.88\, h^2\, {\rm g\, cm^{-3}} \simeq 1.05 \times 10^4\, {\rm eV\, cm^{-3}}$. There is a one to one correspondence between Ω and the spatial curvature of the universe:

$$\rho < \rho_{\rm crit} \iff \Omega < 1 \iff k < 0 \iff \text{open universe}\,, \tag{1.1.16}$$

$$\rho = \rho_{\rm crit} \iff \Omega = 1 \iff k = 0 \iff \text{flat universe}\,, \tag{1.1.17}$$

$$\rho > \rho_{\rm crit} \iff \Omega > 1 \iff k > 0 \iff \text{closed universe}\,. \tag{1.1.18}$$

The curvature radius of the universe is related to the Hubble radius and Ω by

$$R_{\rm curv} = \frac{H^{-1}}{|\Omega - 1|^{1/2}}\,. \tag{1.1.19}$$

In physical terms, the curvature radius sets the scale where the effects of curved space become "pronounced". And in the case of the positively curved model, it is just the radius of the 3-sphere.

The energy content of the universe consists of matter, dark energy and radiation, principally made by photons and neutrinos. Since the photon temperature is accurately known, $T_0 = 2.73 \pm 0.01$ K, the fraction of critical density contributed by radiation is also known: $\Omega_R\, h^2 = 4.2 \times 10^{-5}$, where $h = 0.72 \pm 0.07$ is the present Hubble rate in units of $100\, {\rm km\, s^{-1}\, Mpc^{-1}}$. In particular, recent measurements of the cosmological parameters [1] tell us that the total energy density of the universe is such that

$$\Omega_{\rm now} = 1.00^{+0.07}_{-0.03}\,, \tag{1.1.20}$$

meaning that the present universe is spatially flat, or at least very close to flatness. Restricting to this value $\Omega = 1$, the dark matter density given by TT,TE,EE+lowE+lensing+BAO data sets [1] is

$$\Omega_{\rm DM} h^2 = 0.11933 \pm 0.00091\,, \tag{1.1.21}$$

and the baryon density

$$\Omega_{\rm B} h^2 = 0.02242 \pm 0.00014\,, \tag{1.1.22}$$

and finally, constraints on the matter energy density leads to the dark energy abundance

$$\Omega_\Lambda = 0.6847 \pm 0.0073\,. \tag{1.1.23}$$

Assuming then, that the universe is flat, $k = 0$, the solution of the Friedmann Eq. (1.1.5) can be easily found in terms of the dominant energy component. In particular, for a generic fluid

characterized by an equation of state $\omega \neq -1$, we have

$$\rho \propto a^{-3(1+\omega)}\,, \quad a(t) \propto t^{\frac{2}{3(1+\omega)}}\,, \tag{1.1.24}$$

while, in the case of a flat, cosmological constant dominated universe, $\omega = -1$, we have

$$a(t) \propto e^{H_0 t}\,, \tag{1.1.25}$$

where $H_0 = \sqrt{\frac{\Lambda}{3}}$. This last solution is called de Sitter universe, and it is believed to be a good approximation to the evolution of our universe in both the far past and the far future.

1.2 Shortcomings of the Hot Big Bang model and Cosmic Inflation

We are now going to review some of the shortcomings of the Hot Big Bang model which consists of assuming that the history of our universe has always been dominated by forms of matter with $\omega \geq 0$. We will see that by this assumption, we are led to very non-natural initial conditions for the evolution of the universe. In what follows we will briefly review the initial conditions problems commonly dubbed as the "flatness problem" and the "horizon problem". Let us note that they do not indicate any logical failure Hot Big Bang scenario, rather, that very special initial conditions are required for cosmological evolution to end with a universe that is qualitatively similar to ours.

1.2.1 Flatness Problem

If we look at equation (1.1.15) and assume for simplicity that the expansion is dominated by some form of matter with equation state determined by ω, then, using Eq. (1.1.24), we can derive the relations

$$\dot{\Omega} = H(\Omega - 1)(1 + 3\omega)\,, \quad \frac{\partial \Omega}{\partial \log a} = (\Omega - 1)(1 + 3\omega)\,. \tag{1.2.1}$$

If we assume that $\omega > -1/3$, then (1.2.1) shows that the solution $\Omega = 1$ is a repulsive critical point: if $\Omega > 0$ at some point, it will continue to grow, vice versa, if $\Omega < 0$, it keeps decreasing. For instance, from

$$|\Omega - 1| \propto t^{2/3} \qquad \text{dust domination}\,, \tag{1.2.2}$$

$$|\Omega - 1| \propto t \qquad \text{radiaiton domination}\,, \tag{1.2.3}$$

we can clearly see that any deviation from pure flatness will be amplified in time as a power law. The critical fact is that Ω is observed today to be constrained at a value very close to zero. Given the matter content of the current universe, this means that at earlier times it sure was even smaller. In particular from the evolution (1.1.15), we can make an attempt to obtain a rough estimate of Ω at any time t_i, relating it to the value of the temperature T_i of the universe at such time

$$\frac{|\Omega - 1|_{t=t_i}}{|\Omega - 1|_{t=t_0}} = \frac{(aH)^2_{t=t_0}}{(aH)^2_{t=t_i}} \approx \left(\frac{T_0}{T_i}\right)^2\,, \tag{1.2.4}$$

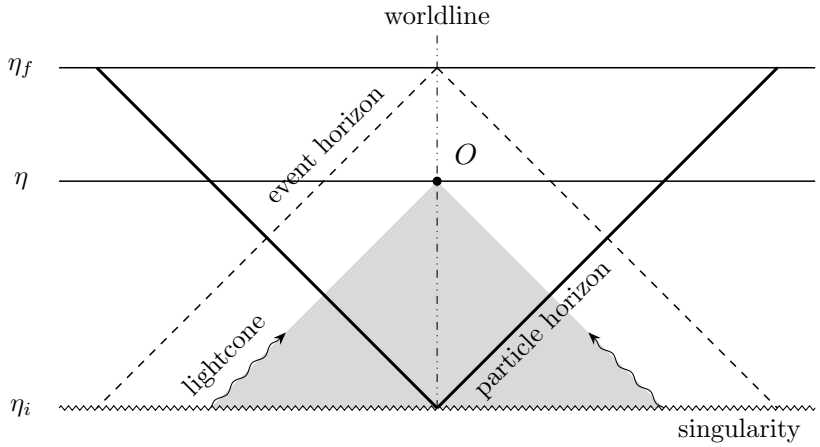

Figure 1.1: Spacetime diagram illustrating the concept of cosmological horizons. The particle horizon describes the maximal distance from which an observer can receive signals. These signals must lie in the past lightcone of the observer. The event horizon is the maximal distance to which the observer can send signals in the future.

where we indicate with t_0 the reference time of the universe today, and with $T_0 = 2.73K \sim 10^{-13}\,\text{GeV}$ the observed CMB temperature. We have considered that the universe was prevalently dominated by radiation, with $H^2 \sim \rho_R \sim a^{-4}$, and used the entropy density conservation [26], to conclude that $a \sim T^{-1}$, where T is the temperature of the universe. Assuming that Einstein equations are valid until the Planck era t_P, when the temperature of the universe is $T_\text{P} \sim 10^{19}\,\text{GeV}$, we have that

$$\frac{|\Omega - 1|_{t=t_\text{P}}}{|\Omega - 1|_{t=t_0}} \approx \left(\frac{T_0}{T_\text{P}}\right)^2 \approx \mathcal{O}(10^{-64})\,. \tag{1.2.5}$$

This is a remarkably small number, and in order to get the correct value of $|\Omega - 1|$ at present times, its value at the initial time must have been fine-tuned to values extremely near zero, but without being exactly zero.

1.2.2 Horizon problem

The size of a causally-connected patch of space-time is determined by the maximum distance travelled by light. We can estimate this, in comoving coordinates $(\eta, r, \theta, \varphi)$, where we introduce the conformal time $\eta = \int \frac{\mathrm{d}t}{a(t)}$. If the universe began at some time t_i, then there is a maximum amount of time for light to have travelled. A point sitting at the origin of space, by the time t could have sent a signal at most to a point at coordinate distance d_h given by

$$d_h(\eta) = \Delta r = \int_{t_i}^{t} \frac{\mathrm{d}t'}{a(t')} = \eta - \eta_i\,, \tag{1.2.6}$$

where we used the differential relation $\mathrm{d}s^2 = 0$, that leads $\mathrm{d}r^2 = a^2(t)\mathrm{d}t^2 = \mathrm{d}\eta^2$, and identified with η_i the initial conformal time of the universe. This distance is the maximum coordinate distance a particle could have travelled in the time interval $[t_i, t]$, and is called the comoving particle horizon. The size of the horizon at time η may be visualized by the intersection of the past light cone of an observer O with the spacelike surface η_i (see Fig. 1.1).

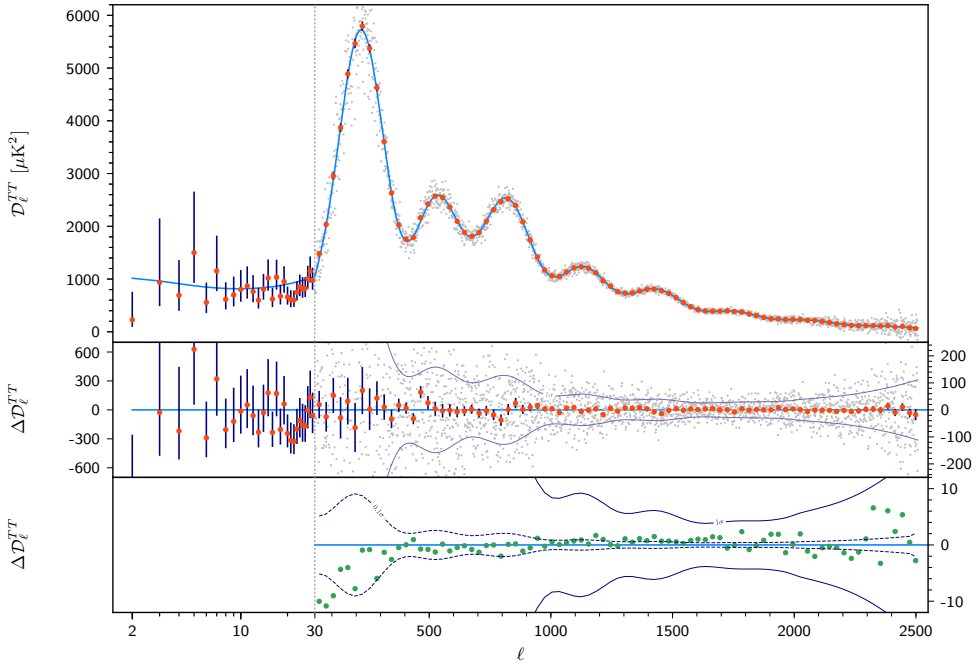

Figure 1.2: Planck 2018 temperature power spectrum. This graph is taken from [27].

The comoving particle horizon can also be written as

$$d_h = \int_{t_i}^{t} \frac{\mathrm{d}t'}{a(t')} = \int_{\log a_i}^{\log a} \mathrm{d}\log a\,(aH)^{-1}\ , \tag{1.2.7}$$

where a_i corresponds to the Big Bang singularity at $\eta = \eta_i$. The causal structure of the spacetime is hence related to the evolution of the comoving Hubble radius, $(aH)^{-1}$. For a radiation (RDU) or a matter dominated universe (MDU), the comoving Hubble radius is a monotonically increasing function of time and the integral in (1.2.7) is dominated by the contributions from late times. In particular, we can estimate that, for both cases, the comoving particle horizon is, indeed, approximately $d_h \sim (aH)^{-1}$. In fact, in a MDU, we have that $H^2 \sim \rho_M \sim a^3$, for which the integral (1.2.7) can be approximated as

$$d_h = \int_{\log a_i}^{\log a} \mathrm{d}\log a\,(aH)^{-1} \sim a^{\frac{1}{2}} \sim (aH)^{-1} \tag{1.2.8}$$

and a similar result can be obtained in the case of a RDU, in which $H^2 \sim a^{-4}$.

According to the standard cosmology [26], once the universe cooled to the point that the formation of neutral hydrogen was energetically favoured, photons of the primordial plasma decoupled and started to move through the universe with a low probability of scattering and became essentially free. This radiation is observed today as CMB, these photons decoupled on the so-called *last scattering surface* (LSS), with a temperature $T_{\mathrm{LSS}} \sim 0.3\,\mathrm{eV}$. Nowadays, the most precise measurement of the CMB features comes from the Planck experiment, which reported a black body spectrum, with temperature $T_0 \sim 2.73\,K \sim 10^{-13}\,\mathrm{GeV}$ and temperature anisotropies $\Delta T/T_0$ of order 10^{-5}.

The maximal observable comoving distance we can observe today is determined by the comoving radius of the last scattering surface:

$$R_{\rm LSS} = \eta_0 - \eta_{\rm LSS} = \int_{\log a_{\rm LSS}}^{\log a_0} \mathrm{d}\log a\,(aH)^{-1} \sim (aH)_0^{-1}\,. \tag{1.2.9}$$

Indeed, before decoupling the universe was opaque. A given comoving scale λ on the last-scattering surface subtends an angle

$$\Delta\theta \simeq \frac{\lambda}{R_{\rm LSS}}\,, \tag{1.2.10}$$

where we have neglected tiny curvature effects. The comoving particle horizon at the last scattering

$$d_{\rm LSS} = \int_{\log a_i}^{\log a_{\rm LSS}} \mathrm{d}\log a\,(aH)^{-1} \sim (aH)_{\rm LSS}^{-1}\,, \tag{1.2.11}$$

where we assumed that the universe was prevalently dominated by radiation until photons decoupled. Thus, two causally-connected points on the LSS have a maximal angular distance $\Delta\theta_{\rm max}$ given by

$$\Delta\theta \simeq \frac{d_{\rm LSS}}{R_{\rm LSS}} \sim \frac{(aH)_0}{(aH)_{\rm LSS}} \sim \left(\frac{T_0}{T_{\rm LSS}}\right)^{1/2} \sim 1.8^\circ\,, \tag{1.2.12}$$

where we considered that after photon decoupling the universe was matter dominated, with $(aH) \sim a^{-\frac{1}{2}} \sim T^{\frac{1}{2}}$, and we used $T_{\rm LSS} \simeq 0.3\,\mathrm{eV}$ and $T_0 \simeq 10^{-13}\mathrm{GeV}$.[1] This angular distance corresponds to a multipole

$$l_{\rm max} = \frac{\pi}{\Delta\theta_{\rm max}} \simeq 200\,. \tag{1.2.13}$$

We conclude that two photons, which on the last-scattering surface were separated by an angle larger than $\Delta\theta_{\rm max}$, corresponding to a multiple smaller than $l_{\rm max} \simeq 200$, were not in causal contact, assuming the universe began in the radiation dominated phase. On the other hand, from Fig. 1.2 it is clear that CMB is extremely isotropic for $l \ll 200$. Photons at the LSS were causally disconnected but shared the same temperature and this requires an extreme fine tuning of the initial conditions of the universe in the absence of a causal origin.

1.2.3 Inflation idea: the shrinking Hubble sphere

The problems mentioned above seem to have a common root: in standard cosmology, the particle content, satisfying $\omega > -1/3$, leads to a time increasing comoving Hubble radius

$$(aH)^{-1} \propto a^{\frac{1}{2}(1+3\omega)} \qquad \Longrightarrow \qquad \frac{\mathrm{d}}{\mathrm{d}t}(aH)^{-1} \propto \frac{1}{2}(1+3\omega)H\,a^{\frac{1}{2}(1+3\omega)} > 0\,. \tag{1.2.14}$$

Then, a simple solution could be to conjecture a phase in the evolution of the universe of *decreasing Hubble radius*, occurred during the early times

$$\frac{\mathrm{d}}{\mathrm{d}t}\,(aH)^{-1} < 0 \quad \Longleftrightarrow \quad \ddot{a} > 0 \quad \Longleftrightarrow \quad \omega < -\frac{1}{3}\,. \tag{1.2.15}$$

[1] Actually, fluctuations in the primordial plasma propagate at the *speed of sound*, which is slightly smaller than the speed of light, $c_s = c/\sqrt{3}$. The corresponding maximal angular distance is then $\Delta\theta_s = \Delta\theta/\sqrt{3} \simeq 1^\circ$.

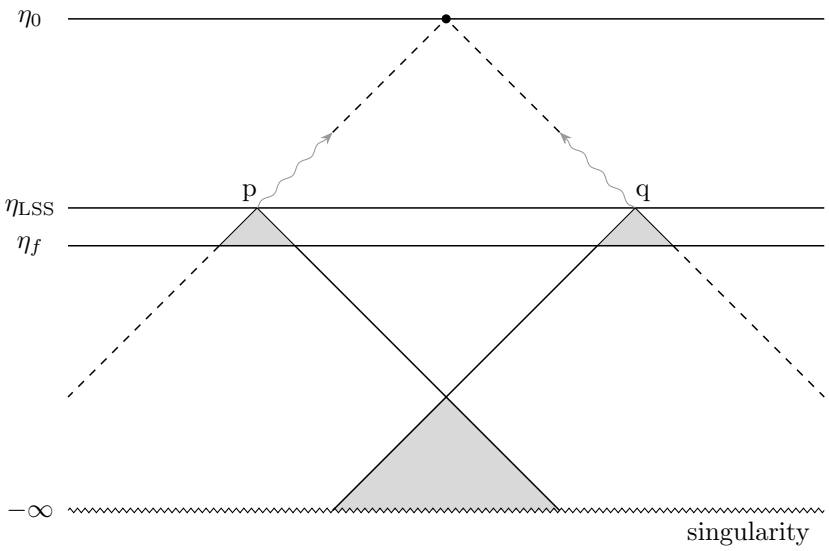

Figure 1.3: Inflationary solution to the horizon problem. All points in the CMB have overlapping past light cones and therefore originated from a causally-connected region of space.

We shall call this era *inflation*. The first implication in (1.2.15) is a direct calculation, while the second follows from the second Friedmann equation (1.1.6):

$$0 < \ddot{a} = -\frac{a}{6\,M_{\rm P}}(\rho + 3p) = -\frac{a\,\rho}{6\,M_{\rm P}}(1+3\omega) \quad \Longrightarrow \quad \omega < -\frac{1}{3}\,. \tag{1.2.16}$$

In this way, we can relate directly and solve both the flatness and horizon problems. We have seen that the time evolution of the fraction of energy density $|\Omega - 1|$ (1.1.15) is determined by the comoving Hubble horizon, if we simply consider a decreasing evolution of the latter for enough time, the problem of flatness is directly solved.

Let us then consider the horizon problem. We have seen that the comoving particle horizon d_h, in standard Big Bang cosmology is dominated by the late times part of the integral (1.2.7). However, if the Hubble radius is instead a decreasing function of time, then the integral (1.2.7) is dominated by the early times part. In particular, assuming the scalar factor dependence in Eq. (1.2.14), we have

$$d_h(\eta) = \eta - \eta_i \propto \frac{2}{1+3\omega}\left[a^{\frac{1}{2}(1+3\omega)} - a_i^{\frac{1}{2}(1+3\omega)}\right]. \tag{1.2.17}$$

Specifically we can set $\eta_i = 0$ for $a_i = 0$ and get $d_h = \eta$. We clearly notice that in the case of inflation, $\omega < -1/3$, the particle horizon receives most of its contribution from early times. In fact, we have now

$$\eta_i \propto \frac{2}{1+3\omega} a_i^{\frac{1}{2}(1+3\omega)} \quad \xrightarrow{a_i \to 0,\ \omega < -\frac{1}{3}} \quad -\infty\,. \tag{1.2.18}$$

In this way, the Big Bang singularity has been pushed to negative conformal times so that there was actually much more conformal time between the singularity and the decoupling of the CMB than we had in the previous framework. Fig. 1.3 shows the spacetime diagram. We denoted the beginning and the end of inflation by η_i and η_f, respectively. If $|\eta_f - \eta_i| \gg \eta_0 - \eta_{\rm LSS}$, where $\eta_{\rm LSS}$ is the conformal time at the decoupling of the CMB, then the past light cones of widely separated

point in the CMB had enough time to intersect, and in this way, there was enough time for heat transfer to erase any initial difference in temperature.

Inflation, then, is supposed to be a period dominated by a form of energy with $\omega \simeq -1$, or equivalently $H \simeq$ const. However, we need a mechanism capable of driving a period of the evolution of the universe with such characteristics. The simplest one is based on the existence of a minimally coupled homogeneous ($\partial_i \varphi = 0$) scalar field with a suitable potential. The total action of the inflaton-gravity system can be

$$S = S_{\rm EH} + S_\varphi = \int \mathrm{d}^4x \sqrt{-g} \left[-\frac{M_{\rm P}^2}{2} R + \frac{1}{2} g^{\mu\nu} \partial_\mu \varphi \, \partial_\nu \varphi - V(\varphi) \right] . \tag{1.2.19}$$

The first term in (1.2.19) is the Einstein-Hilbert action of General Relativity (GR), while the second one represents the action of a minimally coupled scalar field. The idea of inflation is to fill a small region of the early universe with a homogeneously distributed scalar field sitting on top of its potential $V(\varphi)$. Let us calculate the evolution of the space-time. The scalar field stress tensor, that can be obtained through the Noether theorem [25] is

$$T_{\mu\nu} = -\frac{2}{\sqrt{-g}} \frac{\delta S_\varphi}{\delta g^{\mu\nu}} = \partial_\mu \varphi \, \partial_\nu \varphi - g^{\mu\nu} \left(\frac{1}{2} \partial_\rho \varphi \, \partial^\rho \varphi + V(\varphi) \right) . \tag{1.2.20}$$

For a homogeneous field configuration, this leads to the following energy density and pressure

$$\rho_\varphi = \frac{\dot\varphi^2}{2} + V(\varphi) \, , \tag{1.2.21}$$

$$p_\varphi = \frac{\dot\varphi^2}{2} - V(\varphi) \, , \tag{1.2.22}$$

and therefore the equation of state of the inflatonic fluid is

$$\omega_\varphi = \frac{p_\varphi}{\rho_\varphi} = \frac{\frac{\dot\varphi^2}{2} + V(\varphi)}{\frac{\dot\varphi^2}{2} - V(\varphi)} \, . \tag{1.2.23}$$

If the potential energy dominates over the kinetic energy, we then have

$$\dot\varphi^2 \ll V(\varphi) \quad \Longrightarrow \quad \omega_\varphi \simeq -1 < -\frac{1}{3} \, . \tag{1.2.24}$$

In this way, we verified that a scalar field whose energy is dominant in the universe and whose potential energy dominates over the kinetic term, gives the right condition for inflation to take action.

Substituting ρ_φ and p_φ in Eqs. (1.1.5, 1.1.6), and considering a flat FLRW spacetime ($k = 0$), the homogeneous Friedmann equations take the form

$$H^2 = \frac{1}{3\, M_{\rm P}^2} \left[\frac{\dot\varphi^2}{2} + V(\varphi) \right] . \tag{1.2.25}$$

$$\dot H = -\frac{\dot\varphi^2}{2 M_{\rm P}^2} \, , \tag{1.2.26}$$

while the Euler-Lagrange equation of motion for the scalar field is the Klein-Gordon equation

$$\frac{\delta S}{\delta \varphi} = \frac{1}{\sqrt{-g}}\,\partial_\mu\left(\sqrt{-g}\,\partial^\mu\varphi\right) + V_{,\varphi} = 0 \quad \Longrightarrow \quad \ddot{\varphi} + 3H\,\dot{\varphi} + V_{,\varphi} = 0\,. \tag{1.2.27}$$

where $V_{,\varphi} = \frac{\mathrm{d}V}{\mathrm{d}\varphi}$, and $3H\dot{\varphi}$ is the Hubble friction. It can be shown that the condition of a decreasing Hubble radius, in order to obtain inflation, is equal to the condition that the so-called Hubble slow-roll parameter

$$\epsilon_1 \equiv -\frac{\dot{H}}{H^2} < 1\,. \tag{1.2.28}$$

In order to study the homogenous inflationary evolution one generally introduces also the slow-roll parameters

$$\epsilon_2 \equiv \frac{1}{H}\frac{\mathrm{d}\log\epsilon_1}{\mathrm{d}t}\,, \tag{1.2.29}$$

$$\delta \equiv -\frac{\ddot{\varphi}}{H\dot{\varphi}}\,. \tag{1.2.30}$$

We will discuss later the importance of these parameters in a more general framework, defining the hierarchy of Hubble slow-roll parameters.

As already said, inflation occurs when the kinetic energy of the inflaton is small with respect to its total energy density ρ_φ. The parameter δ, related to the acceleration of the scalar field per Hubble time, has to be small in order for inflation to last enough; a large acceleration would rapidly increase the kinetic term compared to the potential. In this way, the friction term in (1.2.27) dominates and the inflaton speed is determined by the shape of the potential. This evolution is called *slow-roll inflation* (SR) and corresponds to the inflaton slowly rolling toward the minimum of the potential. The conditions $\epsilon_1 \ll 1$ and $|\delta| \ll 1$ then legitimate us to neglect the kinetic energy and the acceleration of φ. Therefore we can rewrite the Friedmann and Klein-Gordon equations respectively as

$$H^2 \approx \frac{V}{3\,M_\mathrm{P}^2}\,, \tag{1.2.31}$$

$$3H\dot{\varphi} \approx -V_{,\varphi}\,. \tag{1.2.32}$$

Using the approximate Friedmann equation (1.2.31), we can define new slow-roll parameters, directly related to the properties of the potential

$$\epsilon_1 = -\frac{\dot{H}}{H^2} = \frac{\frac{1}{2}\dot{\varphi}^2}{M_\mathrm{P}^2 H^2} \approx \frac{M_\mathrm{P}^2}{2}\left(\frac{V_{,\varphi}}{V}\right)^2 \equiv \epsilon_V\,, \tag{1.2.33}$$

while taking the time derivative of (1.2.32), leads to

$$\delta + \epsilon_1 = -\frac{\ddot{\varphi}}{H\,\dot{\varphi}} - \frac{\dot{H}}{H^2} \approx M_\mathrm{P}^2\frac{V_{,\varphi\varphi}}{V} \equiv \eta_V\,. \tag{1.2.34}$$

The smallness of the slow-roll parameters ϵ_V and η_V, called potential slow-roll parameters, guarantees that the slope and the curvature of the scalar field potential are sufficiently small to drive an

early epoch of inflation. Within these approximations, it is easy to compute how much inflation is required to solve the flatness and horizon problem.

In general, it is convenient to define a new time variable, called *number of e-foldings* N. This is defined as the logarithm of the scale factor; hence, for generic initial and final values of the scalar field, φ_i and φ_f, we have

$$\Delta N \equiv N_f - N_i = \int_{a_i}^{a_f} \mathrm{d}\log a = \int_{t_i}^{t_f} \mathrm{d}t\, H(t) = \int_{\varphi_i}^{\varphi_f} \mathrm{d}\varphi\, \frac{H}{\dot{\varphi}} \simeq -\frac{1}{M_{\mathrm{P}}^2} \int_{\varphi_i}^{\varphi_f} \mathrm{d}\varphi\, \frac{V}{V_{,\varphi}}\,, \tag{1.2.35}$$

where in the final approximate equality we used the slow-roll conditions (1.2.31, 1.2.32). Let us note that during SR, the amount of inflation ΔN between two values of the scalar field can be calculated without solving the equation of motion.

If the entire observable universe today is smaller than the comoving Hubble horizon at the beginning of inflation

$$(a_0 H_0)^{-1} < (a_i H_i)^{-1}\,. \tag{1.2.36}$$

Then, taking into account that the decrease of the comoving Hubble radius during inflation must compensate for its increase during the standard Big Bang evolution, one can estimate the minimum amount of inflation necessary to solve the flatness and the horizon problem. The amount by which the Hubble radius has grown during the Hot Big Bang evolution can be related to the maximal temperature of the thermal plasma at the beginning of the Hot Big Bang. This is generally called *reheating temperature*, and we identify it as T_R. We furthermore assume that the energy density at the end of inflation was converted very rapidly into the particles of the thermal plasma so that the Hubble radius didn't experience significant growth between the end of inflation and reheating, $(a_R\, H_R)^{-1} \sim (a_f\, H_I)^{-1}$. Then, taking into account that $a \propto T^{-1}$, and that during the radiation domination era $H \propto a^{-2}$ we have that

$$\frac{a_f H_f}{a_0 H_0} \sim \frac{a_R H_R}{a_0 H_0} = \frac{a_R}{a_0} \left(\frac{a_0}{a_R}\right)^2 = \frac{a_0}{a_R} \sim \frac{T_R}{T_0} \sim 10^{28} \left(\frac{T_R}{10^{15}\,\mathrm{GeV}}\right)\,, \tag{1.2.37}$$

where we introduced a reference value of 10^{15} GeV for the reheating temperature. Finally we have, for (1.2.36)

$$\Delta N \equiv \log\left(\frac{a_f}{a_i}\right) > 64 + \log\left(\frac{T_R}{10^{15}\,\mathrm{GeV}}\right) \tag{1.2.38}$$

which is the famous statement that the solution to the horizon problem requires about 60 e-folds of inflation.

1.3 A brief survey of inflationary models

Even restricting ourselves to a simple single-field inflation scenario, the number of models available in the literature is large. We can classify them according to the shape of the scalar field potential and then distinguish among: *large-field*, *small-field* and *hybrid field*. A generic single-field potential can be characterized by two independent mass scales: a "height" Λ^4, corresponding to the vacuum energy density during inflation, and a "width" μ, corresponding to the change in the field value $\Delta\varphi$

during inflation:

$$V(\varphi) = \Lambda^4 f\left(\frac{\varphi}{\mu}\right) , \tag{1.3.1}$$

where f represents naturally the different properties of the potential.

- **Large-field models.** These models are based upon potentials typical of the "chaotic" inflation scenario, in which the scalar field is displaced from the minimum of the potential by an amount usually of the order of the Planck mass $M_{\rm P}$ and evolves towards it. Such models are characterized by $V_{,\varphi\varphi} > 0$ and $0 < \eta_V < 2\epsilon_V$. The generic large-field potentials that can be considered are monomial potentials

$$V(\varphi) = \Lambda^4 \left(\frac{\varphi}{\mu}\right)^p , \tag{1.3.2}$$

  with $p > 1$, and exponential potentials

$$V(\varphi) = \Lambda^4 \exp\left(\frac{\varphi}{\mu}\right) . \tag{1.3.3}$$

  In the chaotic inflation scenario, it is assumed that the universe emerged from a quantum gravitational state with an energy density comparable to that of the Planck density, implying $V(\varphi) \approx M_{\rm P}^4$ and results in a large friction term $3\,H\dot{\varphi}$ from (1.1.5). Consequently, the inflaton will slowly roll down its potential.

- **Small-field models.** These models are the type of potentials that arise naturally from spontaneous symmetry breaking and from pseudo-Nambu-Goldstone models (see [28]). The field starts near an unstable equilibrium point and rolls down the potential to a stable minimum. In general these models are characterized by $V_{,\varphi\varphi} < 0$ and $\eta_V < -\epsilon_V$, where ϵ_V is close to zero. The typical small-field potential is of a polynomial of the form

$$V(\varphi) = \Lambda^4 \left[1 - \left(\frac{\varphi}{\mu}\right)^p\right] , \tag{1.3.4}$$

  with $p > 2$, and can be considered as a lowest-order Taylor expansion of an arbitrary potential around the origin. Furthermore, these models include even potentials which have a logarithmic divergence in the leading derivative at the origin [28].

- **Hybrid models.** The hybrid scenario frequently is realized by models which incorporate inflation into supersymmetry and supergravity [28]. In a typical hybrid inflation model, the scalar field responsible for inflation evolves toward a minimum with non-zero vacuum energy. Such models are characterized by $V_{,\varphi\varphi} > 0$ and $0 < 2\epsilon_V < \eta_V$. We consider generic potentials for hybrid inflation of the form

$$V(\varphi) = \Lambda^4 \left[1 + \left(\frac{\varphi}{\mu}\right)^p\right] , \tag{1.3.5}$$

  with $p \geq 2$. The large-field limit of this potential is just the case of chaotic inflation with a monomial potential; while in the limit of small-field, $\varphi < \mu$, the potential is dominated by the

constant term. The field value at the end of inflation is determined by some other physics, indeed, otherwise we would have, at rest at $\varphi = 0$ an *infinite* period of inflation. Hence, another sector of the theory must be invoked, generally as a coupling to a second scalar field.

There are a number of single-field models that do not fit well into this scheme, for example, logarithmic potentials $V(\varphi) \propto \log(\varphi)$ typical of supersymmetry [28]. Another example is a potential with negative powers of the scalar field $V(\varphi) \propto \varphi^{-p}$ used in intermediate inflation and dynamical supersymmetry inflation. However, the three classes categorized before seem to be good enough for comparing theoretical expectations with experimental data.

1.4 Cosmological perturbations

The model discussed so far describes a homogeneous picture of the universe in which the inflaton evolves generating an inflationary phase and, eventually, will reach a global minimum in its potential ending the accelerated expansion phase. Although inflation was proposed to solve the Big Bang problems, it also predicts an adiabatic spectrum of small fluctuations on top of the homogeneous background. These small fluctuations can be explained as the quantum vacuum fluctuations of the inflaton field: their comoving scale gets stretched during inflation and they cross the horizon and get frozen-out. When they cross the horizon they lose their quantum nature and they can be treated as a classical stochastic field. Eventually, they re-enter the horizon after inflation and they become seeds for the large-scale structures we see today, like galaxies and clusters, and have been imprinted in the CMB anisotropies.

Mathematically, the problem of describing the growth of small perturbations in the context of general relativity reduces to solving the Einstein equations linearized about an expanding background. Hence we apply a semiclassical approximation and consider a background classical field, which in this case is the homogeneous inflaton, and then quantize the perturbation over the background evolution, which here describes the space dependent part of the field.

1.4.1 Massless scalar field in a de Sitter spacetime

Let us first see how the fluctuations of a generic massless scalar test field, that here we call $\delta\varphi$, evolve during a de Sitter era, during which the Hubble rate H is constant. The fluctuations are described by the action

$$S = \frac{1}{2}\int \mathrm{d}^4x\,\sqrt{-g}\,\left[g^{\mu\nu}\,\partial_\mu\left(\delta\varphi\right)\partial_\nu\left(\delta\varphi\right)\right]\,, \tag{1.4.1}$$

with

$$\mathrm{d}s^2 = \mathrm{d}t^2 - e^{2Ht}\,\mathrm{d}\vec{x}^{\,2}, \quad H = \mathrm{const}\,. \tag{1.4.2}$$

It is convenient to reintroduce the conformal time $\eta = \int \frac{\mathrm{d}t}{a(t)}$, which in the de Sitter case is $\eta = -\frac{1}{aH}$. Furthermore, we also have

$$a(\eta) = -\frac{1}{H\eta} \quad (\eta < 0)\,. \tag{1.4.3}$$

The action for the scalar field, expressed in terms of η is

$$S = \frac{1}{2}\int \mathrm{d}\eta\, \mathrm{d}^3\vec{x}\; a^4 \left[\frac{(\delta\varphi')^2}{2a^2} - \frac{1}{2a^2}\left(\vec{\nabla}\delta\varphi\right)^2\right], \tag{1.4.4}$$

where the prime $'$ indicates the derivative with respect to the conformal time η. On defining the new field variable $u = a\,\delta\varphi$ and after integrating by parts, the action can be rewritten as

$$S = \frac{1}{2}\int \mathrm{d}\eta\, \mathrm{d}^3\vec{x}\; \left[(u')^2 - \left(\vec{\nabla}u\right)^2 + \frac{a''}{a}\,u^2\right]. \tag{1.4.5}$$

Let us note that this action is similar to that of a scalar field on a Minkowski spacetime with an effective mass

$$m^2_{\text{eff}} = -\frac{a''}{a} = -\frac{2}{\eta^2}\,. \tag{1.4.6}$$

Conceptually, the problem of quantization of a scalar field $\delta\varphi(\eta,\vec{x})$ in a flat Friedmann universe is reduced to the mathematically equivalent problem of quantizing a free scalar field $u(\eta,\vec{x})$ on a Minkowski spacetime. Indeed, all information about the gravitational interaction is encoded in this time-dependent mass term.

We proceed through the usual procedure for the canonical quantization. First of all, we expand the field $u(\eta,\vec{x})$ in Fourier modes,

$$u(\eta,\vec{x}) = \int \frac{\mathrm{d}^3\vec{k}}{(2\pi)^3}\, u_k(\eta)\, e^{i\,\vec{k}\cdot\vec{x}}\,, \tag{1.4.7}$$

and substituting the expansion back into the action (1.4.5), we find that the Fourier modes $u_k(\eta)$ satisfy a set of decoupled ordinary differential equations

$$u_k'' + \omega_k^2(\eta)\, u_k = u_k'' + \left(k^2 - \frac{a''}{a}\right) u_k = 0\,. \tag{1.4.8}$$

We can qualitatively study the solution in two different regimes:

- in the sub-horizon limit: $k^2 \gg a''/a$, the differential equation takes the form

$$u_k'' + k^2 u_k = 0\,, \tag{1.4.9}$$

  whose solution is a plane wave

$$u_k(\eta) = C_- \frac{e^{-ik\eta}}{\sqrt{2k}} + C_+ \frac{e^{ik\eta}}{\sqrt{2k}}\,, \tag{1.4.10}$$

  where C_- and C_+ are integration constants. We find that fluctuations with wavelength within the horizon oscillate exactly like on a flat spacetime. In the ultraviolet regime, that is for wavelengths much smaller than the horizon scale, one expects that approximating the spacetime as flat is a good approximation and indeed the normalisation of (1.4.10) is that of flat spacetime.

- In the super-horizon limit: $k^2 \ll a''/a$, Eq. (1.4.8) reduces to

$$u_k'' - \frac{a''}{a} u_k = 0\,, \tag{1.4.11}$$

which is satisfied by

$$u_k = C_k\, a + D_k\, a \int^\eta \frac{\mathrm{d}\eta'}{a^2} \approx C_k\, a\,, \tag{1.4.12}$$

where C_k and D_k are integration constants. We can neglect the second term because in a de Sitter universe $a \int^\eta \frac{\mathrm{d}\eta'}{a^2}$ is rapidly decreasing.

Roughly matching the absolute value of the solutions (1.4.10) and (1.4.12) at $k = aH$ ($-k\eta = 1$), we can determine the absolute value of the constant C_k

$$|C_k|\, a = \frac{1}{\sqrt{2k}} \quad \Longrightarrow \quad |C_k| = \frac{1}{a\sqrt{2k}} = \frac{H}{\sqrt{2k^3}}\,. \tag{1.4.13}$$

Going back to the original fluctuation variable $\delta\varphi_k$ we can verify that the fluctuation of the field on super-horizon scales is constant and approximatively equal to

$$|\delta\varphi_k| \simeq \frac{H}{\sqrt{2k^3}}\,. \tag{1.4.14}$$

In the de Sitter case (1.4.6), the approximation just described is not necessary since Eq. (1.4.8) can be solved exactly

$$u_k(\eta) = A_k\, e^{-ik\eta} \left(1 - \frac{i}{k\eta}\right) + B_k\, e^{ik\eta} \left(1 + \frac{i}{k\eta}\right)\,. \tag{1.4.15}$$

This solution reproduces all that we have found by qualitative arguments in the two approximations (1.4.10) and (1.4.12). Let us note that the matching procedure described can be very useful to determine the behaviour of the solution on super-horizon scales when the exact solution is not known. For the time being, we cast aside the problem of specifying the role of the integration constants A_k and B_k, which we will take up in more detail later.

Let us then proceed with the canonical quantization. We promote $u(\eta, \vec{x})$ to a quantum operator and impose the standard equal-time canonical commutation relations

$$\left[\hat{u}(\eta, \vec{x}_1), \hat{u}(\eta, \vec{x}_2)\right] = \left[\hat{\pi}(\eta, \vec{x}_1), \hat{\pi}(\eta, \vec{x}_2)\right] = 0\,, \tag{1.4.16}$$

$$\left[\hat{u}(\eta, \vec{x}_1), \hat{\pi}(\eta, \vec{x}_2)\right] = i\delta^{(3)}(\vec{x}_1 - \vec{x}_2)\,, \tag{1.4.17}$$

where $\hat{\pi}$ is the conjugate momentum of $\hat{u}$, with $\hat{\pi} \equiv \hat{u}'$. We can now expand $\hat{u}$ in the Fourier space to obtain

$$\hat{u}(\eta, \vec{x}) = \int \frac{\mathrm{d}^3 k}{(2\pi)^{\frac{3}{2}}} \left[\hat{a}_{\vec{k}}\, u_k(\eta)\, e^{i\,\vec{k}\cdot\vec{x}} + \hat{a}^\dagger_{\vec{k}}\, u_k^*(\eta)\, e^{-i\,\vec{k}\cdot\vec{x}}\right] \tag{1.4.18}$$

where $k = \left|\vec{k}\right|$ and $\hat{a}_k$, $\hat{a}_k^\dagger$ are the annihilation and creation operators. The creation and annihilation

operators satisfy the induced commutation relations

$$\left[\hat{a}_{\vec{k}_1}, \hat{a}_{\vec{k}_2}\right] = \left[\hat{a}^\dagger_{\vec{k}_1}, \hat{a}^\dagger_{\vec{k}_2}\right] = 0\,, \tag{1.4.19}$$

$$\left[\hat{a}_{\vec{k}_1}, \hat{a}^\dagger_{\vec{k}_2}\right] = \delta^{(3)}(\vec{k}_1 - \vec{k}_2)\,, \tag{1.4.20}$$

and the functions u_k satisfy the classical solution (1.4.15). Inserting the Fourier expansion (1.4.18) in the canonical commutation relations (1.4.19) and using (1.4.16) we obtain the Wronskian normalization condition

$$u_k\,(u_k')^* - u_k^* u_k' = i\,, \tag{1.4.21}$$

which is equivalent to requiring the linear independence of u_k and u_k^*.

To complete the quantization process we must choose the vacuum. In the Minkowski quantum theory, the vacuum is defined as the minimum energy state. Here, the Hamiltonian is time-dependent, thereby it does not have a time-independent eigenstate that could serve as a vacuum. There are various prescriptions to define a suitable vacuum in a general spacetime. On curved spacetime, the vacuum state is commonly defined as the eigenstate $|_{\eta_0}0\rangle$ minimizing the instantaneous Hamiltonian at a fixed time η_0.

Therefore, we first define the vacuum $|_{\eta_0}0\rangle$ such that $\hat{a}_{\vec{k}}\,|_{\eta_0}0\rangle = 0$, $\forall\,\vec{k}$ and considering a generic solution of Eq. (1.4.8) we then evaluate the mean value of the Hamiltonian operator and find the function $u_k(\eta)$ minimizing it. The Hamiltonian is obtained from the action (1.4.5), and, operating the mode expansion (1.4.18) we obtain:

$$\hat{H}(\eta) = \frac{1}{4}\int \mathrm{d}^3k\,\left[\hat{a}_{\vec{k}}\,\hat{a}_{-\vec{k}}\,F^*_{\vec{k}} + \hat{a}^\dagger_{\vec{k}}\,\hat{a}^\dagger_{-\vec{k}}\,F_{\vec{k}} + \left(2\hat{a}^\dagger_{\vec{k}}\,\hat{a}_{\vec{k}} + \delta^{(0)}(0)\right)\,E_{\vec{k}}\right] \tag{1.4.22}$$

where

$$E_{\vec{k}} = \left|u_k'\right|^2 + (k^2 + m^2_{\mathrm{eff}})\,|u_k|^2\,, \qquad F_{\vec{k}} = \left(u_k'\right)^2 + (k^2 + m^2_{\mathrm{eff}})u_k^2\,. \tag{1.4.23}$$

Evaluating the expectation value for a general vacuum state at a fixed time η_0, we obtain the energy. Note that the presence of the divergent term $\delta^{(0)}(0)$ is simply due to an infinite volume normalization factor and can be reabsorbed. The energy density is then

$$\rho(\eta_0) = \langle_{\eta_0}0|\hat{H}(\eta_0)|_{\eta_0}0\rangle = \frac{1}{4}\int \mathrm{d}^3\vec{k}\,\left(\left|u_k'(\eta_0)\right|^2 + (k^2 + m^2_{\mathrm{eff}}(\eta_0))\,|u_k(\eta_0)|^2\right)\,. \tag{1.4.24}$$

For each mode $\vec{k}$, its contribution to the energy must be minimized separately. Thus, for a given $\vec{k}$ we have to determine the initial conditions $u_k(\eta_0)$ and $u_k'(\eta_0)$ as a proxy for the selection of a suitable set of mode functions. Substituting

$$u_k = r_k\,e^{i\alpha_k} \tag{1.4.25}$$

into the consistency relation (1.4.21), we obtain that the functions r_k and α_k obey the following relation

$$r_k^2\,\alpha_k' = \frac{1}{2}\,, \tag{1.4.26}$$

and from Eq. (1.4.23) we have

$$\begin{aligned} E_{\vec{k}} &= (r_k')^2 + r_k^2(\alpha_k')^2 + \omega_k^2\, r_k^2 \\ &= (r_k')^2 + \frac{1}{4r_k^2} + \omega_k^2\, r_k^2\,. \end{aligned} \tag{1.4.27}$$

It is easily seen that (1.4.27) is minimized if $r_k' = 0$ and $r_k = \frac{1}{\sqrt{2k}}$, where we assumed that $\omega_k^2 \sim k^2$. Integrating back, Eq. (1.4.26) gives $\alpha_k = -k\eta$, and hence u_k is:

$$\lim_{\eta\to-\infty} u_k = \frac{1}{\sqrt{2k}}\, e^{-ik\eta}\,. \tag{1.4.28}$$

This last relation fixes the vacuum as the Bunch-Davies vacuum, which is defined as the Minkowski vacuum in the flat spacetime limit. Indeed during inflation the comoving Hubble radius shrinks and therefore one can go sufficiently back in time and find the wavelength of a given mode k inside the Hubble radius. That is $-k\eta \gg 1$ for sufficiently big values of $-\eta$. In this regime, the mode k does not feel the curvature of spacetime and it behaves as in Minkowski spacetime. For de Sitter and the general solution (1.4.15) one fixes the integration constants A_k and B_k to reproduce (1.4.28) and then

$$u_k(\eta) = \frac{e^{-ik\eta}}{\sqrt{2k}}\left(1 - \frac{i}{k\eta}\right)\,. \tag{1.4.29}$$

Let us finally define the *power spectrum*, a useful quantity to characterize the properties of the perturbations. If the perturbations are linear and are a random Gaussian field, so that their Fourier modes are decoupled, they can be decomposed as

$$A(\eta, \vec{x}) = \int \frac{\mathrm{d}^3\vec{k}}{(2\pi)^3} A(\vec{k}) e^{i\vec{k}\cdot\vec{x}}\,, \tag{1.4.30}$$

It is straightforward to define the 2-point function in the Fourier space as

$$\langle A(\vec{k})A(\vec{k}')\rangle = (2\pi)^3\, \mathcal{P}_A(\vec{k})\, \delta^{(3)}(\vec{k} - \vec{k}')\,, \tag{1.4.31}$$

where $\delta^{(3)}(\vec{k} - \vec{k}')$ is the Dirac delta distribution function. The power spectrum for the quantity A is then defined as

$$\mathcal{P}_A(\vec{k}) = \frac{k^3}{2\pi^2}\left|A(\vec{k})\right|^2\,. \tag{1.4.32}$$

As an example, we can consider the scalar fluctuation $\delta\varphi$, and using the final solution for the modes u_k in Eq. (1.4.29), we have

$$\mathcal{P}_{\delta\varphi}(k) = \frac{\mathcal{P}_u(k)}{a^2} = \left(\frac{H}{2\pi}\right)\left[1 + (k\eta)^2\right] \xrightarrow{k\eta\to 0} \left(\frac{H}{2\pi}\right)^2\,. \tag{1.4.33}$$

This is the scale-invariant power spectrum for a de Sitter universe. The amplitude of the fluctuations, on scales larger than Hubble length ($k\eta \to 0$), does not depend on the time at which the fluctuations become larger than the Hubble radius and become frozen in. This scale invariance means that the fluctuations are independent of the energy scale. Let us note that in realistic models of inflation the

time dependence of the Hubble rate is small, otherwise, inflation would never end. To evaluate the effect of a varying $H(t)$, we must calculate the power spectrum (1.4.33) at horizon crossing $k = aH$. For each Fourier mode, this corresponds to a different moment in time, and since H is evolving, this leads to a slight scale dependence of the spectrum

$$\mathcal{P}_{\delta\varphi}(k) \approx \left(\frac{H}{2\pi}\right)^2 \Bigg|_{k=aH} . \tag{1.4.34}$$

1.4.2 Classical relativistic theory of perturbations

In the previous Section, we have assumed that the background geometry is fixed and satisfies restrictive homogeneous conditions. In order to attain a more rigorous and complete study of the theory of quantum cosmological fluctuations we need to set up a proper framework.

We have already seen how we can explain the generation of perturbations of a generic scalar field during a de Sitter expansion. Considering now, that the inflaton field dominates the energy density of the universe during inflation, it is evident that any perturbation in the inflaton field directly affects the energy-momentum tensor, and through the Einstein field equations the structure of spacetime. Schematically

$$\delta\varphi \implies \delta T_{\mu\nu} \implies \delta g_{\mu\nu} . \tag{1.4.35}$$

On the other hand, a perturbation of the metric induces a backreaction on the evolutions of the inflaton perturbation through the perturbed Klein-Gordon equation of the inflaton field

$$\delta g_{\mu\nu} \implies \delta\left[\partial_\mu\partial^\mu - \frac{\partial V}{\partial\varphi}\right] = 0 \implies \delta\varphi . \tag{1.4.36}$$

This schematical reasoning leads us to the important assumption that perturbations of the inflaton field and of the gravitational metric are tightly coupled to each other and have to be studied together.

Mathematically, the problem of describing the evolution of small perturbations in the context of general gravity reduces to solving the Einstein equations linearized about an expanding homogeneous background. In particular, the most convenient procedure which can be undertaken to describe the linear evolution of cosmological perturbation is to split each quantity of interest $X(\eta, \vec{x})$ into two parts, the first being the spatially homogeneous background ${}^{(0)}X(\eta)$, delineated by the superscript ${}^{(0)}$, while the other $\delta X(\eta, \vec{x})$ describing how the "actual" spacetime deviates from the idealized background model. The observational fact that the universe on large scales is nearly homogeneous and isotropic makes this approach reasonable. Furthermore, it was shown that in Robertson-Walker universes solutions of the linearized field approach can be viewed as linearizations of solutions of the full non-linear equations. Hence linear perturbation theory is mathematically well defined.

For a generic observable X we can write the decomposition

$$X(\eta, \vec{x}) = {}^{(0)}X(\eta) + \delta X(\eta, \vec{x}), \qquad |\delta X| \ll \left|{}^{(0)}X\right| \tag{1.4.37}$$

In particular, the decomposition of the metric reads

$$g_{\mu\nu}(\eta, \vec{x}) = {}^{(0)}g_{\mu\nu}(\eta) + \delta g_{\mu\nu}(\eta, \vec{x}) . \tag{1.4.38}$$

wehere the background metric ${}^{(0)}g_{\mu\nu}$ is the flat FLRW metric, introduced in (1.1.1).

The metric perturbations may be categorized into three distinct types: scalar, vector and tensor perturbations. This classification refers to the way in which the fields from which $\delta g_{\mu\nu}$ are constructed transform under three-space coordinate transformations on a constant-time hypersurface. Both vector and tensor perturbations exhibit no instabilities. Vector perturbations decay kinematically in an expanding universe whereas tensor perturbations lead to gravitational waves which do not couple to energy density and pressure inhomogeneities. However, scalar perturbations may lead to growing inhomogeneities which, in turn, have an important effect on the dynamics of matter.

- **Scalar perturbations**. The complete definition of a scalar metric perturbation must take into consideration the proper way scalar perturbations can be inserted in each term of the metric. There are two possible ways that scalar quantities may enter into the spatial part δg_{ij} [29]: either through a multiplicative scalar function ψ or an additive term composed by the covariant derivative of an ulterior scalar function. The covariant derivative being with respect to the background metric g_{ij} of the constant-time hypersurface, that in the spatially flat case ($k = 0$), coincides with ordinary coordinate derivative.

  Finally, we need two more scalar functions: the first in δg_{00} which is invariant under rotations and translations, while the three-dimensional derivative of the second is in δg_{0i}.

  Therefore, the most general form of the scalar metric perturbations is constructed using four scalar quantities: ϕ, ψ, B and E which are functions of space and time coordinates

$$\delta g^{(s)}_{\mu\nu} = a^2(\eta) \begin{pmatrix} 2\,\phi & -B_{,i} \\ -B_{,i} & 2(\psi\delta_{ij} - E_{,ij}) \end{pmatrix} . \tag{1.4.39}$$

- **Vector perturbations**. The vector perturbations are constructed using two three-vectors S_i and F_i satisfying the constraints

$$S^{,i}_{i} = F^{,i}_{i} = 0\,, \tag{1.4.40}$$

  where we transform from upper to lower three-space indices and vice-versa by using the spatial background metric tensor g_{ij} and its inverse g^{ij}. The above constraints are necessary in order to extract exactly only pure vector perturbations. In fact due to SVT decomposition (scalar-vector-tensor) each 3-vector V_i can be decomposed as

$$V_i = \underbrace{V_{,i}}_{\text{scalar}} + \underbrace{\hat{V}_i}_{\text{vector}}, \tag{1.4.41}$$

  where $\hat{V}_i{}^{,i} = 0$. These considerations lead to the following metric vector perturbations:

$$\delta g^{(V)}_{\mu\nu} = -a^2(\eta) \begin{pmatrix} 0 & -S_i \\ -S_i & 2(F_{i,j} + F_{j,i}) \end{pmatrix} . \tag{1.4.42}$$

- **Tensor perturbations**. These perturbations are constructed using symmetric three-tensor

h_{ij} which satisfies the constraints

$$h_i{}^i = 0, \quad h_{ij}{}^{,j} = 0\,. \tag{1.4.43}$$

These constraints mean that h_{ij} does not contain components which transform as scalars or vectors. Thus, the metric for tensor perturbations is

$$\delta g^{(T)}_{\mu\nu} = -a^2(\eta) \begin{pmatrix} 0 & 0 \\ 0 & h_{ij} \end{pmatrix}. \tag{1.4.44}$$

Counting the total number of independent functions we used to form $\delta g_{\mu\nu}$, we find that we have four functions for scalar perturbations (ϕ, ψ, B, E), four for vector perturbations (2 divergenless 3-vectors), and two for the tensor perturbations (a symmetric, traceless, and transverse 3-tensor), adding up to 10, that are the number of independent components of $\delta g_{\mu\nu}$.

In the linear approximation, scalar, vector and tensor perturbations evolve independently and thus can be considered separately.

1.4.3 Gauge-invariant variables and their physical meaning

Until now we have neglected an important aspect of the theory, namely the invariance of the theory under gauge transformations. The metric perturbations, indeed, are not uniquely defined but depend on our choice of coordinates. In particular, when we wrote down the different terms of the perturbed metric, we implicitly assumed a specific time slicing of the spacetime and defined specific spatial coordinates on these time slices.

There are two mathematically equivalent approaches to treat gauge transformations, particularly in the context of small perturbations: the passive and the active ones. In the passive approach, we consider a physical spacetime manifold $\mathcal{M}$ and choose some system of coordinates x^μ on $\mathcal{M}$. A background model is defined by assigning to all functions Q on $\mathcal{M}$ a previously given function ${}^{(0)}Q(x)$. The functions Q may have any kind of tensorial structure, and ${}^{(0)}Q(x)$ are fixed functions of the coordinates, not geometrical objects. Therefore, in a second coordinate system $\tilde{x}^\alpha$ the background functions ${}^{(0)}Q(\tilde{x})$ will have exactly the same functional dependence on $\tilde{x}^\alpha$. The perturbation δQ of the quantity Q in the system of coordinates x^μ is defined as

$$\delta Q(p) = Q(x(p)) - {}^{(0)}Q(x(p))\,, \tag{1.4.45}$$

and can be evaluated for any point $p \in \mathcal{M}$ with associated coordinates $x^\mu(p)$. Similarly, in the second system of coordinates, the perturbation of Q is

$$\delta\tilde{Q}(p) = \tilde{Q}(\tilde{x}(p)) - {}^{(0)}Q(\tilde{x}(p))\,. \tag{1.4.46}$$

Here, $\tilde{Q}(\tilde{x}(p))$ is the value of Q in the new coordinate system at the same point $p \in \mathcal{M}$, and ${}^{(0)}Q(\tilde{x}(p))$ is the same function of $\tilde{x}$ as ${}^{(0)}Q(x(p))$ is of x. The transformation $\delta Q(p) \to \delta\tilde{Q}(p)$ is called gauge transformation associated with the change of variables $x \to \tilde{x}$ on the manifold $\mathcal{M}$.

In the second approach, the active one, we consider two manifolds: the physical manifold $\mathcal{M}$ and a background spacetime $\mathcal{N}$ on which background coordinates x_b are rigidly fixed. Any diffeomorphism $\mathcal{D} : \mathcal{N} \to \mathcal{M}$ induces a system of coordinates on $\mathcal{M}$ via $\mathcal{D} : x_b \to x$. For a given diffeomorphism $\mathcal{D}$ we define the perturbation δQ of the function Q as

$$\delta Q(p) = Q(p) - {}^{(0)}Q(\mathcal{D}^{-1}(p))\,, \tag{1.4.47}$$

where again ${}^{(0)}Q$ is a fixed function defined on the background spacetime. A second diffeomorphism $\tilde{\mathcal{D}} : \mathcal{N} \to \mathcal{M}$ induces a new set of coordinates $\tilde{x}$ on $\mathcal{M}$ via $\tilde{\mathcal{D}} : x_b \to \tilde{x}$ and a different $\delta\tilde{Q}$,

$$\delta\tilde{Q}(p) = \tilde{Q}(p) - {}^{(0)}Q(\tilde{\mathcal{D}}^{-1}(p))\,, \tag{1.4.48}$$

where $\tilde{Q}$ is the value of Q in $\tilde{x}$ coordinates. In this approach, the gauge transformation $\delta Q(p) \to \delta\tilde{Q}(p)$ is generated by the change of correspondence $\mathcal{D} \to \tilde{\mathcal{D}}$ between the manifolds $\mathcal{N}$ and $\mathcal{M}$. We can associate with this change in correspondence the change of coordinates $x \to \tilde{x}$ induced on $\mathcal{M}$.

Both approaches are equivalent; however, the first allows one to connect the gauge transformation with the choice of the system of coordinates on $\mathcal{M}$ in which the perturbations are described. The second view allows one to understand how the amplitudes of the perturbations depend on the correspondence between background manifold $\mathcal{N}$ and physical manifold $\mathcal{M}$.

In both approaches described above one may consider infinitesimal coordinate transformations

$$x \to \tilde{x} = x + \xi\,, \tag{1.4.49}$$

described by four functions ξ of space and time. For a scalar field perturbation $\delta\varphi$ the coordinate transformation induces the variation

$$\delta\varphi \quad \to \quad \delta\tilde{\varphi} = \delta\varphi - {}^{(0)}\varphi'\xi^0\,, \tag{1.4.50}$$

while for a metric perturbation $\delta g_{\mu\nu}$ we have

$$\delta g_{\mu\nu} \to \delta\tilde{g}_{\mu\nu} = \delta g_{\mu\nu} - {}^{(0)}g_{\mu\nu,\gamma}\xi^\gamma - {}^{(0)}g_{\gamma\nu}\xi^\gamma_{,\mu} - {}^{(0)}g_{\mu\gamma}\xi^\gamma_{,\nu}\,, \tag{1.4.51}$$

from which one can calculate the variations of the functions φ, ψ, B and E which constitute the perturbed metric. In particular, if we write the spatial components of ξ as

$$\xi^i = \xi^i_\perp + \zeta^{,i} \quad \text{with} \quad \xi^i_{\perp,i} = 0\,, \tag{1.4.52}$$

the transformation law (1.4.51) for each components become

$$\delta\tilde{g}_{00} = \delta g_{00} - 2a\left(a\xi^0\right)'\,, \tag{1.4.53}$$

$$\delta\tilde{g}_{0i} = \delta g_{0i} + a^2\left[\xi'_{\perp\,i} + (\zeta' - \xi^0)_{,i}\right]\,, \tag{1.4.54}$$

$$\delta\tilde{g}_{ij} = \delta g_{ij} + a^2\left[2\frac{a'}{a}\,\delta_{ij}\,\xi^0 + 2\zeta_{,ij} + \xi_{\perp\,(i,j)}\right]\,. \tag{1.4.55}$$

Combining equations (1.4.53, 1.4.54, 1.4.55) we obtain the transformation laws for scalars, vector and tensor perturbations.

- **Scalar perturbations** transform according to

$$\phi \to \tilde{\phi} = \phi - \frac{1}{a}(a\xi^0)' \,, \tag{1.4.56}$$

$$\psi \to \tilde{\psi} = \psi + \frac{a'}{a}\xi^0 \,, \tag{1.4.57}$$

$$B \to \tilde{B} = B + \xi^0 - \zeta' \,, \tag{1.4.58}$$

$$E \to \tilde{E} = E - \zeta \,. \tag{1.4.59}$$

  The dependence of (1.4.56)-(1.4.59) on two arbitrary functions, ξ and ζ, means that we can use coordinate transformations to cancel two degrees of freedom. Moreover, one can define special combinations of the metric perturbations that do not transform under a change of coordinates. These are the so-called Bardeen variables [26]

$$\Phi \equiv \phi + \frac{1}{a}\left[(B - E')\, a\right]' \,, \qquad \Psi \equiv \psi - \frac{a'}{a}(B - E') \,. \tag{1.4.60}$$

  These gauge-invariant variables are the "real" spacetime perturbations since they cannot be cancelled by a gauge transformation.

- **Vector perturbations** transform according to

$$S_i \to \tilde{S}_i = S_i + \xi'_{\perp\, i} \,, \tag{1.4.61}$$

$$F_i \to \tilde{F}_i = F_i + \xi_{\perp\, i} \,. \tag{1.4.62}$$

  One can construct gauge-invariant quantities, in the same way as before. For example

$$V_i \equiv S_i - F'_i \tag{1.4.63}$$

  do not change under infinitesimal coordinate transformations. These variables describe physical perturbations associated with rotational motions. Usually, they are not relevant during inflation since they rapidly decay in an expanding background.

- **Tensor perturbations** h_{ij} are gauge-invariant by construction since ξ does not contain any tensor component. Tensor perturbations describe primordial gravitational waves.

In general, it is convenient to introduce a gauge-invariant variable to describe the relation between quantum scalar perturbations and observable quantities in cosmology. The intrinsic spatial curvature on hypersurfaces at constant conformal time η and for a flat universe is given by

$${}^{(3)}R = \frac{4}{a^2}\nabla^2\psi \,. \tag{1.4.64}$$

The quantity ψ, defined in (1.4.39) as one of the scalar perturbation terms of the metric, is usually referred to as the *curvature perturbation*. We have seen, however, that the curvature perturbation

ψ is not gauge-invariant, but is defined only on a given slicing, Eq. (1.4.57). We now define the *comoving slicing* as the slicing orthogonal to the world lines of comoving observers. The latter are free-falling and the expansion defined by them is isotropic. This means that there is no flux of energy measured by these observers, that is $T_{0i} = 0$. During inflation these observers measures $\delta\varphi_{\rm com} = 0$ since $T_{0i} \propto \partial_i \delta\varphi(\vec{x}, \eta)\varphi'(\eta)$.

For a transformation on constant time hypersurfaces $\delta\varphi \to \delta\varphi - {}^{(0)}\varphi'\xi^0$ one then has

$$\delta\varphi \to \delta\varphi_{\rm com} = \delta\varphi - {}^{(0)}\varphi'\xi^0 = 0 \implies \xi^0 = \frac{\delta\varphi}{{}^{(0)}\varphi'}\,, \tag{1.4.65}$$

that is $\xi^0 = \frac{\delta\varphi}{{}^{(0)}\varphi'}$ is the time-displacement needed to go from a generic slicing with generic $\delta\varphi$ to the comoving slicing where $\delta\varphi_{\rm com} = 0$. Correspondingly the curvature perturbation ψ transforms (1.4.57) into

$$\psi \to \psi_{\rm com} = \psi + \mathcal{H}\xi^0 = \psi + \mathcal{H}\frac{\delta\varphi}{{}^{(0)}\varphi'}\,, \tag{1.4.66}$$

and we can define the *comoving curvature perturbation* as

$$\mathcal{R} = \psi + \mathcal{H}\frac{\delta\varphi}{{}^{(0)}\varphi'} = \Phi + \mathcal{H}\frac{\overline{\delta\varphi}}{{}^{(0)}\varphi'}\,, \tag{1.4.67}$$

where for the second equality we used the definition (1.4.83) and (1.4.81). This quantity is gauge-invariant by construction and is related to the gauge-dependent curvature perturbation ψ on a generic slicing to the inflation perturbation $\delta\varphi$ in that gauge. By construction, the meaning of $\mathcal{R}$ is that it represents the linear curvature perturbation on comoving hypersurfaces where $\delta\varphi = 0$

$$\mathcal{R} = \psi|_{\delta\varphi=0}\,. \tag{1.4.68}$$

Equations for cosmological perturbations

In this Section, we shall derive the general form of the equations which describe small cosmological perturbations. To do that, we start with the linearized form of Einstein's equations

$$\delta G^{\mu}{}_{\nu} = 8\pi G\, \delta T^{\mu}{}_{\nu}\,. \tag{1.4.69}$$

For the background model described by a homogeneous, isotropic and expanding universe, the Einstein tensor is

$${}^{(0)}G^0{}_0 = 3\,a^{-2}\left(\mathcal{H}^2 + \mathcal{H}\right)\,, \quad {}^{(0)}G^0{}_i = 0\,, \quad {}^{(0)}G^i{}_j = a^{-2}\left(2\mathcal{H}' + \mathcal{H}^2 + \mathcal{H}\right)\,\delta^i{}_j\,, \tag{1.4.70}$$

where $\mathcal{H} = a'/a$. For scalar type metric perturbations with a line element given in (1.1.1), the perturbed Einstein equations can be obtained as a result of straightforward calculations, but what we are really interested in are gauge-invariant quantities with which describing curvature and energy

terms in the Einstein equations. In particular, we can define [29]

$$\overline{\delta G^0{}_0} = \delta G^0{}_0 - \left({}^{(0)}G^0{}_0\right)' (B - E') \,, \tag{1.4.71}$$

$$\overline{\delta G^0{}_i} = \delta G^0{}_i - \left({}^{(0)}G^0{}_0 - \frac{{}^{(0)}G^k{}_k}{3}\right) (B - E')_{,i} \,, \tag{1.4.72}$$

$$\overline{\delta G^i{}_j} = \delta G^i{}_j - \left({}^{(0)}G^i{}_j\right)' (B - E') \,, \tag{1.4.73}$$

and similarly

$$\overline{\delta T^0{}_0} = \delta T^0{}_0 - \left({}^{(0)}T^0{}_0\right)' (B - E') \,, \,, \tag{1.4.74}$$

$$\overline{\delta T^0{}_i} = \delta T^0{}_i - \left({}^{(0)}T^0{}_0 - \frac{{}^{(0)}T^k{}_k}{3}\right) (B - E')_{,i} \,, \tag{1.4.75}$$

$$\overline{\delta T^i{}_j} = \delta T^i{}_j - \left({}^{(0)}T^i{}_j\right)' (B - E') \,. \,, \tag{1.4.76}$$

where $\overline{\delta G^\mu{}_\nu}$ and $\overline{\delta T^\mu{}_\nu}$ are the gauge-invariant counterparts of $\delta G^\mu{}_\nu$ and $\delta T^\mu{}_\nu$.

Using the background equations of motion, Eq. (1.4.69) for small perturbations may be rewritten with the gauge-invariant quantities as

$$\overline{\delta G^\mu{}_\nu} = 8\pi G \, \overline{\delta T^\mu{}_\nu} \,. \tag{1.4.77}$$

The left-hand side of the above equations can be expressed in terms of the gauge-invariant potentials Φ, Ψ (1.4.60) alone. After some algebra, we obtain the following general form of the gauge-invariant equations for cosmological perturbations

$$\nabla^2\Psi + 3\mathcal{H}\Psi - 3\mathcal{H}\left(\Psi' + \mathcal{H}\Phi\right) = 4\pi \, G \, a^2 \, \overline{\delta T^0{}_0} \,, \tag{1.4.78}$$

$$\left(\Psi' + \mathcal{H}\Phi\right)_{,i} = 4\pi \, G \, a^2 \overline{\delta T^0{}_i} \tag{1.4.79}$$

$$\begin{aligned} &\left[\Psi'' + \mathcal{H}\left(2\Psi + \Phi\right)' + \left(2\mathcal{H}' + \mathcal{H}^2\right) + \frac{1}{2}\nabla^2(\Phi - \Psi)\right]\delta_{ij} \\ &\qquad - \frac{1}{2}\left(\Phi - \Psi\right)_{,ij} = -4\pi \, G \, a^2 \, \overline{\delta T^i{}_j} \,. \end{aligned} \tag{1.4.80}$$

From (1.4.80), we see that if there is no anisotropic stress in the matter at linear order, namely $\overline{\delta T^i{}_j} = 0$ for $i \neq j$, we have

$$\Phi = \Psi \,, \tag{1.4.81}$$

and we can write each equation only dependent on Φ. Furthermore, we are interested in inflationary cosmology driven by a single scalar field, which can be decomposed as

$$\varphi(\eta, \vec{x}) = {}^{(0)}\varphi(\eta) + \delta\varphi(\eta, \vec{x}) \,. \tag{1.4.82}$$

Being a scalar quantity, we can define the gauge-invariant counterpart for its perturbation as

$$\overline{\delta\varphi} = \delta\varphi + {}^{(0)}\varphi'(B - E')\,. \tag{1.4.83}$$

We can also obtain the equations of motion for the gauge-invariant scalar field perturbation. Using the form of the energy-momentum tensor for a homogeneous field configuration (1.2.20) and considering Eqs. (1.4.74, 1.4.75, 1.4.76), the equations of motion for perturbations, for no anisotropic stress in the matter, reduce to

$$\nabla^2\Phi - 3\mathcal{H}\Phi' - (\mathcal{H}' + 3\mathcal{H}^2)\Phi = 4\pi G({}^{(0)}\varphi'\,\overline{\delta\varphi}' + V_{,\varphi}\,a^2\,\overline{\delta\varphi})\,, \tag{1.4.84}$$

$$\Phi' + \mathcal{H}\Phi = 4\pi G\ {}^{(0)}\varphi'\,\overline{\delta\varphi}\,, \tag{1.4.85}$$

$$\Phi'' + 3\mathcal{H}\Phi' + (\mathcal{H}' + 2\mathcal{H}^2)\Phi = 4\pi G({}^{(0)}\varphi'\,\overline{\delta\varphi}' - V_{,\varphi}\,a^2\,\overline{\delta\varphi})\,, \tag{1.4.86}$$

Subtracting Eq. (1.4.84) from Eq. (1.4.86), and substituting Eq. (1.4.85) to express $\overline{\delta\varphi}$ as a function of Φ and Φ', one finally finds the classical equation for the evolution of the Bardeen potential Φ

$$\Phi'' + 2\left(\mathcal{H} - \frac{{}^{(0)}\varphi''}{{}^{(0)}\varphi'}\right)\Phi' - \nabla^2\Phi + 2\left(\mathcal{H}' - \mathcal{H}\frac{{}^{(0)}\varphi''}{{}^{(0)}\varphi'}\right)\Phi = 0\,. \tag{1.4.87}$$

Once this equation is solved, the expression for $\overline{\delta\varphi}$ follows from (1.4.85). The second term in the above equation is the Hubble friction, the third term represents the pressure force leading to oscillations, and the last term is the force due to gravity leading to instability. On sub-horizon scales, the solutions describe damped oscillations. On super-horizon scales the oscillations freeze-out and the dynamics is governed by the gravitational force competing with the Hubble friction term.

1.4.4 Cosmological scalar perturbations

In the previous Section, we discussed the classical equations for the cosmological perturbations. Hence, to fully describe the generation and evolution of the inflationary perturbations a quantum treatment is needed. We must note that scalar field fluctuations and metric fluctuations are tightly coupled not only because they are related through Einsteins' equations, but also because of the issue of gauge invariance.

From the above discussion, we know that there is only one physically independent degree of freedom characterizing scalar fluctuations. Therefore the quantum theory of cosmological perturbations consists of the quantization of a single scalar field on an expanding background, where the time-dependence of the classical background leads, after quantization, to particle production. The starting point, which we consider for simplicity, is the action of a minimally coupled scalar field (the inflaton)

$$S = \int \mathrm{d}^4x\,\sqrt{-g}\left[-\frac{M_{\rm P}^2}{2}\,R + \frac{1}{2}g^{\mu\nu}\partial_\mu\varphi\,\partial_\nu\varphi - V(\varphi)\right]\,. \tag{1.4.88}$$

We can now expand the action up to quadratic order in terms of the scalar perturbations. Indeed, the equations for the linear perturbations are the Euler-Lagrange equations derived from a quadratic

Lagrangian

$$S[g_{\mu\nu},\varphi] \simeq S^{(0)}\left[{}^{(0)}g_{\mu\nu},{}^{(0)}\varphi\right] + S^{(2)}\left[{}^{(0)}g_{\mu\nu},\delta g_{\mu\nu},{}^{(0)}\varphi,\delta\varphi\right] . \tag{1.4.89}$$

The term $S^{(1)}$ linear in perturbations vanishes by using the homogeneous equations of motion. The second-order action can be written as that of a scalar field in Minkowski space with a time-dependent mass

$$S^{(2)} = \frac{1}{2}\int \mathrm{d}\eta\,\mathrm{d}^3x\,\left[(v')^2 - \left(\vec{\nabla}v\right)^2 + \frac{z''}{z}\,v^2\right] , \tag{1.4.90}$$

where we have defined the gauge-invariant quantity

$$v \equiv a\overline{\delta\varphi} + z\Phi\,, \tag{1.4.91}$$

called Mukhanov variable, z is defined as $z \equiv a\,\frac{\varphi'}{\mathcal{H}}$ and where we have neglected the superscript ${}^{(0)}$ to indicate background quantities. It is relevant that this action is similar to that of a Klein-Gordon scalar field in a Minkowski spacetime with an effective mass

$$m^2_{\text{eff}} = -\frac{z''}{z}\,. \tag{1.4.92}$$

Conceptually, the problem of quantization is mathematically equivalent to the problem of quantization of a scalar field $v(\eta,\vec{x})$ in Minkowski spacetime interacting with external classical fields [29] and has also many similarities to the analysis of scalar fields in an expanding universe 1.4.1. The time dependence is entirely due to the variable background gravitational field. Thus, the quantization prescription is formally identical to the one presented in Section 1.4.1.

Expanding the field $v(\eta,\vec{x})$ in Fourier modes,

$$v(\vec{x},\eta) = \int \frac{\mathrm{d}^3\vec{k}}{(2\pi)^3}\,v_k(\eta)\,e^{i\,\vec{k}\cdot\vec{x}}\,, \tag{1.4.93}$$

and substituting the expansion back into the action (1.4.90), we find that the Fourier modes $v_k(\eta)$ satisfy a set of decoupled ordinary differential equations of the form

$$v_k'' + \left(k^2 - \frac{z''}{z}\right)v_k = 0\,, \tag{1.4.94}$$

called Mukhanov-Sasaki equation. In general, this equation is difficult to solve, since the function z depends on the background dynamics. We can identify two opposite regimes: i) an early-time regime when each mode is deep inside the horizon and ii) a late-time one when the modes get stretched to become super-horizon. In the former regime, the modes satisfy $k^2 \gg z''/z$ and behave as the standard vacuum fluctuations in Minkowski spacetime

$$v_k(\eta) \simeq \frac{e^{-ik\eta}}{\sqrt{2k}}\,, \tag{1.4.95}$$

where we have fixed the integration constants to adapt the solution to the Bunch-Davies vacuum.

On the other hand, long wavelength modes with $k^2 \ll z''/z$ have solutions given by

$$v_k(\eta) = C_k\, z(\eta) + D_k\, z(\eta) \int^{\eta} \frac{\mathrm{d}\bar{\eta}}{z(\bar{\eta})^2}\,, \tag{1.4.96}$$

where C_k and D_k are integration constants. We can identify important features of the scalar perturbations on super-horizon scales, depending on the behaviour of the solution. On super-horizon scales during slow-roll the modes freeze as the term $z^2 \propto (-\eta)^{-2}$ in the late time $\eta \to 0$ and the second term, the one multiplied by D_k, becomes negligible. In this regime the second contribution in (1.4.96) is negligible and the above solution reduces to

$$v_k(\eta) = C_k\, z(\eta)\,. \tag{1.4.97}$$

The integration constant C_k can be determined by matching the absolute value of the solutions (1.4.95, 1.4.96) at the horizon crossing $k = aH$:

$$|C_k z|_{k=aH} = \frac{1}{\sqrt{2k}} \implies v_k(\eta) = \left(\frac{1}{z(\eta)\sqrt{2k}}\right)_{k=aH} z(\eta)\,. \tag{1.4.98}$$

In general, calculating the power spectrum for a general solution of the Mukhanov-Sasaki equation requires specific knowledge about the evolution of the homogeneous scalar field, as we will analyze in detail in later Chapters. However, it is possible to restrict our analysis to a few interesting cases in which it is possible to extrapolate an approximate solution for the spectrum. Indeed, in a slow-roll regime, we can approximate the expression of the slow-roll parameters to the first order and consider them as constant. It can be demonstrated [30] that in this regime the mass term z''/z can be approximated as

$$\frac{z''}{z} \simeq (aH)^2(1+\epsilon_1-\delta)(2-\epsilon_1) \simeq (aH)^2(2+2\epsilon_1-3\delta)\,. \tag{1.4.99}$$

If we set

$$\frac{z''}{z} = \frac{1}{\eta^2}\left(\nu^2 - \frac{1}{4}\right)\,, \tag{1.4.100}$$

this corresponds to

$$\nu^2 \simeq \frac{3}{2} + (2\epsilon_1 - \delta) \simeq \frac{3}{2} + 3\epsilon_1 - \eta_V \tag{1.4.101}$$

and Mukhanov-Sasaki Eq. (1.4.94) takes the form

$$v_k'' + \left[k^2 - \frac{1}{\eta^2}\left(\nu^2 - \frac{1}{4}\right)\right] v_k = 0\,, \tag{1.4.102}$$

which, for ν real, actually admits a general solution

$$v_k(\eta) = \sqrt{-\eta}\left[C_1(k) H_\nu^{(1)}(-k\eta) + C_2(k) H_\nu^{(2)}(-k\eta)\right]\,, \tag{1.4.103}$$

where $H_\nu^{(1)}$ and $H_\nu^{(2)}$ are the Hankel's functions of the first and second kind, respectively, while C_1 and C_2 are integration constants. If we impose that in the ultraviolet regime $k \gg aH$, the solution

matches the plane-wave solution (1.4.95) and knowing that

$$H_\nu^{(1)}(x \ll 1) \simeq \sqrt{\frac{2}{\pi x}} e^{i\left(x-\frac{\pi}{2}\nu-\frac{\pi}{4}\right)}\,, \qquad H_\nu^{(2)}(x \ll 1) \simeq \sqrt{\frac{2}{\pi x}} e^{-i\left(x-\frac{\pi}{2}\nu-\frac{\pi}{4}\right)}\,, \tag{1.4.104}$$

with $x = -k\eta$, we can set $C_1(k) = \frac{\sqrt{\pi}}{2} e^{\frac{i\pi}{2}\left(\nu-\frac{1}{2}\right)}$ and $C_2(k) = 0$. In this way, the slow-roll solution becomes

$$v_k(\eta) = \sqrt{\frac{\pi}{2}} e^{\frac{i\pi}{2}\left(\nu-\frac{1}{2}\right)} \sqrt{-\eta} H_\nu^{(1)}(-k\eta)\,. \tag{1.4.105}$$

Observing the definition of the comoving curvature perturbation (1.4.67), we notice that

$$\mathcal{R} = \Phi + \mathcal{H}\frac{\overline{\delta\varphi}}{{}^{(0)}\varphi'} = \frac{v}{z}\,, \tag{1.4.106}$$

relating the Mukhanov's variable v with $\mathcal{R}$, allowing us to use the Mukhanov variable to express such comoving quantity which describes the behaviour of scalar cosmological perturbations. We can express the power spectrum of the comoving curvature perturbation in the slow-roll approximation and super-horizon scales using Eq. (1.4.105). In the super-horizon limit [30], we obtain

$$\mathcal{P}_\mathcal{R}(k) = \frac{k^3}{2\pi^2}\left|\frac{v_k}{z}\right|^2 \simeq \frac{1}{2M_\mathrm{P}^2\,\epsilon_1}\left(\frac{H}{2\pi}\right)^2\left(\frac{k}{aH}\right)^{n_s-1}\Bigg|_{k=aH} \simeq \mathcal{A}_s\left(\frac{k}{k_*}\right)^{n_s-1}\,, \tag{1.4.107}$$

where $\mathcal{A}_s$ is the scalar amplitude and k_* is the pivot scale, while $n_s - 1$ is the scalar spectral index

$$n_s - 1 \equiv \frac{\mathrm{d}\log\mathcal{P}_\mathcal{R}}{\mathrm{d}\log k} = 3 - 2\nu = 2\eta_V - 6\epsilon_1\,. \tag{1.4.108}$$

The observational constraints on the scalar amplitude and spectral index are $\mathcal{A}_s = (2.105 \pm 0.010) \times 10^{-9}$ and $n_s = (0.9665 \pm 0.0038)$ from TT,TE,EE+lowE+lensing+BAO measurements at 68% limits [1], considering the pivot mode $k_* = 0.05\,\mathrm{Mpc}^{-1}$.

Gravitational waves from inflation

One of the most relevant and model-independent predictions of inflation is the production of a stochastic background of gravitational waves with an amplitude given roughly by the Hubble scale H during inflation. The simplicity of this prediction means that a measurement of primordial gravitational waves would give clean information about arguably the most important inflationary parameter, namely the energy scale of inflation. Such a background of inflationary gravitational waves could lead to a unique signature in the polarization of the CMB.

The treatment of tensor perturbations is very similar to that of scalar perturbations. Quantum fluctuations in the gravitational fields are generated similarly to those of the scalar perturbations discussed so far. A gravitational wave may be viewed as a ripple of spacetime in the FRLW background metric and, as we have seen in (1.4.44), we can study its evolution by expanding the Einstein-Hilbert action (1.2.19) with respect to the perturbed metric

$$\mathrm{d}s^2 = a^2(\eta)\left[\mathrm{d}\eta^2 - (\delta_{ij} + h_{ij})\mathrm{d}x^i\,\mathrm{d}x^j\right]\,. \tag{1.4.109}$$

The tensor h_{ij} has six degrees of freedom, but as we studied previously, it is also traceless and transverse (1.4.43) and can be described considering only two degrees of freedom, or polarizations, which are usually indicated with $\lambda = +, \times$. To quadratic order in tensor fluctuations, the action takes the form

$$S^{(2)} = \frac{M_{\rm P}^2}{8} \int {\rm d}\eta \, {\rm d}^3x \, a^2 \left[(h'_{ij})^2 - (\vec{\nabla} h_{ij})^2 \right] . \tag{1.4.110}$$

Decomposing in the Fourier space we have

$$h_{ij}(\eta, x) = \int \frac{{\rm d}^3k}{(2\pi)^{3/2}} e^{i\vec{k}\cdot\vec{x}} \left[h_k^+(\eta) \epsilon_{ij}^+(k) + h_k^\times(\eta) \epsilon_{ij}^\times(k) \right] , \tag{1.4.111}$$

where we introduced the normalized polarization tensors

$$\begin{aligned} &\epsilon_{ij}^\lambda = \epsilon_{ji}^\lambda \, , \quad k^i \epsilon_{ij}^\lambda = 0 \, , \quad \epsilon_{ii}^\lambda = 0 , \\ &\epsilon_{ij}^\lambda(-\vec{k}) = \left[\epsilon_{ij}^\lambda(\vec{k}) \right]^* , \qquad \sum_{ij} \left(\epsilon_{ij}^\lambda \right)^* \epsilon_{ij}^{\lambda'} = \delta^{\lambda\lambda'} . \end{aligned} \tag{1.4.112}$$

The action (1.4.110) then becomes

$$S^{(2)} = \sum_{\lambda = \{+,\times\}} \int {\rm d}\eta \, {\rm d}^3\vec{k} \, \frac{a^2}{4} M_{\rm P}^2 \left[\left(\frac{{\rm d}h_k^\lambda}{{\rm d}\eta} \right)^2 - k^2 (h_k^\lambda)^2 \right] . \tag{1.4.113}$$

If we define

$$v_k^\lambda = \frac{a \, M_{\rm P}}{2} \, h_{ij}^\lambda(k) \, , \tag{1.4.114}$$

the equation of motion in the momentum space is

$$(v_k^\lambda)'' + \left(k^2 - \frac{a''}{a} \right) v_k^\lambda = 0 \, , \tag{1.4.115}$$

which is the equation of motion of a massless scalar field in a quasi-de Sitter epoch. We can therefore make use of the mathematical approach learnt in the previous Section to conclude that, on super-Hubble scales, the tensor modes scale like

$$\left| v_k^\lambda \right| = \left(\frac{H}{2\pi} \right) \left(\frac{k}{aH} \right)^{\frac{3}{2} - \nu_T} , \tag{1.4.116}$$

where

$$\nu_T \simeq \frac{3}{2} + \epsilon_1 \, . \tag{1.4.117}$$

Since fluctuations are nearly frozen in on super-Hubble scales, a way of characterizing the tensor perturbations is to compute their spectrum on scales larger than the horizon

$$\begin{aligned} \mathcal{P}_T(k) &\equiv \frac{k^3}{2\pi^2} \sum_{ij} |h_{ij}(k)|^2 = 4 \frac{k^3}{2\pi^2} \sum_{ij} \left(\left| v_k^+ \right|^2 + \left| v_k^\times \right|^2 \right) = \frac{8}{M_{\rm P}^2} \left(\frac{H}{2\pi} \right)^2 \left(\frac{k}{aH} \right)^{n_T} \Bigg|_{k=aH} \\ &\simeq \mathcal{A}_T \left(\frac{k}{k_*} \right)^{n_T} \end{aligned} \tag{1.4.118}$$

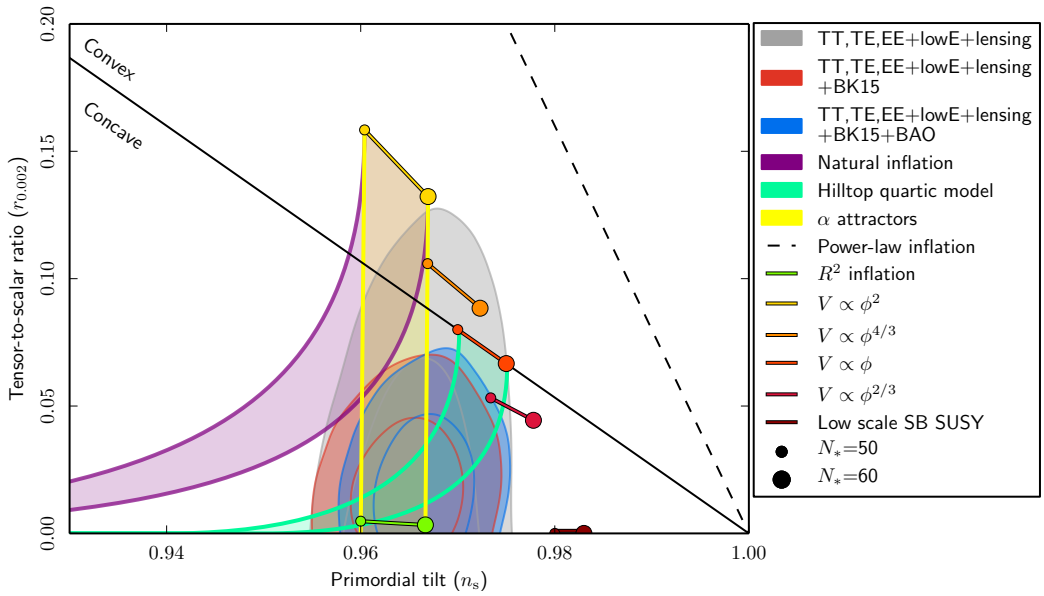

Figure 1.4: Marginalized joint 68% and 95% confidence level regions for n_s and r at $k = 0.002\,\mathrm{Mpc}^{-1}$ from Planck alone and in combination with BK15 or BK15+BAO data, compared to the theoretical predictions of selected inflationary models. Note that the marginalized joint 68% and 95% confidence level regions assume $\mathrm{d}n_s/\mathrm{d}\log k = 0$. The Figure is taken from [24].

where $\mathcal{A}_T$ is the normalization factor for the tensorial power spectrum, and the tensor spectral index n_T is

$$n_T = \frac{\mathrm{d}\log \mathcal{P}_T}{\mathrm{d}\log k} = 3 - 2\nu_T = -2\epsilon_1 \,. \tag{1.4.119}$$

The tensor perturbation is almost scale-invariant. Notice that the amplitude of the tensor modes depends only on the value of the Hubble rate during inflation. This amounts to saying that it depends only on the energy scale associated with the inflaton potential. Hence, a detection of gravitational waves from inflation is therefore a direct measurement of the energy scale associated with inflation.

As of today, there has been no direct and indirect detection of primordial gravitational waves. Observational constraints on the tensor amplitude are usually expressed in terms of the tensor-to-scalar ratio

$$r = \frac{\mathcal{A}_T}{\mathcal{A}_\mathcal{R}} = \frac{8\left(\frac{H}{2\pi M_\mathrm{P}}\right)^2}{\frac{1}{2\epsilon_1}\left(\frac{H}{2\pi M_\mathrm{P}}\right)^2} = 16\epsilon_1 \,, \tag{1.4.120}$$

that leads to the consistency relation

$$r = -8n_T \,. \tag{1.4.121}$$

Since the amplitude of scalar fluctuations has been measured, the tensor-to-scalar ratio quantifies the size of the tensor fluctuations.

Chapter 2

PBH properties and formation

We start by providing a physical description of the PBH formation in the early universe, in order to relate the basic properties of a PBH formation, as their mass and abundance, with the features of primordial curvature perturbation originating from inflation. Let us highlight that we are going to assume the "standard" formation scenario in which PBHs are created out of the collapse of density perturbations when the energy density was dominated by a relativistic fluid, such as radiation or dust.

Following this assumption, we organize this Chapter in the following way. In Section 2.1 we present the mechanism of PBH formation, focusing on the causal process involved with the inflationary quantum fluctuations. In Section 2.2 we describe the principal concepts related to PBH physical description, such as the threshold for collapse into black holes, the corresponding mass and collapse fraction of PBHs, and some of the ingredients and mathematical steps necessary to compute their abundance. In Section 2.3, we determine the amplitude of scalar fluctuations required for producing a certain population of PBH, considering some interesting examples for cosmology. Finally in Section 2.4, we will show how recent studies were able to constrain the PBH abundance in most of the phenomenologically interesting range of masses. Still, we will observe that the study of PBHs may have important consequences, even if they represent only a tiny fraction of the total dark matter.

2.1 PBH formation as a causal process

Primordial black holes may arise from the collapse of large density perturbations in the early universe [31]. We have already studied the quantization and evolution of such perturbations in an expanding universe, and have highlighted the importance of the comoving curvature perturbation $\mathcal{R}$. In fact, apart from providing seeds for the observed cosmic microwave background anisotropies at large scales, the dynamics of the curvature perturbation $\mathcal{R}$ may also be at play for PBH formation.

In order to describe the behaviour of perturbations in the inflationary universe and study their statistical properties, we often label each given perturbation mode (in the Fourier space) with a comoving length scale k^{-1}, measured in units of megaparsec. As shown in Fig. 2.1, we can understand that typically, fluctuations begin their life deep inside the horizon, as quantum fluctuations; then the horizon shrinks during inflation and they leave the horizon to become super-horizon perturbations,

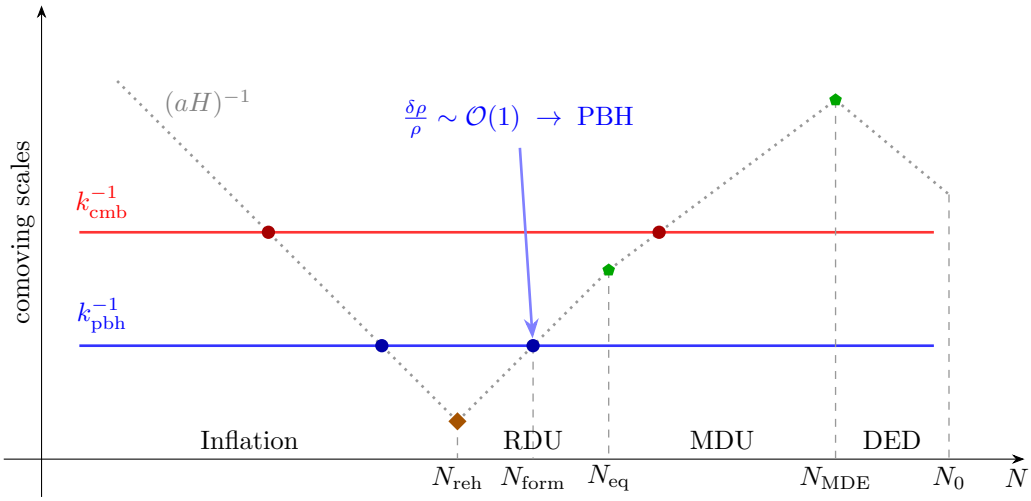

Figure 2.1: A qualitative representation of the time evolution of curvature fluctuations $\mathcal{R}$, with respect to the comoving Hubble radius (dotted lines) in the early universe. In particular, $N_{\rm reh}$ denotes the reheating time, $N_{\rm eq}$ refers to the time of matter-radiation equality, $N_{\rm MDE}$ to matter-dark energy equality, and N_0 denotes the present time. The blue horizontal line indicates the comoving size of a representative small scale perturbation for PBH formation. If the power spectrum associated with these modes is enhanced during inflation, they can transfer their energy density perturbations during radiation domination, and ignite PBH formation upon horizon re-entry at $N = N_{\rm form}$.

and finally re-enter at a later time in the standard Big Bang era.

Considering standard Bunch-Davies "initial conditions" for all scales, we shall assume there is an enhancement of perturbations at smallest length scales below the values relevant for CMB observations at cosmological scales: $\mathcal{P}_\mathcal{R}(k_{\rm pbh}) \gg \mathcal{P}_\mathcal{R}(k_{\rm CMB}) \sim 10^{-9}$ [24]; for this purpose, we consider $k_{\rm pbh} \gg k_{\rm CMB}$ where the former is the wave number associated with PBH formation and the latter the typical wave number of CMB. After the end of inflation, possibly after reheating $N_{\rm rhe}$, the enhanced modes (*e.g.* modes with comoving size of $k^{-1}_{\rm pbh}$) become the seeds of density perturbations during the RDU or the MDU:

$$\delta \equiv \frac{\delta\rho}{\rho}\bigg|_{k=aH} \sim |\mathcal{R}| \sim \mathcal{P}_\mathcal{R}(k_{\rm pbh})^{1/2} \,. \tag{2.1.1}$$

As the Hubble horizon grows compared to the comoving scales k^{-1} during the radiation era, at a certain time the characteristic scale of the perturbations becomes comparable to the horizon scale. When this happens, gravitational forces become active, initiating the contraction of the overdense regions, which can collapse and form PBHs if they are dense enough: $\delta > \delta_c$. Soon after horizon crossing, radiation pressure can rapidly disperse the over-density peaks, and therefore the fate of perturbations is decided at horizon crossing. One finds also that there is only a negligible contribution from PBHs formed from the collapse of sub-horizon modes. This implies that the horizon re-entry is crucial in our understanding of PBH formation as a causal process: in fact, only when the physical wavelength of a perturbation becomes comparable to the causal distance $1/H$, gravity is able to communicate the presence of an over-density and to initiate the gravitational collapse. A schematic diagram that summarizes the discussion above is illustrated in Fig 2.1.

In the following, we shall discuss the relevant quantities involved in PBHs formation such as the

threshold for collapse, the mass and the collapse fraction of PBH, which are crucial to describe the properties and compute the current PBH abundance.

2.2 The relevant quantities for PBH abundance

The threshold collapse

During radiation domination, the background pressure of the relativistic cosmological fluid is very large ($p = w\rho = \rho/3$), meaning that only large amplitude perturbations will experience sufficient gravitational attraction to overcome the pressure forces and collapse into a black hole. We can estimate, following the analysis given by Bernard Carr in 1975 [32], the value required for the over-densities to generate a PBH. In particular, considering a Jeans-type instability argument within Newtonian gravity, Carr estimated that an over-density in RDU would collapse upon horizon re-entry if the *density contrast* δ (2.1.1) satisfies

$$\delta > \delta_c = c_s^2 \,, \tag{2.2.1}$$

where δ_c is the threshold for collapse while c_s^2 is the sound speed of density perturbations, which determines how fast a pressure wave caused by an over-density can travel from the centre to the edge of the perturbation. In a RDU the speed of sound of perturbations is $c_s = 1/\sqrt{3}$ so that its square is directly related to (1.1.8) as $c_s^2 = \omega = 1/3$. Equation (2.2.1) then implies that a perturbation can collapse to form PBHs if its over-density is larger than the pressure exerted by the radiation pressure[1]. A more precise estimate of the threshold δ_c can be obtained both by one-dimensional and three-dimensional GR simulations and even more precisely when the evolution of perturbations is taken into account beyond the linear regime. Recent efforts in this direction (see *e.g.* [33]) show that the threshold values of the density contrast depend on the shape of the density peak, and are in the range $0.4 \leq \delta_c \leq 2/3$. In the following, we shall consider values of δ_c inside this interval.

The mass of PBHs

The mass of the PBHs is approximately given by that contained inside a Hubble patch at the time of collapse t_c: $M(t_c) = (4\pi/3)\,\rho(t_c)/H^3(t_c)$, multiplied by an efficiency factor $\gamma = 0.2$, as suggested in [32]. In particular, we can write

$$M_{\rm pbh}^{(c)} = \gamma\, M\Big|_{a=a_c} = \gamma\, M^{(\rm eq)} \left(\frac{M^{(c)}}{M^{(\rm eq)}}\right) = \left(\frac{a_c}{a_{\rm eq}}\right)^2 \gamma M^{(\rm eq)} \,, \tag{2.2.2}$$

where sub/superscripts "c" and "eq" refer to quantities evaluated at the time of PBH formation and matter-radiation equality respectively, and we used the standard relation $H^2 \propto \rho \propto a^{-4}$ during RDU. Therefore, noting that the horizon mass at the time of equality is given by $M^{(\rm eq)} \simeq 2.8 \times 10^{17}\, M_\odot$ [34], PBH masses can span an incredibly large range of values, in contrast to astrophysical black holes, as they are related to the size of the cosmological horizon and the energy density of the universe at formation time, compared to the same quantities at matter-radiation equality.

[1] See Appendix B for a simple analytic argument that leads to this result.

$M_{\rm pbh}[M_\odot]$	ΔN	$k_{\rm pbh}[{\rm Mpc}^{-1}]$
10^6	14	10^3
$10^0 \; - \; 10^2$	$18 \; - \; 21$	$10^5 \; - \; 10^6$
$10^{-17} \; - \; 10^{-12}$	$34 \; - \; 40$	$10^{12} \; - \; 10^{15}$

Table 2.1: Range of PBH mass w.r.t the corresponding wave-number $k_{\rm pbh}$ of the primordial modes together with the approximate horizon crossing time measured starting from the e-folding number of horizon-exit for the pivot scale $k_{\rm cmb} = 0.002\,{\rm Mpc}^{-1}$, $\Delta \equiv N_{\rm pbh} - N_{\rm cmb} > 0$. The first row refers to the corresponding quantities for a typical Super Massive Black Hole (SMBH) like the SagittariusA* in the center of our galaxy [36]. The third row refers to astroid-mass PBHs that can still account for a significant fraction (or all) of DM density today.

We can relate the PBH mass to the characteristic size of the perturbation that leaves the horizon during inflation and finally collapses to form the corresponding PBH. For this purpose, we can rewrite the PBH mass as [35]

$$M_{\rm pbh}^{(c)} = \left(\frac{\rho_c}{\rho_{\rm eq}}\right)^{1/2} \left(\frac{H_{\rm eq}}{H_c}\right)^2 \gamma M^{(\rm eq)} \; . \tag{2.2.3}$$

Using entropy conservation $g_s(T)\,T^3\,a^3 =$ constant and the temperature dependence of the energy density in the RDU, $\rho \propto g_*(T)\,T^4$, with T indicating the temperature of the cosmological fluid and $g_*(T)$ being the effective number of relativistic degrees of freedom, we can re-express Eq. (2.2.3) as follows [35]

$$\begin{aligned} M_{\rm pbh}^{(c)}(k_{\rm pbh}) &= \left(\frac{g_*(T_c)}{g_*(T_{\rm eq})}\right)^{1/2} \left(\frac{g_s(T_{\rm eq})}{g_s(T_c)}\right)^{2/3} \left(\frac{k_{\rm eq}}{k_{\rm pbh}}\right)^2 \gamma M^{(\rm eq)} \\ &\simeq \left(\frac{\gamma}{0.2}\right) \left(\frac{g_*(T_c)}{106.75}\right)^{-1/6} \left(\frac{k_{\rm pbh}}{3.2\times 10^5\,{\rm Mpc}^{-1}}\right)^{-2} 30 M_\odot \; . \end{aligned} \tag{2.2.4}$$

In the second line we assumed that the effective number of relativistic degrees of freedom in the energy density and entropy are equal, *i.e.* we set $g_*(T) = g_s(T)$ and take $g_*(T_{\rm eq}) \simeq 3.38$, with $k_{\rm eq} \simeq 0.0104\,{\rm Mpc}^{-1}$, accordingly with the latest Planck result [1]. Therefore, Eq. (2.2.4) indicates that for masses of PBHs that could be associated with recent LIGO observations [10], $M_{\rm pbh} \simeq 30 M_\odot$, the peak scale of perturbations responsible for PBH formation is smaller than CMB scales $k_{\rm pbh} \gg k_{\rm cmb}$. For sub-solar mass PBHs, the corresponding peak scale for PBH formation gets progressively smaller. For example, considering the currently allowed sub-lunar range ($M_{\rm moon} \simeq 3.7\times 10^{-8}\,M_\odot$) of PBH masses, $10^{-17} \lesssim M_{\rm pbh}/M_\odot \lesssim 10^{-12}$, which are astrophysical objects that can be the origin for the totality of dark matter, the range of scales associated with PBH formation is quite small: $10^{12} \lesssim k_{\rm pbh}/{\rm Mpc}^{-1} \lesssim 10^{15}$. See Table 2.1 for an easier-to-visualize summary of these considerations.

What's more, given that during a near-de Sitter inflation, the Hubble rate remains nearly constant, $\epsilon_1 \ll 1$, we can also derive an approximate relation between the PBH mass and the number of e-folds $N_{\rm pbh}$ at which the PBH-forming modes leave the horizon during inflation. Considering $H_{\rm pbh} = H_{\rm cmb}\, e^{-\epsilon_1 (N_{\rm pbh} - N_{\rm cmb})}$ and $a_{\rm pbh} = a_{\rm cmb}\, e^{N_{\rm pbh} - N_{\rm cmb}}$, where $N_{\rm pbh} > N_{\rm cmb}$ and we count e-folds

forward in time starting from the horizon exit of the CMB mode.[2]. Considering the relation between the modes and the horizon scale at horizon exit, we can write $k_{\rm pbh}/k_{\rm cmb} = (aH)_{\rm pbh}/(aH)_{\rm cmb} \simeq e^{(1-\epsilon_1)(N_{\rm pbh}-N_{\rm cmb})}$; once plugged in Eq. (2.2.4), assuming $k_{\rm cmb} = 0.002\,{\rm Mpc}^{-1}$, we obtain

$$M^{(c)}_{\rm pbh}(N_{\rm pbh}) \approx 7.7\times 10^{17} M_\odot\, e^{-2(N_{\rm pbh}-N_{\rm cmb})(1-\epsilon_1)} \left(\frac{\gamma}{0.2}\right)\left(\frac{g_*(T_c)}{106.75}\right)^{-1/6} . \tag{2.2.5}$$

Therefore the later the modes leave the horizon compared to CMB scales, with $e^{-2(N_{\rm pbh}-N_{\rm cmb})} \ll 1$, the smaller is the mass of the resulting PBH.

PBH abundance and collapse fraction β

Another important quantity, in this context, is the abundance of PBHs relative to the energy density of other species. In particular, we can compute this quantity during two epochs: today and at PBH formation.

When considering the fraction of PBH density today, we relate the PBH abundance to the present-day dark-matter density introducing the quantity

$$f_{\rm pbh} \equiv \frac{\Omega_{\rm pbh}}{\Omega_{\rm dm}} , \tag{2.2.6}$$

where Ω is defined as (1.1.15), and $\Omega_{\rm dm}$ is currently best constrained by the Planck measurement [1].

We can relate $f_{\rm pbh}$ today to the density fraction of PBH at the epoch of their formation, denoting this quantity with β. If PBH formation occurs in the RDU, and given the different dependence of the energy densities for matter and radiation sources on the scale factor ($\rho_M \propto a^{-3}$ and $\rho_R \propto a^{-4}$), we have

$$\beta \equiv \frac{\rho_{\rm pbh}}{\rho_{\rm tot}} = \left(\frac{H_0}{H_c}\right)^2 \left(\frac{a_c}{a_0}\right)^{-3} \Omega_{\rm dm}\, f_{\rm pbh} , \tag{2.2.7}$$

where the sub-scripts "0" and "c" refer to the present time and the time of PBH formation. In particular, it is possible to determine a subsequent relation directly linked to the mass of PBH at formation [35]:

$$\beta \equiv \left.\frac{\rho_{\rm pbh}}{\rho_{\rm tot}}\right|_{a=a_c} \simeq 1.33\times 10^{-9} \left(\frac{\gamma}{2.0}\right)^{-1/2} \left(\frac{g_*(T_c)}{106.75}\right)^{-1/12} \left(\frac{M^{(c)}_{\rm pbh}}{M_\odot}\right)^{1/2} f_{\rm pbh} . \tag{2.2.8}$$

This expression allows us to extrapolate some information about the process of PBH production. In particular, if PBHs constitute the total DM density today, $f_{\rm pbh} \to 1$, β takes extremely small values since we must restrict to the range of masses $M^{(c)}_{\rm pbh} \sim \mathcal{O}(M_\odot)$. This result reflects the fact that PBHs density in the early universe can be very low.

[2] We used the convention for which the counting of the number of e-folds allows $N_{\rm end} = 0$ at the end of inflation.

2.2.1 Collapse fraction of PBHs at formation

There is another important estimate related to β. We evaluate the PBH abundance at formation through the probability of some perturbation δ to be larger than the threshold δ_c. The estimate of β, in this treatment, is computed using an analogy of the Press-Schechter formalism [37] and is

$$\beta \equiv \frac{\rho_{\rm pbh}}{\rho_{\rm tot}}\bigg|_{a=a_c} \equiv \int_{\Delta_c}^{\infty} {\rm d}\delta\, P(\delta) = \frac{1}{\sqrt{2\pi}\sigma}\int_{\Delta_c}^{\infty} {\rm d}\delta\, e^{-(\delta-\mu)^2/2\sigma^2}\,, \tag{2.2.9}$$

where $P(\delta)$ is the probability distribution function for the over-density δ, and we assume it has a Gaussian form, with mean value μ and variance σ^2. We assume that a perturbation δ will collapse to form BH if its amplitude is larger than a critical value Δ_c. Notice that Δ_c is the critical density contrast and in general is different from the threshold δ_c. For more details on the relation between Δ_c and δ_c we refer to [38]. However, for simplicity, we will continue identifying $\Delta_c = \delta_c$ for the estimates of β.

A crucial parameter of the distribution $P(\delta)$ in (2.2.9) is represented by the variance σ^2. It is clear that for larger values of the variance, the probability of having larger values of the over-density increases and accordingly the value of β.

In particular, using (2.2.8) and (2.2.9), we can estimate the required variance σ^2 that can give rise to a large population of PBH today. Focusing with a distribution with zero mean $\mu = 0$, we have

$$\beta = \frac{1}{\sqrt{2\pi}\sigma}\int_{\delta_c}^{\infty} {\rm d}\delta\, \exp\left(-\frac{\delta^2}{2\sigma^2}\right) = \frac{1}{2}{\rm Erfc}\left(\frac{\delta_c}{\sqrt{2}\sigma}\right) \simeq \frac{\sigma}{\sqrt{2\pi}\delta_c}\exp\left(-\frac{\delta_c^2}{2\sigma^2}\right)\,, \tag{2.2.10}$$

where ${\rm Erfc}(x) = 1 - {\rm Erf}(x)$ is the complementary of the error function, and in the last equality we take $\delta_c \gg \sigma$. In general, this is a quite common and reasonable approximation. We can consider two concrete examples: substituting Eq. (2.2.10) into Eq. (2.2.8) we obtain that a solar mass PBH population with $f_{\rm pbh} = 10^{-3}$ requires $\delta_c/\sigma \simeq 0.7$, whereas for a population with $M^{(c)}_{\rm pbh} = 10^{-12} M_\odot$ and $f_{\rm pbh} = 1$ we need $\delta_c/\sigma \simeq 7.9$. Assuming a threshold of $\delta_c = 0.4$, these results yield respectively $\sigma \simeq 0.06$ and $\sigma \simeq 0.05$. We will analyze in the next Section how these results are related to the power spectrum of the comoving curvature perturbation $\mathcal{R}$.

2.3 PBH properties and primordial scalar fluctuations

We now want to discuss a proper treatment to relate the PBH abundance with the features of the comoving curvature fluctuation $\mathcal{R}$, produced in a quantum state deep inside the horizon and enhanced by cosmic inflation.

Following [33], we assume the comoving curvature perturbation $\mathcal{R}$ is a Gaussian random field. Working in Fourier space, we can perform a gradient expansion controlled by the ratio k/aH and to the linear order one finds [31]

$$\delta(x,t) \simeq \frac{2(1+\omega)}{5+3\omega}\frac{\nabla^2\mathcal{R}(x)}{(aH)^2} + \ldots \implies \delta_k \simeq -\frac{4}{9}\left(\frac{k}{aH}\right)^2 \mathcal{R}_k\,, \tag{2.3.1}$$

where we used $\omega = 1/3$ in the RDU and neglected terms of higher order $O(\mathcal{R}^2)$ in the curvature perturbation. This equation relates the energy fluctuations and curvature fluctuations and allows us to understand the behaviour of the amplitude of curvature perturbation $\mathcal{R}$ necessary to trigger PBH formation.

The relation between the power spectra of over-densities and curvature perturbations is then given by

$$\mathcal{P}_\delta(k) \simeq \frac{16}{81} \left(\frac{k}{aH}\right)^4 \mathcal{P}_\mathcal{R}(k) \,. \tag{2.3.2}$$

In the computation of the density contrast, one should typically use a window function $\mathcal{W}$ to smooth $\delta(t, \vec{x})$ on a comoving scale $R \approx k^{-1} \approx (aH)^{-1}$, relevant for PBH formation. Finally, the relation between the variance of the density contrast δ and the primordial power spectrum (see *e.g.* [39]) is

$$\sigma^2(R) \equiv \langle \delta^2 \rangle_R = \int_0^\infty \mathrm{d}\log q \, \mathcal{W}^2(q, R) \, \mathcal{P}_\delta(q) \simeq \frac{16}{81} \int_0^\infty \mathrm{d}\log q \, \mathcal{W}^2(q, R) \, (qR)^4 \, \mathcal{P}_\mathcal{R}(q) \tag{2.3.3}$$

where $\mathcal{W}$ is the Fourier transform of a real space window function. Common choices of $\mathcal{W}$ include a volume-normalised Gaussian, or a top hat window function, whose Fourier transforms are respectively given by

$$\mathcal{W}(k, R) = \exp\left(-\frac{k^2 R^2}{2}\right) , \qquad \mathcal{W}(k, R) = \frac{3\sin(kR) - 3kR\cos(kR)}{(kR)^3} \,. \tag{2.3.4}$$

If the curvature power spectrum $\mathcal{P}_\delta$ is characterized by a very narrow peak around some wavenumber $k_{\rm phb}$, the integral (2.3.3) can be approximated and gives $\sigma^2 \sim \mathcal{P}_\delta(k_{\rm pbh})$. Then, using Eq. (2.3.2) at horizon entry $k \simeq aH$ (*i.e.* at the time of PBH formation), since $81/16 \sim 5$, we can roughly relate the variance σ to the primordial curvature power spectrum as

$$\mathcal{P}_\mathcal{R}(k_{\rm pbh}) \sim 5\sigma^2 \sim 10^{-2} \,, \tag{2.3.5}$$

where we used the results derived from Eq. (2.2.10). Let us note that a Gaussian PDF for δ requires $\sigma \simeq 0.06$ for $M^{(c)}_{\rm pbh} = M_\odot$ to generate a population of $f_{\rm pbh} = 10^{-3}$ today, considering Gaussian fluctuations. This estimate holds for a wide range of sub-solar PBH masses, and implies that we need a very large amplification of the curvature spectrum perturbation with respect to CMB scales in order to trigger PBH formation:

$$\Delta\mathcal{P}_\mathcal{R} \equiv \frac{\mathcal{P}_\mathcal{R}(k_{\rm pbh})}{\mathcal{P}_\mathcal{R}(k_{\rm cmb})} \sim 10^7 \,. \tag{2.3.6}$$

It is worth mentioning that this estimate does not change much for smaller mass PBHs with $M^{(c)}_{\rm pbh} < 10^{-12} M_\odot$, because the power spectrum has a logarithmic sensitivity on the PBH fraction β. In order to check this last statement, we can invert the expression (2.2.10), and use (2.3.5) to relate primordial power spectrum of curvature perturbation to β as

$$\mathcal{P}_\mathcal{R}(k_{\rm pbh}) \sim 5\sigma^2 \sim \frac{5\delta_c^2}{2\log(1/\beta)} \,. \tag{2.3.7}$$

Now, as an extreme case, we can consider the smallest PBHs $M_{\rm pbh}^{(c)} \simeq 10^{-18} M_\odot$ that can survive until today (not yet evaporated by Hawking radiation) which have the tightest available observational constraints, restricting their current abundance to $f_{\rm pbh} \lesssim 10^{-9}$ [40]. Plugging these values in (2.2.10), we find that the PBH fraction at formation is $\beta \lesssim 10^{-28}$, which in turn leads to the constraint $\mathcal{P}_\mathcal{R}(k_{\rm pbh}) \lesssim 6 \times 10^{-3}$ in (2.3.7) for a threshold of $\delta_c = 0.4$. Therefore, we conclude that for Gaussian perturbations and for any PBH mass of interest, the amplitude of scalar power spectrum relevant for PBH formation requires $\mathcal{P}_\mathcal{R} \sim 10^{-2}$ for any potentially observable PBH fraction f_{pbh} today. The discussion above tells us that a small variation in the amplitude of the power spectrum leads to differences of many orders of magnitude in the fraction of regions collapsing into PBHs, as clearly implied by the exponential dependence of β to $\mathcal{P}_\mathcal{R}$ in (2.3.7). Similarly, a small change in the choice of threshold δ_c could lead to very different estimates in terms of β. For example, focusing on a fixed value of variance $\sigma^2 \simeq 0.05$, β (2.2.10) can change by various orders of magnitude, if we reduce the threshold δ_c by just about 20% :

$$\frac{\beta(\delta_c = 0.4)}{\beta(\delta_c = 1/3)} \simeq 10^{-5}\,, \tag{2.3.8}$$

demonstrating how tuned should be the conditions for producing a cosmologically interesting population of PBHs.

2.4 Constraints on the primordial black hole abundance

In this Section, we review the constraints on the PBHs abundance from different probes, focusing on the phenomenologically interesting mass range, based on the work of [31], [41]. The constraints reported in the literature are derived from a very specific set of assumptions, and it is assumed that all the PBHs have a monochromatic mass function, i.e. they span a mass range $\Delta M \sim M_{\rm pbh}$. However, some more recent works tried to generalize such constraints to the case of extended mass functions [42]. Some constraints may be relaxed or strengthened with model-dependent modifications of the physical processes behind the formation mechanism, such as effects from strongly non-Gaussian fluctuations or the effect of accretion for $M_{\rm pbh} \gtrsim \mathcal{O}(10) M_\odot$ [43] and clustering. In general, there are still uncertainties in both the black hole physics and observations themselves.

A comprehensive summary plot is shown in Fig. 2.2, where the main constraints on the abundance are shown for clarity. We shall organize the discussion on the kind of physical process at the origin of a PBH signature in observations.

Hawking radiation

The lifetime of a PBH due to its evaporation in standard model particles can be approximated as [40]

$$t \approx 10^{64} \left(\frac{M_{\rm pbh}}{M_\odot}\right)^3 \text{yr}\,. \tag{2.4.1}$$

Relation (2.4.1) suggests us that PBHs with $M_{\rm pbh} \lesssim 10^{-16} M_\odot$ evaporate in a time-scale comparable with the age of the universe or even less and the emitted radiation has a black-body spectrum with

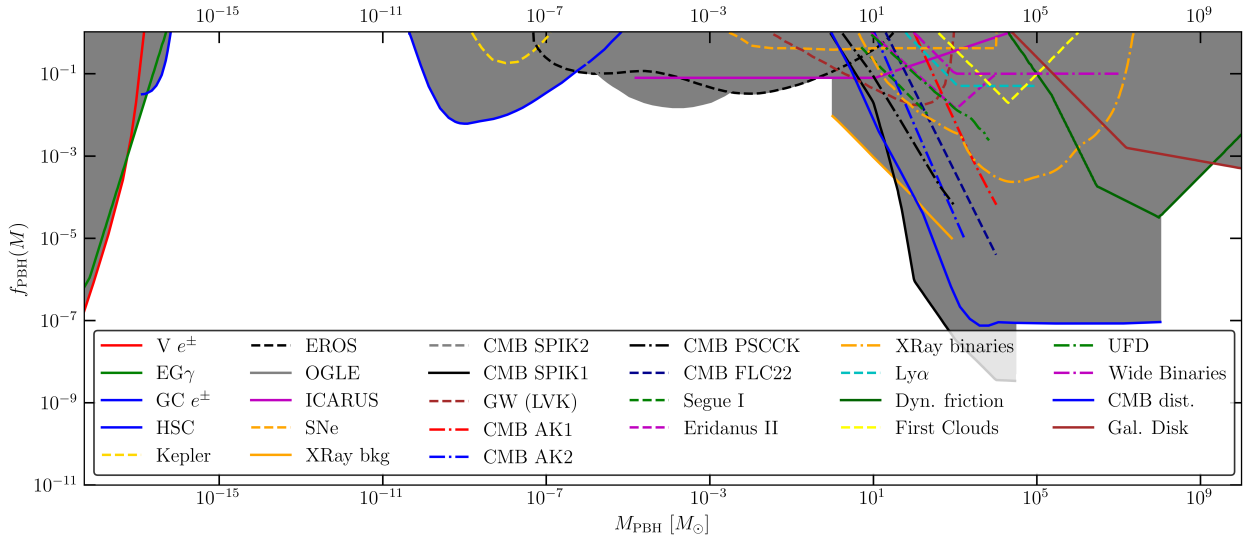

Figure 2.2: We show the most stringent claimed constraints in the mass range of phenomenological interest (Figure taken from [41] and References therein). They come from the Hawking evaporation producing extra-galactic gamma-ray (EGγ), $e^{\pm}$ observations by Voyager 1 (V $e^{\pm}$), positron annihilations in the Galactic Center (GC e^{+}) and gamma-ray observations by INTEGRAL. There are plots related to microlensing searches by Subaru HSC, MACHO/EROS, OGLE and ICARUS. Other constraints come from CMB distortions. In black dashed, we show the ones assuming disk accretion while in black solid the ones assuming spherical accretion. Additionally, constraints coming from X-rays (XRay bkg) and X-Ray binaries (XRay binaries) are shown. Dynamical limits coming from dynamical friction (Dyn. friction), the disruption of wide binaries (Wide Binaries), and the survival of star clusters in Eridanus II and Segue I are also shown.

a temperature $T \propto 1/M_{\rm pbh}$. In particular, as the energy emitted through the Hawking evaporation becomes increasingly larger for lighter BHs, this process may lead to the production of detectable signatures in the case of ultralight PBHs, such as the production of light elements during the Big Bang Nucleosynthesis [40], or affecting the neutron-to-proton ratio at the time of freeze-out of the weak interaction [44]. Other detectable signatures can come from variations of the CMB anisotropies due to the injection of electromagnetic energy for PBHs, for a mass range $[3 \times 10^{13},\ 5 \times 10^{16}]$ g [45].

The most stringent constraints, related to the lightest portion of Fig. 2.2, come from the production of extra-galactic γ-rays [46], $e^{\pm}$ observations by Voyager (V $e^{\pm}$) [47], positron annihilations in the Galactic Center (GC e^{+}) [48] and gamma-ray observations by INTEGRAL [49].

It is important to keep in mind that there is a lack of observational evidence for black hole evaporation, and even if well established theoretically, it is still unclear whether quantum gravity effects would affect or not this process. Although these are all important limitations to account for, it is worth noticing that such very light PBHs, if they exist, are still the ideal target to probe and test the Hawking radiation hypothesis for the first time.

Gravitational lensing

One of the most stringent constraints on PBH as constituents of the dark matter in the universe comes from the microlensing amplification of light. PBHs being very compact objects can lead to significant lensing signatures on the electromagnetic radiation reaching the detectors from background sources. Thus, the most stringent constraints in the mass range $10^{-10} \lesssim M_{\rm pbh} \lesssim 10 M_\odot$

come from microlensing searches by Subaru HSC [50], lensing searches of massive compact halo objects (MACHO) towards the Large Magellanic Clouds [51], fast transient events near-critical curves of massive galaxy cluster Icarus [52] and observations of stars in the Galactic bulge by OGLE [53]. Finally, Ref. [54] constrained $f_{\rm PBH} \lesssim 0.4$ for $M_{\rm PBH} \gtrsim 10^{-2} M_\odot$ from gravitational lensing of type Ia supernovae.

Above $10 M_\odot$, it is essentially impossible to derive bounds due to the fact that the amplification light curve lasts more than a decade, while no microlensing survey has monitored continuously the light from stars for so long. Below $10^{-9} M_\odot$, the wavelength of visible light is comparable to the Schwarzschild radius of the compact object, and we enter the regime of wave optics, where diffraction makes the constraints essentially disappear. One could search for PBHs with $M_{\rm pbh} < 10^{-9} M_\odot$ with light of shorter wavelength, like X-rays or gamma-rays, but sources that emit in those bands are typically not as abundant and stable as stars.

Dynamical effects

The most stringent constraint reported in Fig. 2.2 from dynamical effects is the one denoted as dynamical friction (Dyn. friction) [55]. A large fraction of massive PBHs in the galactic halo may lead to clustering close to the galactic center due to dynamical friction from stars or lighter PBHs, making them lose kinetic energy. Such high concentration would not be allowed by the upper limit on the mass contained in the Galactic center.

The possibility of PBHs above $10 M_\odot$ should induce dynamical heating in highly dark matter dominated ultra-faint dwarf galaxies (UFDGs), such as in Segue I [56] or in Eridanus II [57], allowing them to reach half-light radii larger than 10 parsecs. In general, works in this sense basically exclude $f_{\rm pbh} = 1$ for $M_{\rm pbh} > 10 M_\odot$, and are relatively compelling because they rely on well-known Newtonian gravitational dynamics.

Accretion limits

The accretion of baryonic matter on PBHs leads to various effects both in the early and late-time universe. In fact, the accretion of background gas could lead to a large luminosity for PBHs at early times, having an impact on the CMB temperature and polarization anisotropies, setting limits on the abundance of PBHs between about $10\, M_\odot$ and $10^4\, M_\odot$ [58]. The main idea behind this constraint is the following: in the early universe, PBHs would inevitably affect primordial gas, accreting it. In turn, the consequent emission of high-energy radiation could affect the thermal and ionization histories of the universe, leading to CMB distortions and signatures in the CMB temperature and polarization angular power spectra.

Other constraints come from comparing the late-time emission of electromagnetic signals from interstellar gas accretion onto PBHs with observations of galactic radio and X-ray isolated sources [59] and X-ray binaries [60]. Finally, a cosmology-independent constraint can be set on the PBH abundance based on the absence of gas heating in the interstellar medium due to PBH interactions. Using data from Leo T dwarf galaxy is possible to constrain effects from photon emission, dynamical friction, winds and jets emission from accretion disks, setting a bound on PBHs with masses in the range $[10^{-2}, 10^6]\, M_\odot$ up to the percent level [61, 62].

The strengths of these limits depend on the details of the accretion mechanism and, given the possible complexity of the accretion process, it is possible that those limits significantly change under different assumptions.

Indirect constraints

"Indirect" constraints are considered to be the ones that only probe the standard formation mechanism for PBHs, i.e. limiting the amplitude of primordial curvature perturbations. Those limits at small scales can then be translated into a bound on the PBH abundance. Enhanced primordial density perturbations producing PBHs will also generate CMB μ-distortions [63] by dumping energy into the primordial plasma in the wave-number range $1 \lesssim k/\mathrm{Mpc}^{-1} \lesssim 10^{4.5}$, and strongly constraining PBHs above $M_{pbh} \approx 10^4 M_\odot$. Other effects include the modification of the freeze-out value of the neutron-to-proton ratio at the Big Bang Nucleosynthesis era. In particular, Ref. [64] found that small scale perturbations decrease the n-p ratio, obtaining constraints on the power spectrum of the curvature perturbations as $\mathcal{P}_\mathcal{R} \lesssim 0.018$ on $10^4 \lesssim k/\mathrm{Mpc}^{-1} \lesssim 10^5$. These indirect probes are therefore very interesting to discriminate between the possible PBH formation models in a way that is independent of the complex physical processes that could have impacted the PBH properties. However, those limits would be evaded if PBHs are generated from highly non-Gaussian perturbations boosting the PBH production by enhancing the tail of perturbation distribution while leaving the mean perturbations well below the bounds.

Gravitational waves

In recent years interest in PBHs has intensified because of the detection of gravitational waves (GWs) from coalescing binary black holes by LIGO/Virgo collaboration (LVC) and the possibility that these might be of primordial rather than stellar origin. By requiring the number of detectable events per year not to exceed the rate observed by LVC, one can set a constraint on the PBH abundance [65, 66]. For large values of f_{pbh} close to unity, PBH clustering evolution can reduce the merger rate by enhancing binary interactions in dense environments. However, this effect is not sufficient to reduce the rate to a level that would be compatible with LVC observations in the standard scenario [66, 67].

Additionally, the NANOGrav experiment searching for a stochastic GW background in the frequency range close to $f \simeq 1\mathrm{yr}^{-1}$ would be able to detect the GWs induced at second order by the curvature perturbations responsible for PBH formation. The null observation in the 11-yr dataset was translated into a constraint on the PBH [68]. In particular, less than one part in a million of the total DM mass could come from PBHs in the mass range of $[2 \times 10^{-3}, 7 \times 10^{-1}]\, M_\odot$. As the PBH abundance is exponentially sensitive to the curvature perturbation amplitude constrained by NANOGrav, the current upper bound has large uncertainties when translated in terms of f_{pbh}. Therefore, we take the opportunity to stress that the constraint from the NANOGrav 11-yr data from Ref. [68] has large systematic uncertainties, above all in their choice of the threshold for PBH formation. We stress that this is only applicable for PBHs formed from the collapse of density perturbations and in the absence of non-Gaussianities (see for example [69]. Also, the NANOGrav

collaboration has released the new 12.5 yrs dataset and claimed that the previous constraint should be relaxed due to improved treatment of the intrinsic pulsar red noise [70].

Mass windows: the asteroidal mass range

In this Section, we have reviewed only some of the principal ways to probe and constrain the abundance of PBHs. If one strictly follows the claimed limits and assumes a monochromatic distribution, it seems that there is an open window in the asteroidal mass range $[10^{-16}, 10^{-10}]\,M_\odot$ that can account for the entirety of the dark matter. Indeed, for small mass PBHs, below $10^{-16} M_\odot$, this seems impossible due to limits based on PBH evaporation through Hawking radiation, while above $10^{-10} M_\odot$ we must consider effects coming from microlensing, posing limits up to the solar mass scale, and multiple other astrophysical observations at masses above a solar mass.

Limits that were previously set in this window, by using femtolensing effects [71], an extended original version of HSC microlensing searches [50], dynamical constraints derived requiring the survival of compact objects such as white dwarfs [72] and neutron stars [73], were later on relaxed in the re-analysis performed in Refs. [74–76]. To date, there is general agreement in the literature on the absence of constraints in this interesting mass range.

Besides asteroid mass PBHs, one can also notice that in the solar-mass region, the number of probes is limited by microlensing, and X-ray limits and are not extremely stringent, varying between 10^{-2} and 10^{-1}. Finally, one should note that limits on PBH abundance cohabit with possible positive evidence [77], *e.g.* from detected microlensing events, cosmic background properties supporting the high redshift existence of PBH clusters, and obviously GW observations and the intriguing properties of black hole binary mergers, where most of these evidence point to the stellar-mass region. Taken all these considerations into account, it seems indeed difficulty plausible that all the dark matter is made of planetary-mass or intermediate mass PBHs, above $10 M_\odot$. But both the asteroid-mass region and the stellar mass region remain of very high interest, especially in the context of extended mass distributions. However, strong claims are probably premature given the large level of uncertainties for all the probes.

Chapter 3

Amplification of fluctuations for a minimally coupled inflaton

In the present Chapter, we review two of the principal mechanisms by which it is possible to obtain a sufficient amplification of the power spectrum compatible with the requirement for the production of PBH. As we have learned in the previous Chapter 2, PBH formation is the consequence of a significant enhancement in the curvature power spectrum around a scale $k_{\rm pbh}$, which can be related to the resulting PBH mass spectrum, and is much larger with respect to CMB scales $k_{\rm cmb}$.

In this thesis, we mainly focus on the case of single-field inflation without entering the most general framework of multi-field inflation. Initially, we perform an analysis as model-independent as possible, referring to specific scenarios only when necessary. We start by giving a wide range of possible realizations in order to contextualize how single-field models work for PBH production. Indeed, there are many models of inflation, in the literature, capable of enhancing the primordial spectrum of fluctuations, exploiting, for example, a phase of ultra-slow-roll (USR), the presence of bumps in the inflationary potential, sudden turns of the inflationary trajectory or the resonance during inflation (some examples are [78–81]). This approach outlines all the essential theoretical landmarks and allows us to interpret and understand the physical properties of our results. Instead of analyzing the possible consequences of different inflationary models, we consider particular evolutions of the Hubble parameter and we reconstruct the associated inflation potential accordingly. Within this "reconstruction" approach, we can calculate the features of the resulting spectra and verify if their amplitude is enhanced.

Finally, we use the results found to build complete models of inflation. The goal is to propose a viable model also from a phenomenological perspective, putting together an inflaton potential able to reproduce different phases of inflation. In particular, to have a sufficient amplification of the power spectrum, we expect that the scalar potential has a plateau shape in a non-vanishing field interval $\Delta\phi \neq 0$. As we will see in detail later, this property generates a phase of transient evolution similar to ultra-slow-roll (USR) [82] or constant-roll (CR) [83] depending on the exact profile of the potential around the plateau.

The main discussions and formulas follow the references [35, 84–87].

3.1 Enhancement of scalar perturbation during single-field inflation

The form of the scalar power spectrum in single-field scenarios is obtained by considering the second-order action of scalar perturbations during an inflationary phase. Following the analysis of the cosmological perturbations done in Section 1.4, we perturb the background homogeneous metric describing a (quasi-)de Sitter background with a nearly constant Hubble rate H. We shall work with conformal time $\eta \leq 0$ during inflation. The scalar perturbations can be described in terms of the comoving curvature perturbation $\mathcal{R}$, whose most general quadratic action (to the lowest order in derivatives) can be written as [85]:

$$S_{\mathcal{R}}^{(2)} = \frac{1}{2}\int \mathrm{d}\eta\, \mathrm{d}^3x\, \frac{2a^2(\eta)M^2(\eta)\epsilon_1(\eta)}{c_s^2(\eta)}\left[\mathcal{R}'^2 - c_s^2(\eta)(\vec{\nabla}\mathcal{R})^2\right] . \tag{3.1.1}$$

In this formula, c_s is the sound speed of propagation of curvature perturbations, M is a time-dependent mass, and we recall $\epsilon_1 = -\frac{\dot{H}}{H^2}$ is the slow-roll parameter that guarantees inflation when $\epsilon_1 < 1$. The action (3.1.1) depends on just two independent combinations of these functions of η. In particular, M^2 and ϵ_1 are indistinguishable at the level of linear perturbations; however, it is important to notice that this degeneracy is broken by the background evolution so that it is convenient to keep them separated as it will become clear later.

Let us briefly study the types of field models that lead to the action (3.1.1). If we consider only one scalar field driving inflation, say ϕ, and no other fields are supposed to be relevant during inflation, there is a single independent scalar perturbation and its linear evolution is described by the action (3.1.1). Among these models, the simplest ones are the models with $c_s^2 = 1$ and constant Planck mass $M = M_{\mathrm{P}}$, characterized only by the shape of the potential $V(\phi)$. Assuming that the dynamics eventually reaches the slow-roll attractor, unique features of the potential, such as an inflection point, will give rise to PBH formation (see *e.g.* [11]). This phase is commonly associated with an ultra-slow-roll evolution which is the consequence of a transient period of inflationary evolution in which slow-roll conditions are violated. Potentials with the features required to achieve an amplification of curvature perturbations can find explicit realizations, for example, in models of Higgs inflation [88], alpha-attractors [89], and string inflation [90].

Different models exploit a time dependence for the sound speed c_s^2 and are based on the presence of non-canonical kinetic terms for the inflaton scalar ϕ. The simplest example is that of models whose action is some function $p(X, \phi)$, where $X = -\partial_\mu\phi\partial^\mu\phi/2$, as K-inflation, see *e.g.* [85] for concrete examples. Finally, scenarios with a time-dependent effective Planck mass can be associated with the addition of non-minimal couplings of the inflaton scalar with gravity, as in the Hordeski action and its cosmological applications to G-inflation scenarios [91].

Let us note that scenarios involving a single field rely on similar methods to amplify the power of curvature fluctuations associated with the behaviour of background quantities. Our primary goal is to provide a universal explanation of these methods for amplification, considering M, c_s, and ϵ_1 as functions of time, depending on the background profile evolution during inflation.

To simplify action (3.1.1), we introduce a rescaled conformal time variable that absorbs the

time-dependent c_s and imposes an equal scaling condition on time and space coordinates:

$$\mathrm{d}\bar{\eta} = c_s \mathrm{d}\eta \quad \Longrightarrow \quad S_{\mathcal{R}}^{(2)} = \frac{1}{2}\int \mathrm{d}\bar{\eta}\, \mathrm{d}^3x\, z^2(\bar{\eta}) \left[\mathcal{R}'^2 - (\vec{\nabla}\mathcal{R})^2\right] , \tag{3.1.2}$$

with a prime indicating now a derivative with respect to $\bar{\eta}$, the rescaled conformal time. In analogy for what we have done with the scalar field perturbation $\delta\phi$ in Section 1.4.4, we have introduced the so-called time-dependent "pump field" $z(\bar{\eta})$, with the dimension of a mass and defined by

$$z^2(\bar{\eta}) \equiv \frac{2\, a^2(\bar{\eta})\, M^2(\bar{\eta})\, \epsilon_1(\bar{\eta})}{c_s^2(\bar{\eta})} . \tag{3.1.3}$$

The evolution of $\mathcal{R}$ can be studied mode by mode, in the Fourier space, and the Euler-Lagrange mode equation for $\mathcal{R}_k$ is derived from the action (3.1.2) and has the following form:

$$\frac{1}{z^2(\bar{\eta})}\left[z^2(\bar{\eta})\mathcal{R}_k'(\bar{\eta})\right]' = -k^2\mathcal{R}_k(\bar{\eta}) , \tag{3.1.4}$$

where $k \equiv \left|\vec{k}\right|$ is the modulus of the wave number that labels each given mode. We can notice that the dynamics of the comoving curvature perturbation $\mathcal{R}$ is strongly dependent on the pump field $z(\bar{\eta})$, and more generally on the behaviour of the background quantities M, ϵ_1 and c_s. We can readily see that on super-horizon scales when the right-handed side of equation (3.1.4) is negligible, there exists a solution with $\mathcal{R}_k$ constant, which corresponds to the growing adiabatic mode. It is not necessary for $\mathcal{R}_k$ to remain constant over time after its scale crosses the Hubble horizon. If the decaying mode contributes significantly to $\mathcal{R}$ at horizon crossing, then $\mathcal{R}$ will not become constant until the decaying mode dies out. What is important to note is that the decaying mode is the mode that asymptotically decays in the future, but it may not start decaying right after horizon crossing [87].

To describe scenarios where the size of small-scale curvature fluctuations ($k/aH \gg 1$) differs considerably from large-scale ones ($k/aH \ll 1$), we can implement a gradient expansion approach [35]. This approach consists of starting from the solution in the limit of small $k/(aH)$ and including momentum-dependent corrections that solve (3.1.4) order by order in a $k/(aH)$ expansion. Using this gradient expansion is particularly suitable for our purpose and allows us to comprehend better the physical origin of possible mechanisms of enhancement at small scales. The most general solution of Eq. (3.1.4), up to second-order in powers of $k/(aH)$, can be obtained in terms of the following integral equation

$$\mathcal{R}_k(\bar{\eta}) = \mathcal{R}_k^{(0)}\left[1 + \frac{\mathcal{R}_k^{(0)\prime}}{\mathcal{R}_k^{(0)}}\int_{\bar{\eta}_0}^{\bar{\eta}} \frac{\mathrm{d}\bar{\eta}_1}{\tilde{z}^2(\bar{\eta}_1)} - k^2\int_{\bar{\eta}_0}^{\bar{\eta}} \frac{\mathrm{d}\bar{\eta}_1}{\tilde{z}^2(\bar{\eta}_1)}\int_{\bar{\eta}_0}^{\bar{\eta}_1} \mathrm{d}\bar{\eta}_2\, \tilde{z}^2(\bar{\eta}_2)\frac{\mathcal{R}_k(\bar{\eta}_2)}{\mathcal{R}_k^{(0)}}\right] , \tag{3.1.5}$$

where the sub and super-script (0) denote a reference time, and the tilde over a time-dependent quantity indicates that it is normalized with respect to its value at $\bar{\eta} = \bar{\eta}_0$.

We aim to establish a connection between the curvature perturbation at a later time $\bar{\eta}$ and the same quantity computed at an earlier time $\bar{\eta}_0$. To achieve this, we define $\bar{\eta}_0$ as the time coordinate evaluated soon after horizon crossing, and $\mathcal{R}_k^{(0)}$ as the mode function computed at that time. To

enhance the spectrum of curvature fluctuations at small scales, we can consider two possibilities.

The first option is to use the structure of Eq. (3.1.5), ensuring that contributions within the square brackets become increasingly important as time progresses after horizon crossing. This generates a significant scale dependence for $\mathcal{R}_k(\bar{\eta})$ after horizon crossing, and the possibility to amplify the small-scale curvature spectrum. Alternatively, we can implement some mechanism that leads to significant scale dependence already at horizon crossing, *i.e.* for the quantity $\mathcal{R}_k^{(0)}$, which remains frozen at super-horizon scales. For convenience, we define the following hierarchies of *slow-roll functions*:

$$\epsilon_{i+1} \equiv \epsilon_i^{-1} \frac{\mathrm{d}\epsilon_i}{\mathrm{d}N}\,, \quad s_{i+1} \equiv s_i^{-1} \frac{\mathrm{d}s_i}{\mathrm{d}N} \quad \text{and} \quad \mu_{i+1} \equiv \mu_i^{-1} \frac{\mathrm{d}\mu_i}{\mathrm{d}N}\,, \tag{3.1.6}$$

with $\epsilon_0 = 1/H$, $s_0 = c_s$, and $\mu_0 = M^2$. Let us note that the time coordinate $\bar{\eta}$, is related to the number e-fold N by $\mathrm{d}N = H\mathrm{d}t = (aH/c_s)\mathrm{d}\bar{\eta}$. We observe that the *generalized slow-roll* regime, corresponding to standard attractor dynamics of inflation, holds provided that

$$|\epsilon_i|,\, |s_i|, |\mu_i| \ll 1,\ \forall i \geq 1\,, \tag{3.1.7}$$

which implies that the pump field continuously grows in time $z^2 \propto a^2 \propto (-\bar{\eta})^{-2}$ as $\bar{\eta} \to 0$. As a consequence, the last two terms inside the square brackets in Eq. (3.1.5) decay respectively as $(-\eta)^3$ and $(-\eta)^2$ in the late time limit, and in general are thus referred as "decaying" modes, that rapidly cease to play any role in the dynamics of curvature perturbations. This is the regime typical of slow-roll, where soon after horizon crossing, the curvature perturbation settles into a nearly constant configuration $\mathcal{R}_k^{(0)}$, and their spectrum is almost scale-invariant. In this case, the momentum-dependent terms in Eq. (3.1.5) cannot amplify the curvature spectrum at small scales. This is significant because it suggests that in order to produce PBHs, we need to go beyond the slow-roll conditions of Eq. (3.1.7), as first emphasized in [92].

3.1.1 Enhancement for growing modes

In this Section, we analyze the first of the two possibilities mentioned. We start by noticing the peculiar structure of the integrals within the square parenthesis of Eq. (3.1.5). Suppose that, for a brief time interval, a given mode k experiences a background evolution during which the pump field z rapidly decreases after the horizon exit epoch $\bar{\eta}_0$. Then, the would-be "decaying" mode can grow large. The integrals in the parenthesis of Eq (3.1.5) can affect greatly the nearly constant solution $\mathcal{R}_k^{(0)}$, eventually leading to a late-time value $\mathcal{R}_k(\bar{\eta}) \gg \mathcal{R}_k(0)$ on super-horizon scales. This regime is conceptually different from the slow-roll regime. In this case, the condition for the enhancement of the curvature perturbation can be explicitly expressed in terms of the derivative of the pump field; starting from a general increasing behaviour of the pump field, we expect a change in sign of its derivative, that corresponds to

$$\frac{z'}{z} = \frac{aH}{c_s}\left[1 + \frac{\epsilon_2 - s_1 + \mu_1}{2}\right] < 0\,, \implies \epsilon_2 - s_1 + \mu_1 < -2\,. \tag{3.1.8}$$

This condition implies that $\epsilon_2 - s_1 - \mu_1$ should be of order $\mathcal{O}(1)$ and negative during some period of inflation, violating the slow-roll conditions (3.1.7). In this way, the last terms of $\mathcal{R}$ expansion (3.1.5) can become non-negligible. Such terms are responsible for the enhancement of the power spectrum of curvature fluctuations for a range of scales.

In order to clarify these ideas, we can work with the equation for the curvature perturbation (3.1.4) rewritten as

$$\mathcal{R}_k'' + 2\frac{z'}{z}\mathcal{R}_k' + k^2\,\mathcal{R}_k = 0\,. \tag{3.1.9}$$

It is useful, for numerical purposes, to write this equation in terms of the number of e-folds N, and we can use it as a reference later:

$$\frac{\mathrm{d}^2\mathcal{R}_k}{\mathrm{d}N^2} + (3 - \epsilon_1 + \epsilon_2 - 2s_1 + \mu_1)\,\frac{\mathrm{d}\mathcal{R}}{\mathrm{d}N} + \frac{c_s^2 k^2}{a^2 H^2}\mathcal{R}_k = 0\,. \tag{3.1.10}$$

We can also rewrite, with respect to N the pump field derivative as

$$\frac{1}{z}\frac{\mathrm{d}z}{\mathrm{d}N} = \frac{c_s}{aH}\,\frac{z'}{z} = 1 + \frac{\epsilon_2 - s_1 + \mu_1}{2}\,. \tag{3.1.11}$$

This expression can be integrated to obtain

$$\log\frac{z}{z_0} = (N - N_0) + \frac{1}{2}\int_{N_0}^{N}\mathrm{d}N'\,(\epsilon_2 - s_1 + \mu_1)\,, \tag{3.1.12}$$

where the subscript 0 denotes the horizon crossing time $\bar{\eta}_0$. We then see that $z \propto a \propto e^N$ in the slow-roll regime or, more generally, as long as the combination $(\epsilon_2 - s_1 + \mu_1)$ remains small. In the regime with very long wavelengths with sufficiently (or sufficiently small k/a), the curvature perturbation equation (3.1.9) reduces to

$$\mathcal{R}_k'' + 2\frac{z'}{z}\mathcal{R}_k' \simeq 0\,, \tag{3.1.13}$$

which, after one integration, gives $\mathcal{R}_k' \propto z^{-2}$ and a general solution equal to

$$\mathcal{R}_k \simeq C_{1,k} + 2\,C_{2,k}\int\frac{\mathrm{d}\bar{\eta}'}{z^2(\bar{\eta}')} = C_{1,k} + C_{2,k}\int\frac{c_s^2}{a^3 M^2\epsilon_1\,H}\mathrm{d}N\,, \tag{3.1.14}$$

where $C_{1,k}$ and $C_{2,k}$ are some integration constants which must be determined from the chosen vacuum mode solutions [85]. The first term is the well-known adiabatic mode that is conserved outside the horizon, and that exists due to zero-mode residual symmetries, represented in Eq. (3.1.5) by $\mathcal{R}_k^{(0)}$. The second term, proportional to $C_{2,k}$, instead, for SR becomes the already mentioned decaying mode that typically becomes negligible within a few e-folds after horizon crossing. This is the usual behaviour in the generalized slow-roll regime, where $z \propto a$ and the decaying mode evolves like a^{-3}.

Let us show how the spectrum enhancement can be realized and consider the expression for the

variation of $\mathcal{R}_k$ with the number of e-folds N [85]:

$$\frac{\mathrm{d}\mathcal{R}_k}{\mathrm{d}N} = C_{2,k}\, e^{-3N} \frac{c_s^2}{M^2 \epsilon_1 H} = C_{2,k}\, \exp\left[- \int \mathrm{d}N\ (3 - \epsilon_1 + \epsilon_2 - 2s_1 + \mu_1) \right] , \tag{3.1.15}$$

where we have neglected the time dependence, assuming that each variable is a function of N. We observe that the second mode decays as $a^{-3} \propto e^{-3N}$ in the generalized slow-roll regime. More precisely, the derivative of the curvature perturbation is exponentially suppressed as long as the combination

$$\xi \equiv 3 - \epsilon_1 + \epsilon_2 - 2s_1 + \mu_1 > 0 \, . \tag{3.1.16}$$

If the *friction parameter* ξ is instead negative for some interval of e-folds, the derivative (3.1.15) is no longer suppressed, and the second mode can become the dominant one. Such a growing mode can enhance the power spectrum enough and finally lead to PBHs production. Interestingly, the time variation of the sound speed and the effective Planck mass contribute to ξ through s_1 and μ_1, and this freedom can either guarantee that the second mode never becomes the dominant one or, instead, turn the second mode into a growing one, thus enhancing the power spectrum.

3.1.2 Analysis when the decaying modes are negligible

In this last Section, we continue the analysis started in the previous one, in particular considering the second possible mechanism, which produces an amplification for the curvature amplitude. We note that if the friction term ξ is positive, the leading term $\mathcal{R}_k^{(0)}$ is the only one to survive along the inflationary evolution. What is interesting is that this regime allows us to analytically obtain an equation for the power spectrum and calculate an explicit relation between PBHs formation properties and the slow-roll parameters.

In order to see this, it is convenient to rewrite Eq. (3.1.4), adopting the canonical normalization for the scalar perturbation $v_k(\bar{\eta}) = z(\bar{\eta})\mathcal{R}_k(\bar{\eta})$:

$$v_k''(\bar{\eta}) + \left(k^2 - \frac{z''}{z} \right) v_k(\bar{\eta}) = 0 \, . \tag{3.1.17}$$

We assume that the pump-field z is monotonically increasing in time in order to have the decaying mode at super-horizon scales. The treatment is identical to the case of a scalar perturbation reviewed in section 1.4.4. In fact, we can identify two asymptotic regimes for each mode k: i) an early-time regime, when each mode is deep inside the horizon and ii) a late-time one, when the modes get stretched to become super-horizon. On the one hand, in the former regime, the modes satisfy $k^2 \gg z''/z$ and behave as the standard vacuum fluctuations in Minkowski space-time

$$v_k(\bar{\eta}) \simeq \frac{e^{-ik\bar{\eta}}}{\sqrt{2k}} \, . \tag{3.1.18}$$

On the other hand, long wavelength modes with $k^2 \ll z''/z$ have solutions given by

$$v_k(\bar{\eta}) \simeq C_1(k)\, z(\bar{\eta}) + C_2(k)\, z(\bar{\eta}) \int \frac{\mathrm{d}\bar{\eta}}{z^2(\bar{\eta})} \, , \tag{3.1.19}$$

that was already found in Eq. (3.1.14). From the previous discussion, we neglect the last term in Eq. (3.1.19) that rapidly decays away. Soon after horizon crossing, the canonical perturbation will stabilize around the solution $v_k = z\, C_{1,k}$. Using the field redefinition, we can identify the constant mode as the curvature perturbation at late times $C_{1,k} = \mathcal{R}_k = \mathcal{R}_k^{(0)}$. In order to determine its expression, we match the solutions around horizon crossing time $\bar{\eta} = \bar{\eta}_0$, and we obtain

$$|C_1(k)|^2 = |\mathcal{R}_k^{(0)}|^2 = \frac{1}{2k\, z^2(\bar{\eta}_0)} = \frac{1}{2k} \frac{c_s}{2M^2 a^2 \epsilon_1}\bigg|_{\bar{\eta}=\bar{\eta}_0} . \tag{3.1.20}$$

We can approximatively identify the matching time, with the condition

$$k = \frac{aH}{c_s} , \tag{3.1.21}$$

and write the late-time power spectrum as

$$\mathcal{P}_{\mathcal{R}}(k) = \frac{k^3}{2\pi^2} \left|\frac{v_k(\bar{\eta})}{z(\bar{\eta})}\right|^2 = \frac{k^3}{2\pi^2} \left|\mathcal{R}_k^{(0)}\right|^2 = \frac{k^3}{2\pi^2} |C_1(k)|^2 = \frac{H^2}{8\pi^2\, \epsilon_1\, c_s\, M^2} . \tag{3.1.22}$$

From Eq (3.1.22), we observe that in order to realize a non-negligible boost of the power spectrum, it is sufficient to have a regime in which ϵ, c_s and M^2 rapidly decrease.

3.2 Model in General Relativity

After having illustrated the principal mechanisms of amplification pertinent to the single-field inflation scenario, we will try to apply these procedures to solve viable inflation models, able to produce the seven-order of magnitude enhancement required for PBH formation. In order to simplify the analysis, we first focus on canonical single-field models, in which $c_s = 1$ and $M = M_{\rm p}$, and the hierarchies associated with them are absent, $s_i = 0$ and $\mu_i = 0$.

The properties of the dynamics of the background slow-roll parameters are then determined by the features of the field potential $V(\varphi)$. In order to find the complete form for our model potential, we reconstruct it starting from a given evolution of H. In particular, the reconstruction is relevant to model the amplification phase since SR can be easily obtained with a nearly flat region in the potential.

3.2.1 Evolution with "Constant" SR parameters

Before examining some examples of "complete" potentials directly, we shall restrict the analysis to the amplification phase. Let us start with the evolution of cosmological perturbations considered in the previous Sections. The main formula (3.1.9) governs the evolution of cosmological fluctuations. In order to extrapolate the same results obtained in Sections 3.1.1 and 3.1.2 one can introduce as

a new time the dimensionless variable [1] $\zeta = k/(aH)$, that allows us to rewrite Eq. (3.1.9):

$$\zeta^2 \frac{\mathrm{d}^2\mathcal{R}_k}{\mathrm{d}\zeta^2} + \left[\frac{\epsilon_1\epsilon_2 - 2(1-\epsilon_1)\frac{\mathrm{d}\log z}{\mathrm{d}N}}{(1-\epsilon_1)^2}\right]\zeta\frac{\mathrm{d}\mathcal{R}_k}{\mathrm{d}\zeta} + \frac{\zeta^2}{(1-\epsilon_1)^2}\mathcal{R}_k = 0\,. \tag{3.2.2}$$

In the long-wavelength limit ($\zeta \ll 1$), the last term is negligible, and assuming that the SR parameters are constant, and considering that $\frac{\mathrm{d}\log z}{\mathrm{d}N} = 1 + \epsilon_2/2$ from Eq. (3.1.11), we note the equation admits a constant solution and a solution proportional to ζ^β, where

$$\beta = \frac{3 - 4\epsilon_1 + \epsilon_2 + \epsilon_1(\epsilon_1 - 2\epsilon_2)}{(1-\epsilon_1)^2}\,. \tag{3.2.3}$$

If ζ^β decreases in time, the constant solution dominates in the $\zeta \to 0$ limit. This is what happens for de Sitter and SR. In contrast, if ζ^β increases in time, it dominates in the $\zeta \to 0$ limit. This is what occurs for USR leading to a very different spectrum from de Sitter and SR, since its amplitude increases in time. The non-constant solution of (3.2.2) is

$$\mathcal{R}_k \propto \left(\frac{k}{aH}\right)^\beta \sim e^{-\beta(1-\epsilon_1)\,N}\,, \tag{3.2.4}$$

and it increases or decreases depending on the sign of

$$\Phi \equiv \beta(1-\epsilon_1) = \frac{3 - 4\epsilon_1 + \epsilon_2 + \epsilon_1(\epsilon_1 - 2\epsilon_2)}{1-\epsilon_1}\,, \tag{3.2.5}$$

increasing if $\Phi < 0$ and decreasing if $\Phi > 0$. Only in the latter case the spectral index of the primordial spectrum can be analytically calculated using the definition (1.4.108)

$$n_s - 1 = \frac{\mathrm{d}\log\mathcal{P}_\mathcal{R}}{\mathrm{d}\log k}\,. \tag{3.2.6}$$

We have examined the conditions for Φ and $n_s - 1$ capable of producing a blue-tilted spectrum, and such conditions are exact if the SR parameters are constant trend. Still one can apply the results to other cases, such as SR inflation, in which the parameters are close to zero, and one can expand the formulae to first order for consistency. Also, the inflationary phases in which SR parameters have a constant limit for large a can be studied with the approach illustrated above. In these cases, we typically obtain parameter hierarchies in which ϵ_i approach constant values different from 0 for even or odd values of i, while the remaining parameters become null.

Indeed, assuming $\epsilon_i \overset{N\to\infty}{=} l_i + L_i(N)$ where $\lim_{N\to\infty} L_i(N) = 0$ and applying the typical recursive definition of slow-roll parameters, we have

$$\epsilon_i\epsilon_{i+1} \equiv \frac{\mathrm{d}\epsilon_i}{\mathrm{d}N} \overset{N\to\infty}{=} L_{i,N}(N)\,, \tag{3.2.7}$$

[1] For ζ we have the differential relations

$$\frac{\mathrm{d}}{\mathrm{d}\eta} = -aH(1-\epsilon_1)\zeta\frac{\mathrm{d}}{\mathrm{d}\zeta}\,, \qquad \frac{\mathrm{d}^2}{\mathrm{d}\eta^2} = (aH)^2(1-\epsilon_1)^2\left[\zeta^2\frac{\mathrm{d}^2}{\mathrm{d}\zeta^2} + \frac{\epsilon_1\epsilon_2}{(1-\epsilon_1)^2}\zeta\frac{\mathrm{d}}{\mathrm{d}\zeta}\right]\,. \tag{3.2.1}$$

which implies $\lim_{N\to\infty}\epsilon_{i+1}=0$, considering that $\lim_{N\to\infty}L_{i,N}(N)=0$, and in particular

$$\epsilon_{i+1}\overset{N\to\infty}{=}\frac{L_{i,N}(N)}{l_i+L_i(N)}\,. \tag{3.2.8}$$

Following the same procedure, we obtain the relation

$$\epsilon_{i+2}\equiv\frac{\mathrm{d}\log\epsilon_{i+1}}{\mathrm{d}N}\overset{N\to\infty}{=}\frac{L_{i,NN}(N)}{L_{i,N}(N)}+\epsilon_{i+1}\,. \tag{3.2.9}$$

We can, therefore, have different limits for our slow-roll parameters, depending on the behaviour of $L_i(N)$ and in particular of the limit $\lim_{N\to\infty}L_{i,NN}(N)/L_{i,N}(N)$. For example, if $L_i(N)\sim e^{-\gamma N}$, where $\gamma>0$ we have

$$\epsilon_{i+2}\overset{N\to\infty}{=}-\gamma+\epsilon_{i+1}\,, \tag{3.2.10}$$

and we can derive the asymptotic value for each element in the hierarchy

$$\lim_{N\to\infty}\epsilon_i=l_i\,,\quad \lim_{N\to\infty}\epsilon_{i+1+2n}=0\,,\quad \lim_{N\to\infty}\epsilon_{i+2n}=-\gamma\,. \tag{3.2.11}$$

Thus, due to their definition, an infinite sequence of slow-roll parameters can assume alternate "constant" values in the limit for N going to infinity. It is also worthwhile to observe that similar results can be achieved for other hierarchies of SR parameters, always because of the recursive definition of slow-roll parameters themselves. Indeed, the same approach can also be extended to the hierarchies of "scalar field flow functions" that are defined by $\delta_0=\varphi/\varphi_0$ and $\delta_i\,\delta_{i+1}=\mathrm{d}\delta_i/\mathrm{d}N$. In general, the ϵ_i's and the δ_i's are connected through the homogeneous Friedmann and Klein-Gordon equations and, as we will show later, can be used simultaneously to solve more general problems.

3.2.2 GR with a minimally coupled inflaton

In this Section, we will analyze a specific type of inflaton potential that describes a set of transient solutions of inflations used for amplification, with SR parameters approximatively constant for large a. We will start by briefly describing how to reconstruct the potential from the homogeneous Friedmann equations, then we will estimate the amount of amplification in the spectrum, we can achieve. Our purpose is to study the transient and then use the result to build phenomenologically valid inflationary models that possibly lead to PBHs production. We will study the two possible mechanisms for spectrum amplification discussed previously, analytically and numerically, as we will see in the following Sections.

Let us, therefore, take again the homogeneous Friedmann equations

$$H^2=\frac{1}{3\,\mathrm{M_P^2}}\left(\frac{1}{2}\dot{\varphi}^2+V(\varphi)\right)\,, \tag{3.2.12}$$

$$\dot{H}=-\frac{\dot{\varphi}^2}{2\,\mathrm{M_P^2}}\,, \tag{3.2.13}$$

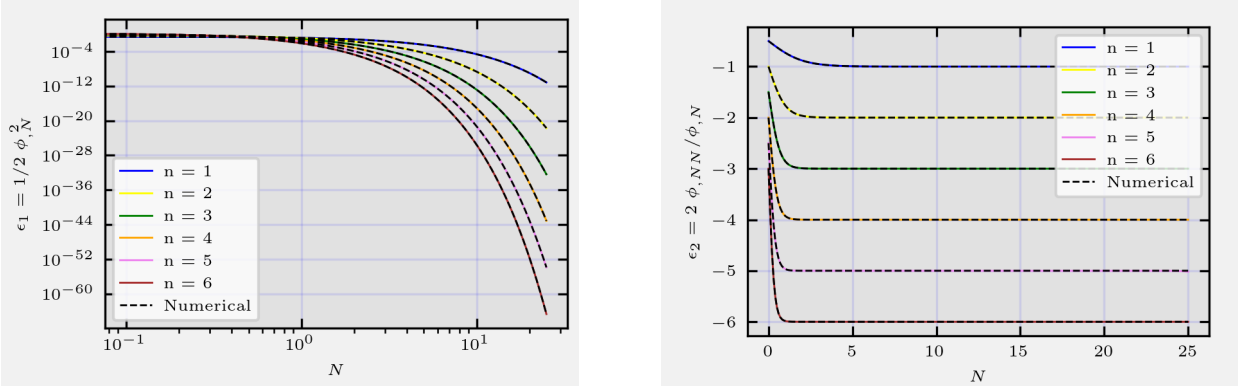

(a) (b)

Figure 3.1: First and second slow-roll parameters, Eqs (3.2.17) and (3.2.18), respectively on the left and right figures, as a function of *e-folds* N. These figures represent the analytical behaviour of the slow-roll parameters for different values of the initial parameter n, while m is kept fixed at 1/2. Nevertheless, it does not enter directly into the evaluation. We confront these results with n the numerical evaluation, considering the simple case of α, $A = 1$.

which leads to

$$\mathrm{M_p^2}\, H^2\,(3 - \epsilon_1) = V. \tag{3.2.14}$$

Given an analytical solution for the Hubble parameter $H = H(N)$, this last equation can be used to reconstruct the potential. In particular, considering that

$$\epsilon_1 = \frac{1}{2\mathrm{M}_P^2}\left(\frac{\mathrm{d}\varphi}{\mathrm{d}\log a}\right) \tag{3.2.15}$$

we can obtain a direct relation between the slow-roll parameters and the homogenous inflaton.

Let us start with the following ansatz for the Hubble parameter

$$H = H_0\left(\alpha + \frac{A}{a^n}\right)^m, \tag{3.2.16}$$

where A, α, n, $m > 0$, and we recall that the scale factor follows $a \sim e^N$. This type of solution involves a de Sitter-type attractor in the future $H \to \alpha^m H_0 = \text{const}$. Note that the transient is determined by a trend $A/a^n \sim e^{-nN}$, which is analogous to the behaviour of the SR hierarchy in Eq.(3.2.11). We can verify this analytically by observing the following:

$$\epsilon_1 = m \cdot n\,\frac{A}{\alpha a^n + A} = m\,\epsilon_3 = m\,\epsilon_5 = \cdots = \xrightarrow{a\to\infty} 0\,, \tag{3.2.17}$$

while

$$\epsilon_2 = -n\frac{\alpha a^n}{\alpha a^n + A} = \epsilon_4 = \epsilon_6 = \cdots = \xrightarrow{a\to\infty} -n\,, \tag{3.2.18}$$

where $a > [(m \cdot n - 1)\, A/\alpha]^{1/n}$ is necessary in order to satisfy the inflation condition ($\ddot{a} > 0$). We can exploit the form of the slow-roll parameters (3.2.17) to analytically solve Eq. (3.2.15):

$$\exp\left(\frac{\varphi - \varphi_0}{\mathrm{M}_P}\sqrt{\frac{n}{2m}}\right) = \frac{x+1}{x-1}\frac{x_0 - 1}{x_0 + 1}\,, \tag{3.2.19}$$

where now $x \equiv A^{-1/2}\sqrt{\alpha a^n + A}$ with x, $x_0 > 1$, and both φ_0 and x_0 are constants of integration. Considering that $x \to \infty$ for large a, we have that the field converges to the value φ_∞

$$\varphi_\infty \equiv \varphi_0 + \mathrm{M_P}\sqrt{\frac{2m}{n}}\log B_0\,, \tag{3.2.20}$$

where $B_0 = (x_0 - 1)/(x_0 + 1)$. We can now solve Eq. (3.2.19), and obtain a relation between x and φ,

$$x = \frac{\exp\left(\frac{\varphi-\varphi_0}{\mathrm{M}_P}\sqrt{\frac{n}{2m}}\right) + B_0}{\exp\left(\frac{\varphi-\varphi_0}{\mathrm{M}_P}\sqrt{\frac{n}{2m}}\right) - B_0}\,, \quad \text{and} \quad a^n = \frac{A(x^2-1)}{\alpha}\,, \tag{3.2.21}$$

which can be properly inverted to finally the form of the potential

$$V = H_0^2\left(\frac{\alpha x^2}{x^2-1}\right)^{2m}\left(3 - \frac{n\cdot m}{x^2}\right)\,, \tag{3.2.22}$$

where we have simply used Eq. (3.2.14), substituting for H and ϵ_1 with respect to $a = a(\varphi)$. We avoid explicitly presenting the total form of the potential in terms of the inflaton field, for any choice of the parameters n and m, since it is a complicated function with exponentials of φ. It is interesting to note that for $n = 6$ and $m = 1/2$, we obtain a constant potential $V = 3\alpha\, H_0^2$ and the typical prescription of USR in the ansatz (3.2.16), as we have already mentioned in the introduction. In any case, what we can note is the behaviour of the potential around $\varphi \sim \varphi_\infty$,

$$V \simeq 3H_0^2\alpha^{2m}\left[1 + \frac{n}{4}\left(1 - \frac{n}{6}\right)\left(\frac{\varphi-\varphi_\infty}{M_p}\right)^2\right]\,, \tag{3.2.23}$$

which allows us to study our results in an approximative way. We can now estimate the consequences of this background evolution on the inflationary spectrum. The value of Φ is

$$\Phi = \frac{3 - 4\epsilon_1 + \epsilon_2 + \epsilon_1(\epsilon_1 - 2\epsilon_2)}{1-\epsilon_1} \xrightarrow{a\to\infty} 3 - n\,. \tag{3.2.24}$$

The late time limit (3.2.24) allows us to distinguish models when perturbations $\mathcal{R}_k$ are amplified, after their horizon exit, namely with $n > 3$. On the other hand, for $0 < n < 3$, we clearly have decreasing cosmological perturbations $\mathcal{R}_k$ with a late-time dominance of the constant mode 3.1.2. In this case, the spectral index can be analytically calculated, following (3.2.6), as

$$n_s - 1 = n > 0\,, \tag{3.2.25}$$

which implies that the amplitude of the spectrum is blue tilted, *i.e.* increase with the wave number k. We can therefore conclude that in general relativity with an inflaton minimally coupled to the gravitational field, inflation described by the transient (3.2.16) given by a potential very similar to (3.2.22) leads to a period of amplification of the inflationary spectrum.

3.2.3 Outline of the model

In this Section, we discuss the consequences of a three-stage potential model, following a construction analogous to that presented by H. Motohashi, S. Mukohyama and M. Oliosi [93]. The potential considered drives an initial slow-roll period (SR1), which satisfies observational constraints obtained by the Planck Collaboration [24], an intermediate stage (GR) determined by the potential in Eq. (3.2.22) or with asymptotic behaviour given by Eq. (3.2.23) and leading to amplification, and finally, a final slow-roll stage that leads to the end of inflation. We do not consider the eventual reheating phase at the end of the entire inflationary era, which can, however, be implemented.

The first phase of SR will be described by a Starobinsky potential based on one of the inflationary models most compatible with observations [94]. The Starboinsky model reproduces a quasi-de Sitter phase obtained as a self-consistent solution of the vacuum Einstein's equations modified by the one-loop corrections of quantized matter fields. The potential can be derived from the Starobinsky action

$$S_S = \frac{1}{2}\int \mathrm{d}x^4\sqrt{-g}\left(M_p^2 R + \frac{R^2}{6m^2}\right) \tag{3.2.26}$$

after an appropriate conformal transformation which allows to derive the following Straobinsky potential

$$V_{\mathrm{S}}(\varphi,\varphi_s) = m^2\, M_{\mathrm{P}}^2\left(1-\exp\left(-\sqrt{\frac{2}{3}}\,\frac{\varphi-\varphi_s}{M_{\mathrm{P}}}\right)\right)^2 . \tag{3.2.27}$$

With respect to the usual formulation, we have introduced, for model-building purposes, a field shifting parameter φ_s. That allows us to fix with a certain freedom the exact point of transition between the three stages. We have already studied the expected amplification and analytic behaviour of the intermediate stage potential (3.2.22) in the previous Section. The third phase of inflation is similar to the first one, and we describe it through a Starobinsky-like potential.

We consider that our complete potential, comprising all the specific details of each inflationary stage, is composed as follows:

$$\begin{aligned} V(\varphi) = {} & V_{\mathrm{GR}}(\varphi)\,\Theta_{d_1}(\varphi_1-\varphi)\,\Theta_{d_2}(\varphi-\varphi_2) \\ & + V_{\mathrm{SR1}}(\varphi,\varphi_{s1})\,\Theta_{d_1}(\varphi-\varphi_1) \\ & + V_{\mathrm{SR2}}(\varphi,\varphi_{s2})\,\Theta_{d_2}(\varphi_2-\varphi)\,, \end{aligned} \tag{3.2.28}$$

where, in order to obtain as smooth as possible transitions, we use a "step" function of the form:

$$\Theta_d(x) = \frac{1}{2}\left[1+\tanh\left(x/d\right)\right] . \tag{3.2.29}$$

The variation of parameter d allows us to tune the amplitude around which the transition takes place, and satisfy certain conditions on the time duration of the transitions and duration of each

stage. Thus, following all the prescriptions the overall potential takes the following form

$$
\begin{aligned}
V(\varphi) = 3H_0^2 M_{\rm p}^2 \left[1 + \frac{n}{4}\left(1 - \frac{n}{6}\right)\left(\frac{\varphi - \varphi_\infty}{M_p}\right)^2\right] \Theta_{d_1}(\varphi_1 - \varphi)\, \Theta_{d_2}(\varphi - \varphi_2) \\
+ m_1^2 M_{\rm P}^2 \left(1 - \exp\left(-\sqrt{\frac{2}{3}}\frac{\varphi - \varphi_{s1}}{M_{\rm P}}\right)\right)^2 \Theta_{d_1}(\varphi - \varphi_1) \\
+ m_2^2 M_{\rm P}^2 \left(1 - \exp\left(-\sqrt{\frac{2}{3}}\frac{\varphi - \varphi_{s2}}{M_{\rm P}}\right)\right)^2 \Theta_{d_1}(\varphi_2 - \varphi)\,.
\end{aligned}
\tag{3.2.30}
$$

The field values φ_1 and φ_2 represent the values around which the transitions occur In particular, we considered $\varphi_1 > \varphi_2$. All the parameters are set in order to have a continuum and smooth potential in all the field ranges of evolution: due to the fact that we consider two phases of Starobinsky inflation, we need two different sets of parameters and thus m_1, φ_{s1} determine the stage SR1, and m_2, φ_{s2} for the second slow-roll phase. The intermediate phase is indicated with the sub-script GR. The value of the parameters φ_{s1} and φ_{s2} crucially determine the evolution during the slow-roll phases. Let us note that the transition between the three stages is not instantaneous but occurs around a specific scalar field value φ. The initial value of the background field is set to $\varphi(N = 0) = 1$, in Planck units, where $N = 0$ corresponds to the horizon exit of the pivot mode $k_0 = 0.0002\,\mathrm{Mpc}^{-1}$, such that $k_0 = a_0 H_0$, where a_0 and H_0 are the initial values of the scale factor and Hubble function. The first SR stage needs to reproduce the CMB spectrum observed by the Planck experiment [24]. In particular, we have set the first transition φ_1 to occur after at least $N \sim 5$ e-folds after the CMB scales exit of the horizon [93]. The value of the field at the second transition, φ_2, instead is less constrained, in the sense that the only requirement needed to be satisfied is the form of the power spectrum, which is not affected by this phase. Finally, we must impose the continuity relation between the three stages

$$
V_{GR}(\varphi_1) = V_{SR1}(\varphi_1) \implies m_1^2 = H_0^2 \frac{1 + \frac{n}{4}\left(1 - \frac{n}{6}\right)\left(\frac{\varphi_1 - \varphi_\infty}{M_p}\right)^2}{\left(1 - \exp\left(-\sqrt{\frac{2}{3}}\frac{\varphi_1 - \varphi_{s1}}{M_{\rm P}}\right)\right)^2}\,, \tag{3.2.31}
$$

$$
V_{GR}(\varphi_2) = V_{SR2}(\varphi_2) \implies m_2^2 = H_0^2 \frac{1 + \frac{n}{4}\left(1 - \frac{n}{6}\right)\left(\frac{\varphi_2 - \varphi_\infty}{M_p}\right)^2}{\left(1 - \exp\left(-\sqrt{\frac{2}{3}}\frac{\varphi_2 - \varphi_{s2}}{M_{\rm P}}\right)\right)^2}\,. \tag{3.2.32}
$$

Let us briefly comment on the solution of the homogeneous Fridmann and Klein-Gordon equations for the background variables φ and H, which allows us to determine the Hubble slow-roll hierarchy ϵ_i. The background evolution for the scalar field driving inflation is determined by the system of equations:

$$
H^2 = \frac{V/M_{\rm p}^2}{3 - \frac{1}{2M_{\rm p}^2}\varphi_{,N}^2}\,, \tag{3.2.33}
$$

$$
\varphi_{,NN} + \left(\frac{1}{2}\varphi_{,N}^2 - 3\right)\left(\varphi_{,N} + \frac{V_{,\varphi}}{V}\right) = 0\,. \tag{3.2.34}
$$

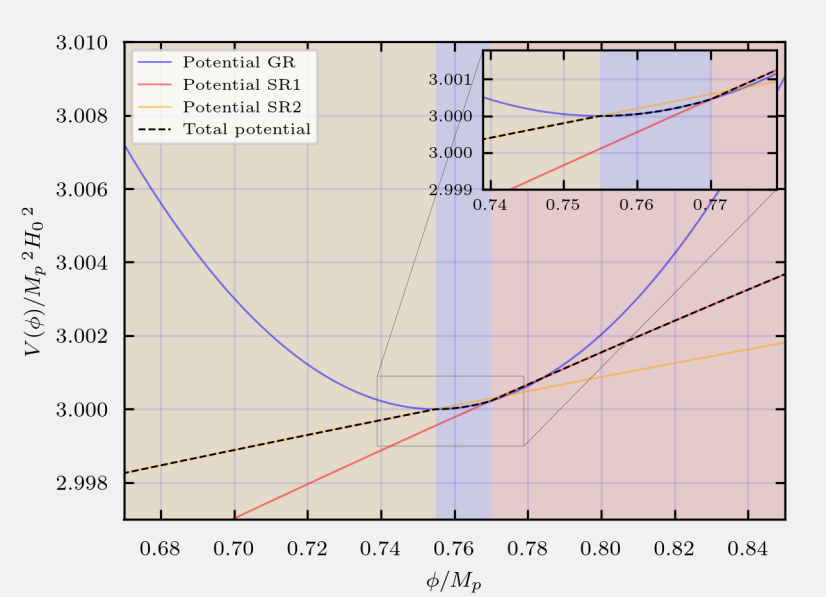

Figure 3.2: Total potential presented in Eq. (3.2.30), where we considered as a working example the parameters in Tab. 3.1, with $n = 2$ and $m = 1/2$. We have highlighted the three regimes with different colours: red (SR1), blue (GR) and orange (SR2). In particular, we have chosen to represent only a small interval around the field value $\varphi \sim \varphi_\infty$, the actual point in the field evolution determining the amplification.

In this scenario the pump field z is $z = a\sqrt{2\epsilon_1}\, M_{\rm p}$. The condition required to realize the desired growth in the spectrum depends upon the evolution in time of ϵ_1, and in particular, its behaviour during the transient regime (GR). In particular, as we notice in Fig. 3.2, at the end of the intermediate phase, we have a local extremum at φ_∞, a common feature for constant-roll-like models. As the scalar field, during its evolution, passes through such a flat region with negligible potential gradient, the acceleration term $\ddot{\varphi}$ is balanced by the Hubble friction term in the Klein-Gordon equation (1.2.27), and the inflation speed is no longer controlled by the scalar potential. This significantly affects the values of the inflaton velocity during the transient non-attractor phase and inevitably leads to the violation of the slow-roll conditions:

$$\epsilon_2 \equiv \frac{\epsilon_{1,N}}{\epsilon_1} = \frac{2\varphi_{,NN}}{\varphi_{,N}} = -2\left(3 - \epsilon_1 + \frac{V_{,\varphi}}{H^2\,\varphi_{,N}}\right), \tag{3.2.35}$$

hence $\epsilon_2 > -6$ for transient CR phase ($V_{,\varphi} < 0$). We emphasize that since the non-slow-roll inflationary era is characterized by a large negative ϵ_2 for a brief interval of e-folds, the pump field, as well as the first slow-roll parameter ϵ_1, quickly decay during this stage. Indeed

$$\epsilon_2 \equiv \frac{{\rm d}\log\epsilon_1}{{\rm d}N} \implies z^2 \propto \epsilon_1 \propto e^{-|\epsilon_2|\Delta N}, \tag{3.2.36}$$

where we assumed ϵ_2 is constant during the non-attractor phase.

Stability analysis for the transient evolution

We have verified the importance of the slow-roll parameter ϵ_2 in determining the behaviour of the pump field z and thus affecting the time evolution of $\mathcal{R}$. We have already studied in detail how the

power spectrum behaves in the case of the non-attractor stage described by potential (3.2.23), and, in particular, we have found an analytical solution for the background field in such regime (3.2.19). For practical use in our description, it is useful to rewrite such relation as $\varphi = \varphi(N)$, then

$$\varphi_{\rm GR}(N) = \varphi_0 + 2M_{\rm P}\sqrt{\frac{2m}{n}}\left[\text{arcCoth}\left(\sqrt{1+e^{nN-\tilde{A}}}\right) - \text{arcCoth}\left(\sqrt{1+e^{nN_0-\tilde{A}}}\right)\right], \tag{3.2.37}$$

where we stress again that the sub-script GR identify the amplification phase. The parameters φ_0 and N_0 are the initial field value and time. We made an arbitrary choice for the parameters α and A in Eq. (3.2.19), in order to simplify the form of the relation. In particular, we have redefined the parameter $A = a_0^n\, e^{\tilde{A}}$ and considered $\alpha = 1$. The factor α appears only as a normalization term of the Hubble parameter and of the potential, and without any loss of generality, can be reabsorbed with other normalization constants.

Let us note that depending on n the solution (3.2.37) may be unstable. A superficial analysis of our equations would suggest that we can control the final evolution of fluctuations by simply manipulating the potential parameter n, as we have seen in Eqs.(3.2.24, 3.2.25). However, from a stability point of view, we have assumed that our analytical solutions are the attractors of the evolution during the transient stage (GR). This is not true as can be shown by analyzing how the slow-roll parameter ϵ_2 behaves in the large a limit.

We can conveniently approximate our equations in the large a limit and starting from the definition of the slow-roll parameter ϵ_2 derived in Eq. (3.2.35) after some algebra one obtains the second-order differential equation:

$$\frac{\epsilon_{1,NN}}{\epsilon_1} - \left(\frac{\epsilon_{1,N}}{\epsilon_1}\right)^2 = 2\epsilon_{1,N} - 2\left[\frac{V_{,\varphi\varphi}}{H^2} + \left(2\epsilon_1 - \frac{\epsilon_{1,N}}{\epsilon_1} - 6\right)\left(\epsilon_1 - \frac{1}{4}\frac{\epsilon_{1,N}}{\epsilon_1}\right)\right]. \tag{3.2.38}$$

This equation is exact and allows us to study the evolution of the slow-roll parameters in a general form. However, we will use it in the large a limit in order to understand what is the attractor behaviour when our field approaches φ_∞. In such a limit, we can rewrite Eq. (3.2.15) introducing some approximations. In particular, we can express the term $V_{,\varphi\varphi}/H^2$ in terms of the potential parameter n and m, in order to have a clear understanding of how the shape of the potential is related to stability. By considering Eq. (3.2.14) and collecting the potential term we have

$$(3-\epsilon_1) = \frac{V}{M_{\rm P}^2\, H^2} \xrightarrow{\epsilon_1 \to 0} H^2 = \frac{V}{3\, M_{\rm P}^2}, \tag{3.2.39}$$

where, following the expected behaviour in (3.2.17), we used the fact that $\epsilon_1 \to 0$, close to φ_∞. Now, we can approximate the potential around the point φ_∞, and if we consider the approximated behaviour (3.2.23) we have that

$$\frac{V_{,\varphi\varphi}}{V} \simeq \frac{2n(n-6)}{M_{\rm P}^2\,\left[n(n-6)(\varphi-\varphi_\infty)^2 - 24\right]} \xrightarrow{\varphi \to \varphi_\infty} \frac{n(6-n)}{12\, M_{\rm P}^2}, \tag{3.2.40}$$

and

$$\frac{V_{,\varphi\varphi}}{H^2} \approx \frac{n(6-n)}{4}. \tag{3.2.41}$$

The equation (3.2.38) can then be simplified to

$$\frac{\epsilon_{1,NN}}{\epsilon_1} - \frac{1}{2}\left(\frac{\epsilon_{1,N}}{\epsilon_1}\right)^2 \simeq 5\epsilon_{1,N} + 12\epsilon_1 - 4\epsilon_1^2 - 3\,\frac{\epsilon_{1,N}}{\epsilon_1} - \frac{n(6-n)}{2}\,. \tag{3.2.42}$$

This last equation cannot be solved exactly and needs further approximations. Since $\epsilon_{1,NN}$, $\epsilon_{1,N} \sim O(\epsilon_1)$ and assuming that ϵ_2 is nearly constant (3.2.18) in the large a limit, we have that $\epsilon_{1,N} = \epsilon_1\,\epsilon_2$ and $\epsilon_{1,NN} = \epsilon_{1,N}\,\epsilon_2 + \epsilon_2\,(\epsilon_1\,\epsilon_3)$ by definition, then we observe that the leading term is of order ϵ_1. Keeping only the leading terms leads to

$$\frac{\epsilon_{1,NN}}{\epsilon_1} - \frac{1}{2}\left(\frac{\epsilon_{1,N}}{\epsilon_1}\right)^2 + 3\,\frac{\epsilon_{1,N}}{\epsilon_1} + \frac{n(6-n)}{2} = 0\,. \tag{3.2.43}$$

This differential equation is the following first order equation for $\epsilon_2 \equiv \frac{\epsilon_{1,N}}{\epsilon_1}$,

$$\epsilon_{2,N} + 3\epsilon_2 + \frac{1}{2}(\epsilon_2)^2 + \frac{n(6-n)}{2} = 0\,. \tag{3.2.44}$$

It is a non-linear differential equation of the first order, called the "generalized Riccati equation". We can solve this equation through a function redefinition that allows us to transform the non-linear structure into a second-order linear differential equation. Indeed, we may substitute the function ϵ_2 with

$$\epsilon_2 = 2\,\frac{\chi_{,N}}{\chi}\,, \tag{3.2.45}$$

where χ is an arbitrary continuous and differentiable function in N. After having simplified all the terms, we obtain from Eq. (3.2.44)

$$\chi_{,NN} + 3\chi_{,N} + \frac{n(6-n)}{4}\,\chi = 0\,, \tag{3.2.46}$$

which admits the simple general solution

$$\chi(N) = C_1 e^{-\frac{n}{2}N} + C_2 e^{\frac{n-6}{2}N}\,, \tag{3.2.47}$$

where C_1 and C_2 are arbitrary integration constants different from zero. We have obtained the general solution for the equation (3.2.44),

$$\epsilon_2(N) = \frac{(n-6)e^{(n-3)N} - K\,n}{K + e^{(n-3)N}}\,, \tag{3.2.48}$$

where we introduced the integration constant $K = C_1/C_2$. This result deserves some comment because it allows us to understand the stability of the solutions (3.2.37) in relation to the behaviour of the slow-roll parameter ϵ_2 in the large a regime. At this point, we can easily calculate the limit for $N \to \infty$ for our ϵ_2 (3.2.48), leading to

$$\epsilon_2 \xrightarrow{N\to\infty} \begin{cases} -n\,, & \text{if } n < 3\,, \\ n-6\,, & \text{if } n > 3\,, \end{cases} \tag{3.2.49}$$

i.e. for $n < 3$ the solution is stable while for $n > 3$ the solution is unstable. Considering what

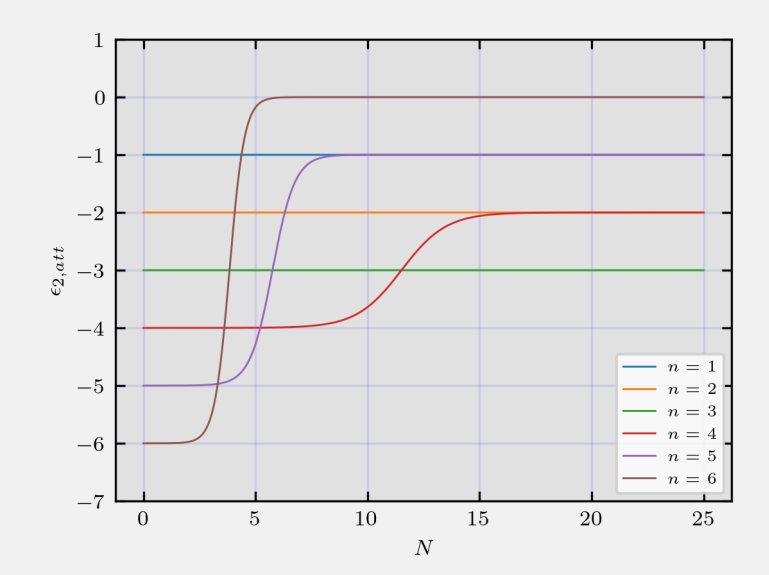

Figure 3.3: Analytical solutions for ϵ_2 derived by the Riccati equation (3.2.44), taken for different values of the parameter n. We have chosen $K = 10^5$ to highlight the transient behaviour for solutions with $n > 3$.

we studied in Section 3.2.2, we know that for $n < 3$, we have a blue-tilted spectrum but not growing solutions of the perturbations. In this case, the analytical solution is an attractor and $\epsilon_2 \to -n$ is respected. However, in the case $n > 3$, we note that the attractor value for ϵ_2 is now $\epsilon_2 \simeq n - 6 > -3$. In this regime, we can nevertheless obtain a sufficient amplification of the spectrum, but the condition required for the existence of the growing mode of the perturbations is not stable.

This result shows that the evolution of slow-roll parameter ϵ_2 has a transient, more or less steep towards the attractor $n - 6$. Moreover, as can be seen in Fig. 3.3, the transition time between one solution and the other, in the case of $n > 3$, is determined by the value of integration constant K: if K is sufficiently large, the departure from the solution $\epsilon_2 = -n$ occurs later. Indeed, considering a fixed value K and for increasing values of n, the transition to the associated attractor $n - 6$ is much faster and occurs much earlier due to the exponential behaviour of our solution. In situations where the value of n is high, we will show that there will be specific transition phases that lead to the amplification of perturbations and an increase in the spectrum. At the time N_1, at which the transition takes place, i.e. $\varphi(N_1) = \varphi_1$, we need to constrain our numerical solution φ to be as near as possible to the analytical solution (3.2.37) in the intermediate phase. In order to do so, we can adjust our free parameters, once fixed n and m. We have the following conditions

$$\begin{cases} \varphi_{\rm GR}(N_1) = \varphi_1 \,, & \Longrightarrow \quad \varphi_0 = \varphi_1 \,, \; N_0 = N_1 \,, \\ \varphi_{{\rm GR},N}(N_1) = -\sqrt{\frac{2mn}{1+e^{nN-\tilde{A}}}} \simeq \varphi_{{\rm SR1},N}(N_1) & \Longrightarrow \quad \tilde{A} = nN_1 - \log\left[\frac{2nm}{\varphi_{{\rm SR1},N}(N_1)^2} - 1\right] \,, \end{cases} \tag{3.2.50}$$

where the former gives us an estimate of the value φ_∞ towards which the field converges and where

n	φ_1	φ_∞	φ_2	d_1	d_2
1	$\frac{8}{10}$	0.77058	$\varphi_\infty + 2\times10^{-6}$	10^{-3}	2×10^{-6}
2	$\frac{77}{100}$	0.75495	$\varphi_\infty + 2\times10^{-6}$	10^{-3}	2×10^{-6}
3	$\frac{74}{100}$	0.72973	$\varphi_\infty + 15\times10^{-7}$	10^{-3}	15×10^{-7}
4	$\frac{715}{1000}$	0.70714	$\varphi_\infty + 2\times10^{-6}$	10^{-3}	10^{-6}
5	$\frac{705}{1000}$	0.69867	$\varphi_\infty + 10^{-6}$	10^{-3}	10^{-6}
6	$\frac{7}{10}$	0.69470	$\varphi_\infty + 2\times10^{-7}$	10^{-3}	2×10^{-7}

Table 3.1: Parameters considered for our working model. For numerical purposes, we also present the numerical estimate for φ_∞ in each configuration obtained through the evaluation of Eq. (3.2.56).

we have the maximum amplification. In particular, we have

$$\varphi_\infty = \varphi_1 - 2\sqrt{\frac{2m}{n}}\,\mathrm{arcCoth}\left(\sqrt{1+e^{nN_1-\tilde{A}}}\right) = \varphi_1 - 2\sqrt{\frac{2m}{n}}\,\mathrm{arcCoth}\sqrt{\frac{2n\,m}{\varphi_{\mathrm{SR1},N}(N_1)^2}}\,. \tag{3.2.51}$$

We must note that the expected value of φ_∞ is directly determined by the value of the derivative $\varphi_{SR1,N}(N1)$. We can then estimate this value numerically through a preliminary simulation of the field's evolution in the first slow-roll stage (SR1). In contrast, as we shall see later, it is also possible to determine the analytical approximate solution for the (SR1) phase and then obtain an analytical estimate for φ_∞ directly linked to the initial condition of the problem. In what follows, we analyze the complete model for different values of the parameters n, studying the amplification of the spectrum in the different cases and comparing the numerical results with our estimates.

3.2.4 Numerical Results

In this Section, we will discuss the numerical simulations and their outcome using the parameters listed in Table 3.1. We consider different choices of n to study a wide range of possible evolutions including decaying and enhanced perturbation solutions of the Mukhanov-Sasaki equations (3.1.17). The value of m is, in general, arbitrary and mainly serves as a normalization factor, and it is not particularly relevant in our analysis, as previously mentioned. We set the initial conditions and adjust the transition periods properly to ensure that the scalar and tensor spectral power produced during the first phase of SR is within observational limits. Ideally, the transition between the first slow-roll phase and the intermediate regime must be smooth and the transition should occur at the proper value φ_1. To determine the details of the second transition, we must also consider the desired distribution function of PBH. The second transition should stop the amplification of the power spectrum after having reached the threshold amplitude for sufficient PBH production. When the model is used to produce PBHs as DM candidates, this guarantees that the PBH mass distribution is peaked enough to satisfy the window allowed by current observational constraints. Thus, we can choose for each instance of the parameter n, different values for the parameters φ_2 and d_2 in order that the second transition occurs after a sufficient number of e-folds, in order to produce the chosen abundance of PBH.

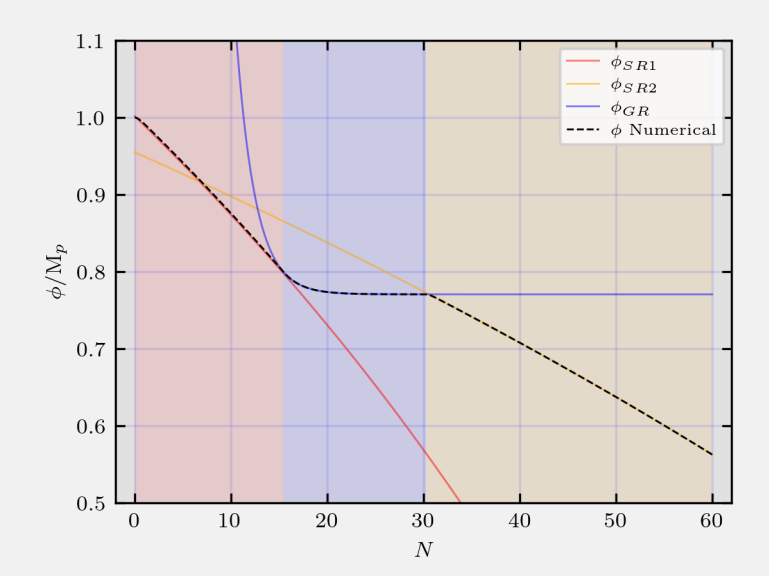

Figure 3.4: Time evolution of the background scalar field in the case $n = 1$. We have highlighted each evolution stage, comparing it with the analytical or approximate estimate.

In this work, we considered six different models with m fixed to $1/2$, while n has an integer value between 1 and 6. The main parameters we considered for our simulations are listed in Tab. 3.1, while for each simulation we kept the values of

$$\varphi_0 = 0.5\,, \quad \varphi_{s1} = -5\,, \quad \varphi_{s2} = -6\,, \tag{3.2.52}$$

where we recall that φ_0 is the initial value of the field evolution and φ_{s1}, φ_{s2} are the translation parameters φ_s in the Starboinsky potential (3.2.27) in Planck units. In Fig. 3.4 we plot the full evolution of the background field φ, where we have also plotted the solutions for each potential phase. In particular, we already discussed the analytical procedure to obtain the solutions from the ansatz (3.2.16). Although there is no complete analytical solution, we can also obtain an approximated solution for the background in the slow-roll regime. We can use Eqs. (1.2.31, 1.2.32), which combined and rewritten using the time variable N become

$$\varphi_{,N} \simeq -M_{\rm P}^2 \frac{V_{,\varphi}}{V} = -\frac{2\sqrt{\frac{2}{3}}\exp\left(-\sqrt{\frac{2}{3}}\frac{\varphi-\varphi_s}{M_{\rm P}}\right)}{1-\exp\left(-\sqrt{\frac{2}{3}}\frac{\varphi-\varphi_s}{M_{\rm P}}\right)} \simeq -2\sqrt{\frac{2}{3}}\exp\left(-\sqrt{\frac{2}{3}}\frac{\varphi-\varphi_s}{M_{\rm P}}\right)\,, \tag{3.2.53}$$

Indeed, considering $\varphi_s \sim 5\,M_{\rm P}$, we have that the denominator can be approximated to 1, and the differential equation has an analytical solution. We can integrate by separating the variables and obtain the solution for the slow-roll regimes

$$\varphi_{SR}(N) = \varphi_s + \sqrt{\frac{3}{2}}\log\left[K_0 - \frac{8}{3}N\right]\,, \tag{3.2.54}$$

where K_0 is an integration constant. This value can be obtained from the initial conditions for the problem, or by comparison with the numerical solution in the first and third stages of the

evolution. In what follows, we used the first most simple approach. We compare this solution with the numerical solution of the complete Klein-Gordon problem. The actual usefulness of this procedure, however, comes from the fact that we can analytically estimate the value of $\varphi_{,N}(N_1)$ to insert in Eqs (3.2.50) and (3.2.51) in order to estimate the right set of parameters for the intermediate phase (GR). In particular, the complete results are

$$\tilde{A} = nN_1 - \log\left[\frac{nm}{2}\left(2\sqrt{\frac{2}{3}}N_1 - K_0\right)^2 - 1\right], \tag{3.2.55}$$

$$\varphi_\infty = \varphi_1 - 2\sqrt{\frac{2m}{n}}\,\mathrm{arcCoth}\left[\sqrt{\frac{mn}{2}}\left|2\sqrt{\frac{2}{3}}N_1 - K_0\right|\right]. \tag{3.2.56}$$

In Fig. 3.5, we present the evolution of the slow-roll parameter ϵ_2, considering each different evolution for n. As we shall see, the transient period is well represented by the analytical solution estimate $\epsilon_2 = -n$. Indeed, through the analytical estimate (3.2.56), we could find sufficiently stable background field solutions during the transient phase. We can also note a peculiar feature related to the duration of the intermediate phase (GR); as n increases and considering very similar parameters (Tab. 3.1), the transient phase decreases in duration. This can be seen directly from determining the value φ_∞. Indeed, from Eq. (3.2.20), we note that for increasing values of n, the function $\frac{\mathrm{arcCoth}(n)}{\sqrt{n}}$ is decreasing, bringing the value φ_∞ closer to the transition point φ_1.

From the solutions for the homogeneous variables, we are able to solve the Mukhanov-Sasaki equation (3.1.17) with Bunch-Davies initial conditions and thus derive the power spectrum for the curvature perturbation $\mathcal{R}_k$ (the numerical prescription is described in the App. A). We group our results in four different plots, represented in Fig. 3.6 (a), (b), (c) and (d), to highlight their differences. In particular, we decided to compare in couples the spectrums obtained for $n = \{1, 5\}$ and $n = \{2, 4\}$. Indeed, because of the analysis carried out in Section 3.2.3, we expect a similar behaviour of the slow-roll parameter ϵ_2, and we wanted to compare the different shape of the spectrum for constant and "increasing" solutions of $\mathcal{R}_k$. We separated instead the cases $n = \{3, 6\}$ for which we do not have a similar behaviour but are nevertheless interesting and $n = 6$ is ultra-slow-roll. The modes that exit the event horizon during the first phase of SR, should respect the CMB Planck measurement constraints.

We can notice that for all the cases, the power spectrum grows in amplitude towards small scales, exhibiting a peak for $k_{\mathrm{peak}} \gg k_{\mathrm{cmb}}$, where its value depends on the duration of the intermediate phase (GR). We observe that for both the cases $n = \{1, 2\}$, the amplification of the spectrum satisfies the analytical expectation $n_s - 1 = n$. In the remaining cases, the spectrum presents a peculiar feature: at the beginning of the amplification we observe a steady initial growth proportional to k^4, and there is a pronounced dip, occurring at scales that exit the horizon a few e-folds before the time of the first transition. Close to the peak instead the slope is less steep and is determined by the attractor value of the slow-roll parameter ϵ_2 (3.2.49), with a power law seemingly compatible with k^{6-n}. Let us mention [79] that the dip is physically due to a disruptive interference between the "constant" mode of curvature fluctuation at super-horizon scales and the "decaying" mode that is becoming active and ready to contribute to the enhancement of the spectrum. The position and

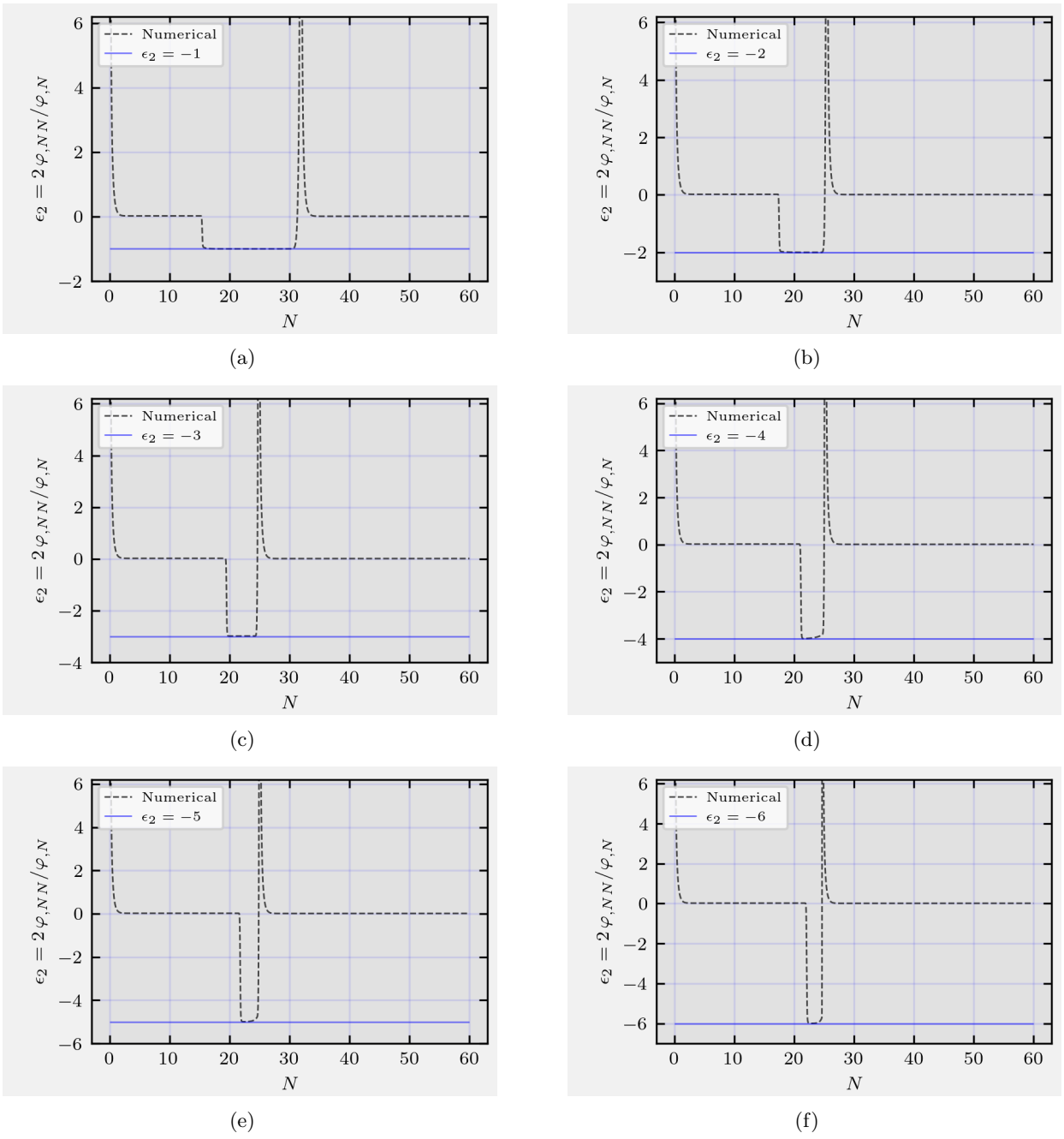

Figure 3.5: Time evolutions for the slow-roll parameters ϵ_2 for each configuration of the parameter n. We show the numerical solution in a dashed black line and, in coloured lines, the expected constant value during the transient phase GR. We can notice that for different values of n, we have a smaller duration of the intermediate stage.

depth of the dip are calculable in terms of other features of the spectrum, at least in the limit of a short duration of the amplification epoch. It is found that the position of the dip in momentum space is proportional to the inverse fourth root of the enhancement of the spectrum, and the depth of the dip is proportional to the inverse square root of the enhancement of the spectrum.

We observe that oscillations of the spectrum are present, particularly in the second half of the spectrum, relative to small scales after the peak. These oscillations can be understood, considering

n	ΔN	$M_{\rm pbh}^{(\Delta N)}/M_\odot$	$k_{\rm pbh}/{\rm Mpc}^{-1}$	$M_{\rm pbh}/M_\odot$	f_{pbh}
1	29.1	6.44×10^{-11}	2.18×10^{11}	6.45×10^{-11}	1.63×10^{-2}
2	26.1	1.46×10^{-5}	4.58×10^{8}	1.46×10^{-5}	1.11×10^{-1}
3	25.5	5.09×10^{-5}	2.45×10^{8}	5.10×10^{-4}	1.96×10^{-2}
4	25.9	2.52×10^{-5}	3.49×10^{8}	2.53×10^{-5}	2.24×10^{-2}
5	25.6	4.03×10^{-5}	2.76×10^{8}	4.04×10^{-5}	1.36×10^{-2}
6	23.2	5.51×10^{-3}	2.36×10^{7}	5.52×10^{-3}	3.83×10^{-2}

Table 3.2: Estimate of the mass of the PBH, both using the time duration ΔN between the exit of PBH-forming modes and the exit of CMB modes, through Eq. (2.2.5) and identifying the peak mode k_{pbh} of the spectrum Eq. (2.2.4). The abundance f_{pbh} is evaluated through the approximated result for the collapse fraction (2.2.9), with $\delta_c = 0.4$.

that the transitions between the slow-roll and amplification phases are characterized by a rapid variation of the slow-roll parameter ϵ_1. This rapid variation generates a large variation of the mass term $\frac{z''}{z}$, in the Mukhanov-Sasaki equation, leading to oscillations in the evolution of the absolute value for the complex mode of curvature crossing the horizon during the transition. This generates a spiral elongation of the mode in the complex plane of $\mathcal{R}$, which appears as an oscillation in the power spectrum.

Finally, we present in Tab. 3.2, the estimated result for the mass and abundance of PBH, derived from the simulations for each choice of n. We have estimated the mass of the PBH both using Eqs. (2.2.4) and (2.2.5). In the first case, we assumed that each parameter at its proxy value, determining the position of the peak of the spectrum $k_{\rm pbh}$. In the latter, we have considered a quasi-de Sitter evolution, with $\epsilon_1 \sim 0$, evaluating $N_{\rm pbh}$ as the time of horizon exit of the peak mode $k_{\rm pbh}$. We can note that both cases give the same approximative value of $M_{\rm pbh}$. We have considered an interesting set of masses $M_{\rm pbh} \in \left[10^{-11}, 10^{-3}\right] M_\odot$, compatible with the constraints presented in Fig. 2.2. The value of $f_{\rm pbh}$ was determined inverting (2.2.8), and estimating the collapse fraction with (2.2.10), considering $\delta_c = 0.4$, and $\sigma^2 \sim \mathcal{P}_\mathcal{R}(k_{\rm pbh})/5$.

3.3 Constraints on the power spectrum with PTA

The direct detection of gravitational waves (GWs), with the first LIGO detection of a merger of two black holes, opened a new era of the exploration of the early universe. Stochastic gravitational wave background (SGWB) is originated from a superposition of many unresolved GW sources, of both astrophysical and cosmological nature, which can be detected by searching for correlated signals between multiple detectors. Recently, four pulsar timing array (PTA) collaborations, namely NANOGrav [15, 16], PPTA [17, 18], EPTA [19, 20], and CPTA [21], all announced the strong evidence of a SGWB in the nanohertz frequency band [1, 100] nHz. However, the origin of this signal, whether from supermassive black hole binaries or other cosmological sources, is still under investigation (see [95] for References). A promising explanation of such a signal could be given by scalar-induced gravitational waves (SIGWs) accompanying the formation of primordial black holes, which is the main target of this thesis. Other physical phenomena can source the PTA frequency band, such as cosmological phase transitions or cosmic topological defects (see for examples [96]

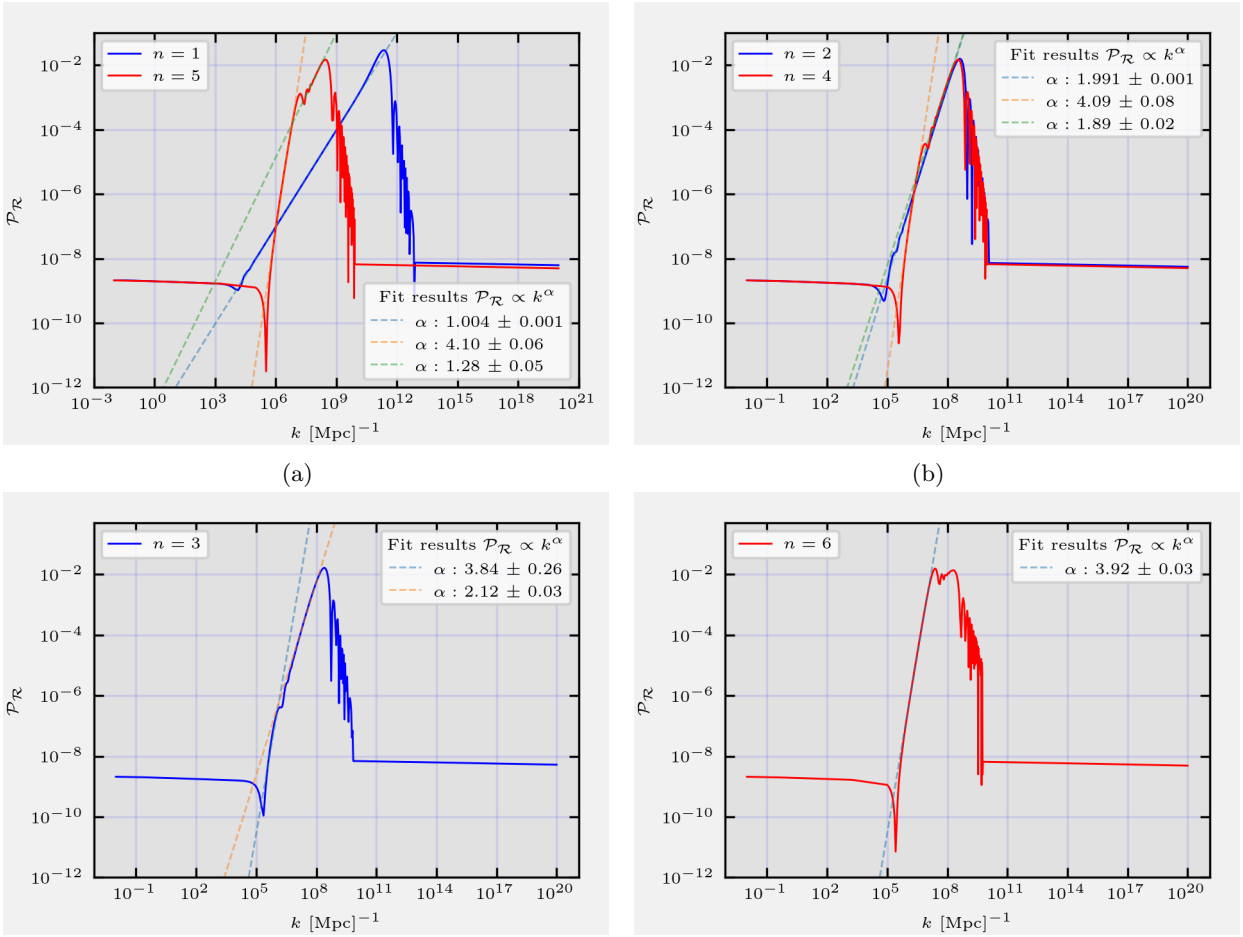

Figure 3.6: Power spectrum of the comoving curvature perturbation for the cases $n = \{1, 5\}$ (a) and $n = \{2, 4\}$ (b). We can notice a relative spectrum enhancement, $\Delta\mathcal{P}_\mathcal{R} \sim 10^7$, between large CMB and small PBH-formation scales. For both the cases $n = \{1, 2\}$, the power index satisfies the relation (3.2.25). For $n = \{4, 5\}$ instead, we have an initial maximum growth proportional to k^4, for modes that exit the horizon during the first slow-roll phase.

and [97] respectively).

The SIGWs can be traced back to scalar perturbations generated during the inflationary epoch. In particular, large scalar over-densities are seeded by the primordial curvature perturbation generated during inflation and can be responsible for the induced GWs in RDU. For more references on the mathematical formalism for the production of SIGWs see [95]. SIGWs, therefore, may offer valuable insights into the physics of the very early universe and can be detected not only by PTAs but also by space-based GW detectors such as LISA [98], Taiji [99], TianQin [100], and DECIGO [101]. Being related to the PBH formation, significant emission of SIGWs requires the amplitude of the power spectrum of the primordial curvature perturbations to be around $\mathcal{P}_\mathcal{R} \sim 10^{-2}$. In particular, to account for the observed gravitational wave signal detected by PTAs, the curvature power spectrum must possess at least one high peak at intermediate scales, which, as we have already discussed, can be achieved through inflationary models with special features.

The main goal of this Section is to compare the results obtained from our inflationary models

Parameters	Prior	Posterior	$\log \mathcal{B}$
$\log_{10} \mathcal{A}$	$U[-3, 1]$	$-0.88^{+0.81}_{-0.36}$	0.46
α	$U[0, 5]$	$2.33^{+1.72}_{-1.14}$	
β	$U[0, 5]$	$2.22^{+1.87}_{-1.54}$	
$\log_{10} k_p/\mathrm{Mpc}^{-1}$	$U[5, 10]$	$7.91^{+0.88}_{-0.44}$	

Table 3.3: The priors, maximum posterior values, 1-σ credible intervals bounds of posteriors and Bayes factor for a BPL model of the primordial curvature power spectrum using NANOGrav 15-yr data set [95].

(Section 3.2.3) to the preliminary analysis in Ref. [95]. In this article, the authors study the constraints on different shapes of the power spectrum from the PTAs dataset in a model-independent way. In particular, to describe a single-peak primordial curvature power spectrum, various parameterizations were employed, such as a monochromatic δ-function form, a box form, a lognormal form, and a broken power law form. A Bayesian analysis was employed on the NANOGrav 15 years to investigate these different parametrizations of the power spectrum. We shall use their results to test our inflationary models against the production of SIGW.

We used as a main reference the analysis performed for a power spectrum with a broken power law (BPL) form:

$$\mathcal{P}_{\mathcal{R}}^{(\mathrm{BPL})}(k) = \frac{\mathcal{A}(\alpha+\beta)}{\beta(k/k_p)^{-\alpha} + \alpha(k/k_p)^{\beta}} + \mathcal{A}_s \left(\frac{k}{k_*}\right)^{n_s-1} \tag{3.3.1}$$

where $\mathcal{A}_s$ and $n_s - 1$ are the CMB power spectrum amplitude and tilt fixed at $\mathcal{A}_s = 2.1 \times 10^{-9}$ and $n_s - 1 = 0.965$ with $k_* = 0.05\,\mathrm{Mpc}^{-1}$. The priors and best-fit parameters of the Bayesan analysis reported in [95] are presented here in Tab. 3.3. The marginal distribution of the parameter β is plotted in Fig. 3.7. Let us note that such a distribution is essentially unable to constrain β, *i.e.* the form of the peak of the power spectrum after the amplification stage is substantially unconstrained. This essentially translates in the absence of constraint of the final part of inflation (third region of our potential).

We must stress that the principal goal of this analysis is to perform a qualitative comparison of the power spectra obtained in Section 3.2.3 for the production of PBH with the posterior results listed in Tab. 3.3. The best-fit parameters obtained for our models are presented in Tab. 3.4. It is important to notice that the main feature of the power spectrum is given by the parameter α, which describes the amplification phase and is related to the shape of the inflaton potential. In contrast, the position of the peak k_p and the relative amplitude $\mathcal{A}$ of the spectrum can be tuned by a different choice of the parameters of the model and are not very interesting for the reconstruction. They can be modified by simply varying the position of the second part of the potential and its duration. Then, we can compare the results obtained for the parameter α with the posterior result listed in Tab. 3.3 and with the marginal distribution in Fig. 3.8. We remind that in the case of amplifying potentials with $n > 3$, the transient solution is unstable and the amplification of the spectrum occurs in two phases. As we have already mentioned, the power spectra presented in Fig. 3.6, for $n \geq 3$ present an initial steep-growth proportional to k^4 right after the dip, before relaxing to a less steep slope determined by the attractor value of ϵ_2 (3.2.49). In such cases, we then decided

n	$\log_{10}\mathcal{A}$	α	β	$\log_{10} k_p/\mathrm{Mpc}^{-1}$
1	-1.527 ± 0.002	1.12 ± 0.03	3.4 ± 0.1	11.35 ± 0.02
2	-1.775 ± 0.004	1.90 ± 0.02	3.0 ± 0.2	8.59 ± 0.04
3	-1.745 ± 0.003	2.06 ± 0.03	3.3 ± 0.3	8.36 ± 0.05
4	-1.82 ± 0.01	1.88 ± 0.02	2.8 ± 0.2	8.51 ± 0.03
5	-1.82 ± 0.02	1.34 ± 0.02	3.3 ± 0.2	8.46 ± 0.01
6	-1.80 ± 0.05	3.66 ± 0.05	2.9 ± 0.3	7.352 ± 0.003

Table 3.4: Fit of the power spectrum for a BPL form for models presented in Fig. 3.6.

to consider the possibility, not investigated in the numerical analysis, that for some choices of the parameters of the model, the transition between the first slow-roll stage (SR1) and the transient phase is smooth enough to just have a steep-growth proportional to k^4. In Fig. 3.8 such cases are plotted with vertical dashed lines. The corresponding slope is obtained from the fit of the initial growth of the spectra presented in Fig. 3.6. Let us note that for some of the cases analyzed the value of α is not so close to the maximum of the distribution, however, the cases $n = 1$ and $n = 5$ are certainly mildly favoured. We expect, by extrapolating the behaviour found for integer values of n, that some value of n in [1, 1.5] and [4.5, 5] is slightly more favoured by data.

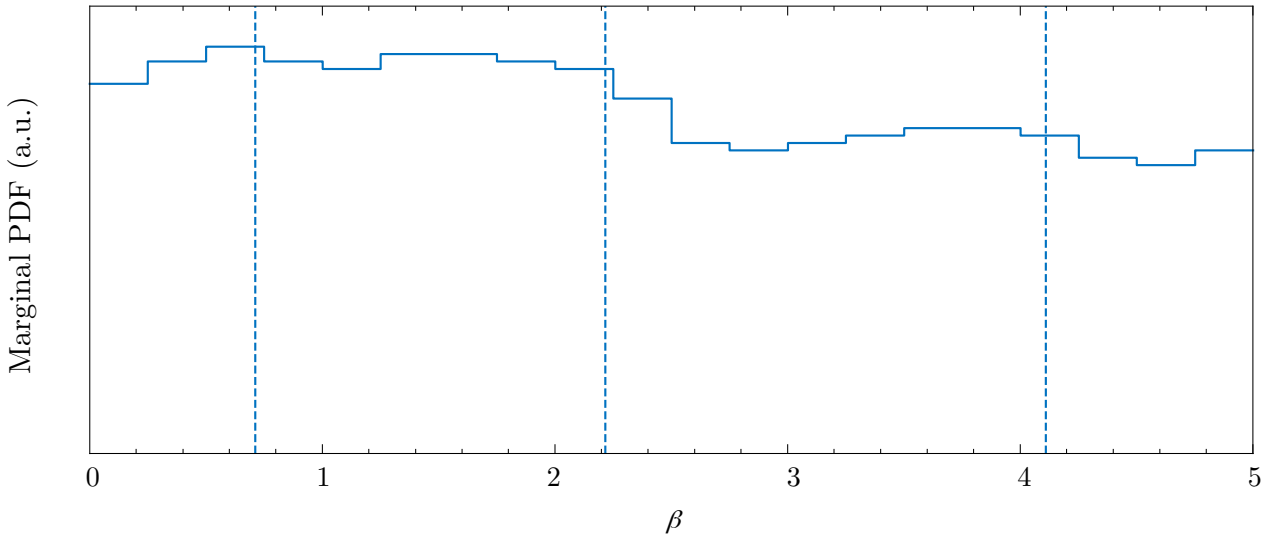

Figure 3.7: Marginal distribution of the parameter β obtained from the Bayesan analysis performed in [95]. The distribution is prevalently uniform and it gives no relevant information on the shape of the power spectrum after the peak.

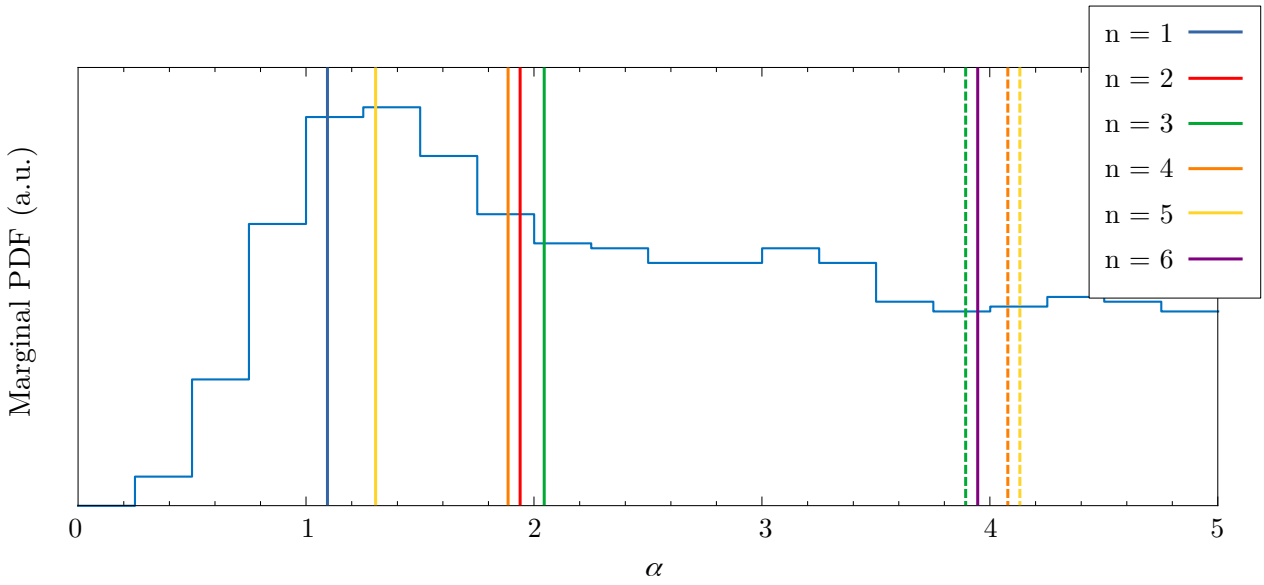

Figure 3.8: Marginal distribution of the parameter α obtained from the Bayesan analysis performed in [95]. We superimpose the results obtained from the fit of the growth of the power spectra for our inflationary models. The solid lines reproduce the best-fit values of α listed in Tab. 3.4, while the dashed ones correspond to the estimated values of α, assuming that the peak is reached with the maximum possible steep of the growth proportional to k^4, presented in Fig. 3.6.

Chapter 4

Amplification in Induced Gravity models

The inflationary paradigm is widely accepted as a valid description of the early universe and is supported by current data. We have seen how it is able to explain the flatness and homogeneity of the universe and the spectrum of primordial density fluctuations imprinted in the CMB. However, as scalar fields play an important role in driving inflation, it is interesting to study the case in which the scalar inflaton is non-minimally coupled to gravity. General Relativity is a description of gravity which passes many observational tests at low energy. In contrast, at Planck energies, and generally in the very early universe, several theoretical reasons lead to possible generalizations of the gravity sector due to quantum effects where the inflaton is non-minimally coupled [102–104].

The first proposal following these ideas is the work of Brans and Dicke [105], in which gravitational effects are described also by the dynamics of a non-massive scalar field on a Riemann manifold. Such a theory has been developed from Mach's principle, according to which inertia must arise from the general mass distribution of the universe. The model consisted of a new massless scalar field whose inverse was associated with the gravitational Newton coupling. Such a field was shown to dynamically evolve in the presence of matter and led to cosmological predictions differing from General Relativity.

A similar theory, assigning a dynamical origin to the gravitational coupling, was proposed again in 1967 by Sakharov [106]. In his article, he highlighted that quantum corrections at one-loop of the dynamics of a scalar field on a curved spacetime generate Einstein's cosmological constant and an action term similar to Einstein-Hilbert's action. In this sense, we can say that in a theory consisting of a single scalar field we can generate through a quantum process the gravity action, which is, in a certain sense, "induced".

Some years later a similar model was proposed by Zee [107] who incorporated the spontaneous symmetry-breaking idea and gravity. This idea was inspired by recent successes in the description of the electro-weak interaction. There a pointwise 4-fermion interaction with a coupling constant with the dimension of an inverse squared mass was explained as the exchange of massive vector bosons. This explained also the mass dimension of the coupling constant and the smallness of such a coupling, $G_F \sim 1/M_W^2$. In this framework, the concept of spontaneous symmetry breaking was

rediscovered causing some scalar field to have a vacuum expectation value v, generating then the mass of the intermediate boson, $G_F \sim 1/M_W^2 \sim 1/v^2$. In analogy, we can think of the gravitational Newton's constant arising as the expectational vacuum value of some scalar field.

In this Chapter, we indeed study such theories, called Induced Gravity models with the inflation playing also the role of the scalar field associated with Newton's constant. These are a natural generalisation of GR and, even if they were introduced many years ago, recently have become more and more attractive. When quantum effects become large enough a non-minimal coupling to gravity naturally arises in the presence of a scalar field which then affects the observed Newton's constant. Higgs inflation, in particular, is described by a non-minimally coupled model in which the inflaton is identified with the scalar Higgs field, responsible for both inflation and the generation of the primordial inhomogeneities. This model is nowadays favoured by observations and reconciles, within a common framework, Planck scale and Standard Model physics. Let us note that the inflaton-Higgs scalar is non-minimally coupled to gravity however inflation occurs at energies where induced-gravity action dominates on the Einstein-Hilbert term.

In this Chapter, we first describe the formalism and the homogenous dynamics in the Induced Gravity model. We then formalize the problem of perturbations in such a context and briefly study what are the conditions for obtaining an amplification of the power spectrum. In analogy with the previous Section, we restrict to the description of a transient phase of the evolution of the scalar field with nearly constant slow-roll parameters. Once the requirements for such an amplification are studied, we introduce another reconstruction procedure, to build the amplifying potential. The reconstruction method is similar to the Hamilton-Jacobi one, and it is known as the "superpotential" method [108]. It is commonly applied to cosmological models with scalar fields. In this method, the Hubble parameter, instead of being parametrized as a function of the scale factor a, is instead considered as a function of the scalar field φ. In general, the two methods, the one illustrated in the previous chapter and the superpotential one, supplement each other and allow to construct different cosmological models with the required properties. The advantage of the second approach is that it allows one to construct models without having to invert complicated relations between the scalar field and the scale factor. In particular, we shall discuss the form of an inflaton potential able to generate a de Sitter attractor phase, that leads to amplification.

The final part of the Chapter consists of building a complete model of inflation in IG in a similar fashion to what was done for General Relativity (Chapter 3). In particular, we illustrate how building an amplification model considering growing or decreasing solutions of the curvature perturbation $\mathcal{R}$. We study the attractor behaviour in different cases, obtaining results similar to those already obtained in the context of General Relativity, for the ansatz (3.2.16). The goal is to obtain a model with a satisfying amplification of the power spectrum, to be considered for the primordial black holes production.

4.1 Induced Gravity inflation

In Induced Gravity a scalar field is coupled in a non-minimal way to the gravitational sector and the scalar field-gravity system can be described by the action [109]

$$S = \int \mathrm{d}x^4 \sqrt{-g} \left[\frac{g^{\mu\nu}}{2} \partial_\mu \varphi \partial_\nu \varphi - \frac{\gamma \varphi^2}{2} R - V(\varphi) \right] , \tag{4.1.1}$$

where γ is a dimensionless, positive definite parameter giving the non-minimal coupling between the scalar field φ and gravity, and φ is the scalar field that determines the effective Newton's constant and we henceforth consider as the inflation. Suppose that $V(\varphi)$ is such that it is minimized when $\langle \varphi \rangle = \varphi_0$ we see that action (4.1.1) reduces to Einstein's action (1.2.19) with the identification [107]

$$\langle \varphi \rangle = \frac{M_\mathrm{P}}{\sqrt{\gamma}} \implies G_N = \frac{1}{8\pi} \frac{1}{\gamma \langle \varphi \rangle^2} . \tag{4.1.2}$$

We also impose that the potential at the minimum satisfies $V(\varphi_0) = 0$ in order not to have residual vacuum energy at the end of inflation. The model of inflation considered belongs to the single-field scenario and we leave the more complex multi-field case to future applications.

Assuming a spatially flat Robertson-Walker background metric (1.1.1), the variation of the above homogeneous action leads to the following set of independent equations

$$H^2 = \frac{1}{3\gamma \varphi^2} \left[\frac{\dot{\varphi}^2}{2} + V(\varphi) \right] - 2H \frac{\dot{\varphi}}{\varphi} , \tag{4.1.3}$$

$$\ddot{\varphi} + 3H \dot{\varphi} + \frac{\dot{\varphi}^2}{\varphi} = - \frac{V_{\mathrm{eff},\varphi}}{1 + 6\gamma} , \tag{4.1.4}$$

where we used the usual notation for time and field differentiation and defined

$$V_{\mathrm{eff},\varphi} \equiv \frac{\mathrm{d}V}{\mathrm{d}\varphi} - 4 \frac{V}{\varphi} . \tag{4.1.5}$$

The equation (4.1.4) determines the time evolution of the field, and is the generalised form of the Klein-Gordon equation. With respect to the equation (1.2.27) we have an additional quadratic time derivative term for the field, and a term for the potential, defined through the effective potential (4.1.5). The effective potential plays the same role as the potential in the minimal coupling case. The Eq. (4.1.3) instead is the generalised form of Friedmann equation in a flat homogeneous and isotropic background spacetime. In particular, it is interesting to notice that potential slow-roll conditions are now different, and in general in order to have a slow time evolution for the field $\dot{\varphi} \ll H\varphi$, we do not require the potential to be almost flat $V_{,\varphi} \sim 0$, but, from (4.1.5), we need a potential with a quartic dependence on φ: $V \propto \varphi^4$.

It is well known that, by a suitable conformal transformation and a redefinition of the scalar field, one can map a minimally coupled theory, defined in the so-called Einstein Frame (EF), into a non-minimally coupled one, in the Jordan-Frame (JF) [110]. In particular, considering the conformal

transformation

$$\tilde{g}_{\mu\nu} = \Omega^2 \, g_{\mu\nu} \,, \tag{4.1.6}$$

$$\mathrm{d}\tilde{\varphi}^2 = \frac{1+6\gamma}{\Omega^2} \, \mathrm{d}\varphi^2 \,, \tag{4.1.7}$$

$$\tilde{V}(\tilde{\varphi}) = \Omega^{-4} \, V(\varphi) \,, \tag{4.1.8}$$

where $\Omega^2 = \frac{\gamma\varphi^2}{M_{\rm P}^2}$, we can rewrite, up to boundary terms, the action in Eq. (4.1.1) in the EF as:

$$S_E = \int \mathrm{d}^4 \sqrt{-\tilde{g}} \left[\frac{\tilde{g}^{\mu\nu}}{2} \partial_\mu \tilde{\varphi} \partial_\nu \tilde{\varphi} - \frac{M_{\rm P}^2}{2} \tilde{R} - \tilde{V}(\tilde{\varphi}) \right] . \tag{4.1.9}$$

The variation of Eq. (4.1.9) then leads to a set of equations analogous to those obtained from the action (1.2.19). Let us note that the spectral index of the curvature perturbations and that of gravitational waves are invariant under conformal transformations and can be calculated in the simpler Einstein frame.

However, other important quantities in cosmology are not left invariant under conformal transformations, like the Hubble parameter H. It is then important to distinguish between the two frames, emphasising which one is to be considered the physical one. Henceforth, for us, the Jordan frame will be the physical one, and it is principally the frame in which we derive all our results.

4.1.1 Homogeneous dynamics and the Hubble and scalar field flow functions

As briefly mentioned in Section 3.2.1, we can introduce the slow-roll parameters that conveniently describe the dynamics of the scalar field, the so-called "scalar field flow functions" hierarchy defined by $\delta_0 = \varphi/\varphi_0$, with φ_0 indicating an arbitrary initial value for the field, and $\delta_{n+i} = \mathrm{d}\log\delta_i/\mathrm{d}N$, with $i \geq 1$. Differently from the case of Einstein Gravity, we can not express the evolution of inflationary linear fluctuations only in terms of the Hubble slow-roll functions ϵ_i but we need also this second kind of functions δ_i. However, combining Eqs. (4.1.3) and (4.1.4) we can find following relation between the two hierarchies

$$\epsilon_1 = \frac{\delta_1}{\delta_1 + 1} \left(\frac{\delta_1}{2\gamma} + 2\delta_1 + \delta_2 - 1 \right) . \tag{4.1.10}$$

and higher order ϵ_i's can be obtained by differentiating (4.1.10).

It is interesting to also determine the exact solutions of the homogeneous dynamics in both the Einstein and Jordan Frame, observing the peculiar differences between them. We can write the equations of motion in terms of the SR parameters in order to find these solutions. In the context of the minimally coupled case (EF) we have from (3.2.12)

$$\tilde{\delta}_1^2 \frac{\tilde{\varphi}^2}{M_{\rm P}^2} = \tilde{\epsilon}_1 \quad \Longrightarrow \quad \tilde{\delta}_1 + \tilde{\delta}_2 = \frac{\tilde{\epsilon}_2}{2} \,, \tag{4.1.11}$$

and we can rewrite the Klein-Gordon equation (1.2.27) as

$$\tilde{\delta}_2 + \tilde{\delta}_1 - \tilde{\epsilon}_1 + \frac{\tilde{\delta}_1}{\tilde{\epsilon}_1}\frac{\mathrm{d}\log\tilde{V}}{\mathrm{d}\log\tilde{\varphi}}(3-\tilde{\epsilon}_1) = 0\,. \tag{4.1.12}$$

We have here used the new notation with the superimposed tilde ˜ sign to indicate Einstein Frame quantities. From Eqs. (4.1.11, 4.1.12), we can easily observe that no solutions with $\tilde{\delta}_1$ and $\tilde{\epsilon}_1$ simultaneosly constant and different from zero exist while a non-trivial solution can be found for the case $\tilde{\epsilon}_2 = 0$, $\tilde{\delta}_1 = \pm\sqrt{\epsilon_1}\,M_{\rm P}/\varphi$ with $\tilde{V} \propto \exp\left(\sqrt{\epsilon_1}\varphi/M_{\rm P}\right)$. This kind of solution is the well-known power law inflationary solution [109].

Proceeding now into the Induced Gravity gravity case, the dynamical equations (4.1.11, 4.1.12) must be now replaced by a combination of Eqs. (4.1.3,4.1.4), and on using the definition of slow-roll parameters, we obtain

$$\epsilon_1 = \left[3\left(\delta_1 - 4\gamma + \gamma\frac{\mathrm{d}\log V}{\mathrm{d}\log\varphi}\right) + \delta_1\left(6\gamma - \frac{\delta_1}{2}\right)\frac{\mathrm{d}\log V}{\mathrm{d}\log\varphi} + \delta_1(\delta_1+\delta_2)\right]\frac{1}{\delta - 6\gamma}\,. \tag{4.1.13}$$

Despite the involved form of the equation, we can still easily find an exact, non-trivial solution being the counterpart of the one found in the minimally coupled case. In fact, considering $\epsilon_2 = \delta_2 = 0$, with a monomial potential

$$V = V_0\left(\frac{\varphi}{\varphi_0}\right)^n\,, \tag{4.1.14}$$

we have

$$\delta_1 = -\frac{\gamma(n-4)}{1+\gamma(n+2)}, \qquad \epsilon_1 = \frac{\gamma(n-2)(n-4)}{2+2\gamma(n+2)}\,. \tag{4.1.15}$$

It is interesting to notice the presence of two different de Sitter-like solutions. The form of the slow-roll parameter ϵ_1 clearly suggests that for quartic $n = 4$ and quadratic $n = 2$ potentials, the Hubble parameter is constant $\epsilon_1 = 0$. In particular, we have that in the quartic case $\delta_1 = 0$ and the field is frozen, while in the quadratic one $\delta_1 = \frac{2\gamma}{1+4\gamma}$.

4.1.2 Cosmological perturbations

We have already studied the quantization of linear scalar perturbations in the case of a homogenous and isotropic background, for the minimally coupled inflaton. The result was the derivation of the Mukhanov-Sasaki equation for the gauge invariant quantity v (1.4.91). The same approach can be applied in this context.

Following the prescription presented in [111], we work in the uniform curvature gauge, which corresponds to imposing $\psi = 0$ for the scalar component of the perturbed metric term $\delta g_{\mu\nu}$, implying that spatial curvature vanishes. In this way, the scalar curvature perturbations produced by quantum fluctuations of the inflaton can be described through the comoving curvature perturbation $\mathcal{R}(x) = H\delta\varphi(x)/\dot{\varphi}$, where $\delta\varphi(x)$ is the scalar inflaton perturbation. Ignoring surface terms, we can expand to the second order the action (4.1.1) with respect to $\delta\varphi$, and removing all non-physical

degrees of freedom, we can derive the action [111]

$$S^{(2)} = \frac{1}{2}\int \mathrm{d}t\,\mathrm{d}^3\vec{x}\,a^3 Z\left\{\delta\dot{\varphi}^2 - \frac{1}{a^2}\left(\nabla\delta\varphi\right)^2 + \frac{1}{a^3 Z}\frac{H}{\dot{\varphi}}\frac{\mathrm{d}}{\mathrm{d}t}\left[a^3 Z\frac{\mathrm{d}}{\mathrm{d}t}\left(\frac{\dot{\varphi}}{H}\right)\right]\right\}. \tag{4.1.16}$$

The structure of the action is very similar to that in Eq. (1.2.19). In the case of IG, we have [109]

$$Z \equiv \frac{H^2\varphi^2(1+6\gamma)}{(\dot{\varphi}+H\varphi)^2} = \frac{1+6\gamma}{(1+\delta_1)^2}\,. \tag{4.1.17}$$

The action (4.1.16) leads then to the perturbation equation, in the Fourier space given by

$$\delta\ddot{\varphi}_k + \left(3H + \frac{\dot{Z}}{Z}\right)\delta\dot{\varphi}_k + \left[\frac{k^2}{a^2} - \frac{1}{a^3 Z\,\varphi\delta_1}\frac{\mathrm{d}}{\mathrm{d}t}\left(a^3 Z\frac{\mathrm{d}}{\mathrm{d}t}\left(\varphi\,\delta_1\right)\right)\right]\delta\varphi_k = 0\,, \tag{4.1.18}$$

and the Fourier component $\delta\varphi_k$ is related to the comoving curvature perturbation Fourier component $\mathcal{R}_k$, in uniform gauge, through

$$\mathcal{R}_k = H\frac{\delta\varphi_k}{\dot{\varphi}}\,. \tag{4.1.19}$$

The above equation can be rewritten by introducing a new field variable

$$v_k(t) \equiv z\frac{H}{\dot{\varphi}}\delta\varphi_k = z\mathcal{R}_k\,, \qquad z(t) \equiv \frac{a\dot{\varphi}}{H}\sqrt{Z}\,, \tag{4.1.20}$$

as

$$v_k'' + \left(k^2 - \frac{z''}{z}\right)v_k = 0\,, \tag{4.1.21}$$

where a prime denotes a derivative with respect to the conformal time η. In particular, we have

$$\begin{aligned}\frac{z''}{z} \equiv (aH)^2 f_{MS} = (aH)^2\Big[&\delta_1^2 + \delta_2^2 + (3-\epsilon_1)(\delta_1+\delta_2+1)\delta_2\delta_3 \\ &+ \frac{\delta_1\delta_2}{1+\delta_1}\left(\epsilon_1 + \delta_1 - 3\delta_2 - \delta_3 + \frac{2\delta_1\delta_2}{1+\delta_1} - 2\right) - 1\Big]\end{aligned} \tag{4.1.22}$$

where we defined the function $f_{MS} = f_{MS}(\epsilon_i,\,\delta_i)$.

Also gravitational waves are produced during inflation. Tensorial perturbations are traceless and with a transverse polarization. They are described by two degrees of freedom described by the field variable $h_{s,k}$, where $s = \{\times, +\}$. In IG the Fourier modes of tensor perturbations satisfy the following equation [109]

$$\ddot{h}_{s,k} + (3H + 2H\,\delta_1)\dot{h}_{s,k} + \frac{k^2}{a^2}\,h_{s,k} = 0\,. \tag{4.1.23}$$

On setting $T_{s,k} \equiv \frac{1}{\sqrt{2}}a\varphi\sqrt{\gamma}\,h_{s,k}$ the above equation can be rewritten as:

$$T_{s,k}'' + \left[k^2 + M_T^2(\eta)\right]T_{s,k} = 0\,, \tag{4.1.24}$$

where

$$M_T^2(\eta) = -(aH)^2\left[2 - \epsilon_1 + \delta_1(3 + \delta_1 + \delta_2 - \epsilon_1)\right]\,. \tag{4.1.25}$$

Before discussing some examples for the reconstruction of a potential, let us stress that the construction of a potential given H is not as straightforward as for GR with a minimally coupled inflaton. In particular, we can easily obtain exact potentials only for certain values of the parameters following the procedure similar to that described after Eq. (3.2.16) for a minimally coupled inflaton.

Given $H = H(a)$ we can calculate the SR parameters in the large a limit. Since $\lim_{a\to\infty}\epsilon_1 = 0$ we expect from Eqs. (4.1.10, 4.1.13) two possible field hierarchies δ_i: (a) $\lim_{a\to\infty}\delta_1 = 0$ and $\lim_{a\to\infty}\delta_2 \neq 0$, or (b) $\lim_{a\to\infty}\delta_2 = 0$ and $\lim_{a\to\infty}\delta_1 \neq 0$ and satisfying the relation

$$\delta_{1,\infty} = \frac{2\gamma}{1+4\gamma}\,. \tag{4.1.26}$$

These results follow from the functional dependence of $H(a)$ inherited by ϵ_1 and δ_i's and by the general result obtained from (3.2.11), which is applied here to the SR hierarchy δ_i. Notice that in contrast with the minimally coupled case, two different de Sitter trajectories are present in IG, and they are associated with two different evolutions of the inflaton field. Using Eq. (4.1.13) in the same limit for a, one obtains that the potential, on the attractor, must satisfy

$$\frac{\mathrm{d}\log V_\infty}{\mathrm{d}\log\varphi} - 4 = 0 \implies V_\infty \propto \varphi^4 \tag{4.1.27}$$

in the (a) case and

$$\frac{\mathrm{d}\log V_\infty}{\mathrm{d}\log\varphi} - 4 = -2 \implies V_\infty \propto \varphi^2 \tag{4.1.28}$$

in the case (b). We can now proceed to evaluate the full hierarchy of δ_i's. Starting from Eq. (4.1.10) and differentiating we find

$$\epsilon_2 = \frac{\delta_2\left[(1+4\gamma)\delta_1^2 + 2\gamma(\delta_2+\delta_3-1) + 2\delta_1(1+4\gamma+\gamma\delta_3)\right]}{(1+\delta_1)\left[(1+4\gamma)\delta_1 + 2\gamma(\delta_2-1)\right]}\,, \tag{4.1.29}$$

and, by further differentiation, the ϵ_i's with arbitrary large i can be obtained.

In order to study the amplification in the IG context, and similarly to what we did in the previous Chapter, we calculate Φ and $n_s - 1$. It can be shown that [12]

$$\Phi = 1 - \epsilon_1 - \frac{\epsilon_1\epsilon_2}{1-\epsilon_1} + \left(2 + 2\delta_1 + \delta_2 - \frac{\delta_1\delta_2}{1+\delta_1}\right)\,. \tag{4.1.30}$$

If we evaluate Φ with respect to the hierarchies (a), with $V_\infty \propto \varphi^4$ and (b), with $V_\infty \propto \varphi^2$, one observes that only constants and terms linear in the SR parameters remain. Moreover, considering $\epsilon_{1,\infty} = 0$, Φ can be simplified to

$$\Phi = 3 + 2\delta_1 + 2\delta_2\,, \tag{4.1.31}$$

which can be negative only for the hierarchy (a) (growing solutions) but is strictly positive for the second hierarchy (b), provided we restrict ourselves to positive values of the non-minimal coupling γ.

If no growing solution exists, an amplification of the spectrum is only possible if the spectrum

is blue-tilted. We can estimate the spectral index $n_s - 1$, simplifying the parametric function $f_{\rm MS}$, obtaining the following expression for the scalar spectral index [12]

$$n_s - 1 = 3 - \sqrt{1 + 4(\delta_1^2 + \delta_2^2 + 3(1 + \delta_1 + \delta_2) - 1)}\,. \tag{4.1.32}$$

4.2 Potential Reconstruction and amplification

We have already illustrated that a conformal transformation can map non-minimally coupled theories in General Relativity with a minimally coupled scalar field. We would like to use this transformation to implement a reconstruction procedure for the IG potential leading to an enhancement of the power spectrum [108]. The procedure can be generalized to all models described by an arbitrary action

$$S_G = \int \mathrm{d}^4\sqrt{-g}\left[\frac{1}{2}g^{\mu\nu}\partial_\mu\varphi\partial_\nu\varphi - U(\varphi)R + V(\varphi)\right]\,, \tag{4.2.1}$$

where $U(\varphi)$ and $V(\varphi)$ are differentiable function of the scalar field φ, where the first determine the gravity-scalar coupling and the second is the field potential. This procedure is similar to the Hamilton-Jacobi method and also referred to as the "superpotential" method since it uses the homogenous scalar field to parametrise the evolution.

In the Einstein case, the advantages of the superpotential reconstruction method are based upon the fact it is possible to derive the final structure of the potential without having to integrate or invert functions.

Considering a spatially flat FLRW universe, the Einstein equations derived from the variation of the action (4.2.1) have the form

$$6UH^2 + 6\dot{U}H = \frac{1}{2}\dot{\varphi}^2 + V\,, \tag{4.2.2}$$

$$2U(2\dot{H} + 3H^2) + 4\dot{U}H + \ddot{U} + \frac{\dot{\varphi}^2}{2} - V = 0\,, \tag{4.2.3}$$

where the dot denotes the differentiation with respect to the cosmic time t and H is the usual Hubble parameter. At the same time, we can also derive the field φ evolution equation

$$\ddot{\varphi} + 3H\dot{\varphi} + V_\varphi = 6(\dot{H} + 2H^2)U_{,\varphi}\,. \tag{4.2.4}$$

We can combine Eqs. (4.2.2, 4.2.3) to obtain

$$4U\dot{H} - 2\dot{U}H + 2\ddot{U} + \dot{\varphi}^2 = 0\,. \tag{4.2.5}$$

If we assume that the scalar field φ undergoes a monotonic evolution we can introduce the operator

$$\frac{\mathrm{d}}{\mathrm{d}t} = F(\varphi)\frac{\mathrm{d}}{\mathrm{d}\varphi}\,, \qquad \text{where then } \dot{\varphi} = F(\varphi)\,. \tag{4.2.6}$$

We can then rewrite Eq. (4.2.5) considering $H = H(\varphi)$ and substituting $\dot{\varphi}$ and $\ddot{\varphi} = F_{,\varphi}F$, we obtain

$$4UH_{,\varphi} + 2(F_{,\varphi} - H)U_{,\varphi} + (2U_{,\varphi\varphi} + 1)F = 0\,, \tag{4.2.7}$$

where now H is a function of φ. This equation contains three functions of φ and, given two of them, the third one can be obtained through the integration of a linear differential equation. Therefore, if U and F are given, then $H(\varphi)$ can be obtained as

$$H(\varphi) = -\left[\int^{\varphi} \mathrm{d}\bar{\varphi}\, \frac{2F_{,\bar{\varphi}}U_{,\bar{\varphi}} + (2U_{,\bar{\varphi}\bar{\varphi}} + 1)F}{4U^{3/2}} + c_0\right]\sqrt{U(\varphi)} \tag{4.2.8}$$

where c_0 is an integration constant, and similarly, given $H(\varphi)$ and $U(\varphi)$, we can express $F(\varphi)$ as:

$$F(\varphi) = \left[\int^{\varphi} \mathrm{d}\bar{\varphi}\, \frac{U_{,\bar{\varphi}}H - 2UH_{,\bar{\varphi}}}{U_{,\bar{\varphi}}}\, e^{\Upsilon} + \bar{c}_0\right] e^{-\Upsilon(\varphi)} \tag{4.2.9}$$

where

$$\Upsilon(\varphi) \equiv \frac{1}{2}\int^{\varphi} \mathrm{d}\bar{\varphi}\, \frac{2U_{,\bar{\varphi}\bar{\varphi}} + 1}{U_{,\bar{\varphi}}}\,. \tag{4.2.10}$$

and $\tilde{c}_0$ is another integration constant. Let us notice that, in the minimally coupled case ($U =$ constant), the $F_{,\varphi}$ contribution cancels in Eq. (4.2.5) and correspondingly Eq. (4.2.9) no longer holds. Indeed Eq. (4.2.5) becomes an algebraical equation which fixes F in terms of $H_{,\varphi}$. In such case, for any function $H(\varphi)$ the reconstruction procedure can be analytically fulfilled and the potential obtained as a function of φ.

Once the three functions of φ are calculated, the corresponding potential $V(\varphi)$ can be easily obtained by inverting the Friedmann equation (4.2.2)

$$V(\varphi) = 6UH^2 + 6U_{,\varphi}FH - \frac{1}{2}F^2 = 6H^2U\left(1 + 3\frac{U_{,\varphi}^2}{U}\right) - \frac{(F - 6U_{,\varphi}H)^2}{2}\,. \tag{4.2.11}$$

However, any non-minimally coupled model can be transformed to the corresponding EF through a conformal transformation and a field redefinition. In such a frame through the Friedmann Eq. (3.2.12), the relation

$$\frac{\mathrm{d}\tilde{H}}{\mathrm{d}t} = -\frac{1}{2M_{\mathrm{P}}}\left(\frac{\mathrm{d}\tilde{\varphi}}{\mathrm{d}t}\right)^2 \quad\Longrightarrow\quad \tilde{F} = -2M_{\mathrm{P}}\tilde{H}_{,\varphi} \tag{4.2.12}$$

is valid. If one then expresses F and H in the JF through the corresponding quantities in the EF, that we called $\tilde{F}$ and $\tilde{H}$, and then uses the relation (4.2.12) here, then the reconstruction in the JF can be studied using a single function and its derivative, namely $Y(\varphi) \equiv \tilde{H}(\tilde{\varphi}(\varphi))$ where $\tilde{\varphi}$ is the inflaton in Einstein frame.

At the homogeneous level, one has the following relations between the JF (φ, U, N, a) and the EF ($\tilde{\varphi}$, $\tilde{U}$, $\tilde{N}$, $\tilde{a}$):

$$\tilde{N} = \sqrt{\frac{U}{\tilde{U}}}\,N\,, \qquad \tilde{a} = \sqrt{\frac{U}{\tilde{U}}}\,a\,, \tag{4.2.13}$$

and

$$\tilde{H} = \sqrt{\frac{\tilde{U}}{U}}\left(1 + \frac{1}{2HU}\frac{\mathrm{d}U}{\mathrm{d}t}\right) H\,, \qquad \tilde{F} = \frac{\tilde{U}}{U}\sqrt{1 + 3\frac{U_{,\varphi}^2}{U}}\, F\,, \tag{4.2.14}$$

where the time derivative $\mathrm{d}/\mathrm{d}t$ is w.r.t the cosmic time in JF. These two relations may be inverted to obtain

$$H = \sqrt{\frac{2U}{M_{\rm P}}^{\,2}}\left(Y + \frac{2U_{,\varphi}Y_{,\varphi}}{1 + 3U_{,\varphi}^2/U}\right)\,, \qquad F = -\sqrt{2U}M_{\rm P}^2\frac{4UY_{,\varphi}}{1 + 3U_{,\varphi}^2/U} \tag{4.2.15}$$

and one may check by direct substitution that H and F in (4.2.15) satisfy Eq. (4.2.7).

Let us note that, starting from any given, non-singular, function $Y(\varphi)$ one is able to reconstruct a model having $\dot{\varphi}$ and H given by (4.2.15) and correspondingly express its potential by (4.2.11). One may argue that the same potential can be obtained by simply exploiting the mapping between the potentials in the associated Jordan and Einstein frames. Indeed this is only possible provided the integral which expresses the relation between $\tilde{\varphi}$ and φ can be analytically performed, and this only occurs for specific choices of $U(\varphi)$. However, we can impose conditions for Y, leading to specific inflationary evolutions in the Jordan Frame, and reconstruct the corresponding potential form.

We leave behind the general formalism and focus then on the simple case of Induced Gravity, with $U = \frac{\gamma\varphi^2}{2}$. The superpotential formalism previously discussed allows us to derive the two field functions:

$$F = -\alpha\varphi^3\, Y_{,\varphi}\,, \qquad H = \beta\varphi\, Y + \alpha\varphi^2\, Y_{,\varphi} \tag{4.2.16}$$

where $\beta \equiv \sqrt{\gamma}/M_{\rm P}$ and $\alpha \equiv 2\gamma\,\beta/(1+6\gamma)$. We can use these relations to express the slow-roll parameters for both the Hubble and the scalar field hierarchies in terms of $Y(\varphi)$ and its derivatives:

$$\delta_1 = \frac{\dot{\varphi}}{H\varphi} = \frac{F}{H\varphi} = -\frac{\alpha\varphi\, Y_{,\varphi}}{\beta Y + \alpha\varphi\, Y_{,\varphi}}\,, \tag{4.2.17}$$

$$\delta_2 = \frac{F}{H}\frac{\mathrm{d}\log\delta_1}{\mathrm{d}\varphi} = \frac{\alpha\beta\varphi\left(Y_{,\varphi}Y - \varphi Y_{,\varphi}^2\varphi + Y_{,\varphi\varphi}\,Y\varphi\right)}{(\beta Y + \alpha\varphi\, Y_{,\varphi})^2}\,. \tag{4.2.18}$$

and

$$\epsilon_1 = -\frac{\dot{H}}{H^2} = -\frac{FH_{,\varphi}}{H^2} = \frac{\alpha\varphi\, Y_{,\varphi}\left(\beta Y + \alpha\varphi^2\, Y_{,\varphi\varphi} + (2\alpha+\beta)\varphi\, Y_{,\varphi}\right)}{(\beta Y + \alpha\varphi\, Y_{,\varphi})^2} \tag{4.2.19}$$

If the inflaton evolves to some attractor φ_∞ with, without loss of generality, $\varphi_\infty > 0$ then Y can be Taylor expanded around it

$$Y(\varphi) = \sum_{n=0}^{\infty} y_n\left(\frac{\varphi}{\varphi_\infty} - 1\right)^n\,. \tag{4.2.20}$$

In the Taylor expansion (4.2.20) $y_0 > 0$ and $y_1 = 0$ in order for $\delta_1(\varphi_\infty) = 0$. This particular result allow us to estimate the large a limit of the parameter δ_2:

$$\delta_{2,\infty} = -\frac{2\alpha}{\beta}\frac{y_2}{y_0}\,, \tag{4.2.21}$$

which must be different from zero in order for the hierarchy δ_i to behave as (3.2.11). In this way, we can impose the late time field evolution through the Taylor coefficients (y_0, y_1, y_2) of the field function Y, and as we have seen before writing the corresponding potential. The reconstructed form

of such a potential is then

$$\begin{aligned} V &= 3\gamma\varphi^4(\beta Y + \alpha\varphi\, Y_{,\varphi})^2 - 6\gamma\varphi^4(\alpha\varphi Y_{,\varphi})(\beta Y + \alpha\varphi\, Y_{,\varphi}) - \frac{\varphi^4}{2}(\alpha\varphi\, Y_{,\varphi})^2 \\ &= \frac{\gamma^2\varphi^4\left[3(1+6\gamma)Y^2 - 2\gamma\varphi^2 Y_{,\varphi}^2\right]}{(1+6\gamma)M_{\rm P}^2}\,. \end{aligned} \tag{4.2.22}$$

Let's finally check the behaviour of the homogenous variables φ and H close to φ_∞. Approximating, to the leading order, $Y(\varphi) \approx y_0 + y_2(\varphi/\varphi_\infty - 1)^2$ and expanding both F and H accordingly, we obtain

$$\dot\varphi \approx -2y_2\alpha\,\varphi_\infty^2\left(\frac{\varphi}{\varphi_\infty} - 1\right)^2, \qquad H \approx \beta\varphi_\infty y_0\left[1 + \left(1 + 2\frac{\alpha}{\beta}\frac{y_2}{y_0}\right)\left(\frac{\varphi}{\varphi_\infty} - 1\right)\right] \tag{4.2.23}$$

where we observe that H approaches the constant value linearly on varying the field φ and δ_0 has a "time" dependence determined by

$$\delta_0 = \frac{\varphi}{\varphi_\infty} \simeq 1 + \exp\left(-2\alpha\, y_2\varphi_\infty\, t\right) \simeq 1 + \exp\left(-2\frac{\alpha}{\beta}\frac{y_2}{y_0}\, N\right) \tag{4.2.24}$$

where we approximated the relation between t and N through the limit value of H in (4.2.23). Let us note that the expected exponential behaviour of $L_i(N)$ in (3.2.7) is obtained. A very simple potential possibly leading to amplification can be obtained by the exact expression: $Y = y_0 + y_2\,(\varphi/\varphi_\infty - 1)^2$. In such a case $\varphi Y = y_2\varphi/\varphi_\infty$ and the potential is

$$V(\varphi) = \frac{\gamma^2\varphi^4 y_0^2\left\{3(1+6\gamma)\left[1 + \frac{y_2}{y_0}\left(\frac{\varphi}{\varphi_\infty} - 1\right)^2\right] - 8\gamma\frac{\varphi^2}{\varphi_\infty^2}\left(\frac{\varphi}{\varphi_\infty} - 1\right)^2\right\}}{(1+6\gamma)M_{\rm P}^2}\,. \tag{4.2.25}$$

We can actually estimate the features of the resulting spectrum. In the de Sitter limit we have a transient evolution of the scalar field, and, for a large, one finds:

$$\Phi = 3 - \frac{4\alpha}{\beta}\frac{y_2}{y_0} = 3 - \frac{8\gamma}{1+6\gamma}\frac{y_2}{y_0} \tag{4.2.26}$$

and

$$n_s - 1 = 3 - \frac{3 + \left(18 - 8\frac{y_2}{y_0}\right)\gamma}{1+6\gamma}\,. \tag{4.2.27}$$

The parameters y_0, y_2 are related to "n" in (3.2.16). On substituting $\varphi(N)$ of (4.2.24) in $H(\varphi)$ of (4.2.23) and being $a \sim e^N$ one has:

$$n = \frac{y_2}{y_0}\frac{8\gamma}{1+6\gamma}\,. \tag{4.2.28}$$

Indeed, we note that the factor y_2/y_0 determines both the shape of the potential and the late time

value of the slow-roll parameters:

$$\delta_{2,\infty} = -\frac{n}{2}\,, \tag{4.2.29}$$

$$\Phi = 3 - n\,, \tag{4.2.30}$$

$$n_s - 1 = 3 - \sqrt{(n-3)^2} = n\,. \tag{4.2.31}$$

From a model-building perspective, we expect to have, in order to obtain a sufficient amplification of the spectrum for both decreasing ($0 < n < 3$) and growing mode fluctuations $\mathcal{R}_k$ ($n > 3$), a value of the parameter $n \sim (y_2/y_0)\gamma \sim \mathcal{O}(1)$, that is the main assumption we will consider henceforth.

4.3 Outline of the model

Let us now proceed and construct a complete inflationary model in IG. The approach used is identical to the one described in Section 3.2.3. We introduce a three-stage potential in order to impose three distinct phenomenological requirements. We consider an initial slow-roll period (SR1) consistent with CMB observations, in which generating a power spectrum with a power-law functional form $\mathcal{P}_\mathcal{R}(k) = \mathcal{A}_s(k/k_*)^{n_s-1}$, with $\mathcal{A}_s \simeq 2.1 \times 10^{-9}$ and $n_s - 1 \simeq 0.965$, with $k_* = 0.05\,\mathrm{Mpc}^{-1}$. The intermediate stage (IG) is described by an inflationary evolution driven by a potential with a form described in Eq. (4.2.25) and finally we have a second slow-roll phase (SR2) which stops any further amplification and leads to the end of inflation.

From a model-building perspective, we consider a slow-roll evolution driven by a Landau-Ginzburg potential, of the form

$$V_{LG} = \frac{\mu}{4}(\varphi^2 - \varphi_0^2)^2\,. \tag{4.3.1}$$

This kind of potential has the same structure as a Higgs potential, and it was considered in the first work of Zee [107]. This kind of potential presents some interesting features [109, 112]: it has a minimum in $\varphi = \varphi_0$ and a relative maximum in $\varphi = 0$, $V(\varphi) \geq 0$ and allows both large and small field configuration. These features lead to inflationary predictions in agreement with observations, given suitable values of the parameters of the potential μ and φ_0.

The final potential has the form given by

$$\begin{aligned} V(\varphi) = {} & \frac{\gamma^2\varphi^4 y_0^2\left\{3(1+6\gamma)\left[1+\frac{y_2}{y_0}\left(\frac{\varphi}{\varphi_\infty}-1\right)^2\right] - 8\gamma\frac{\varphi^2}{\varphi_\infty^2}\left(\frac{\varphi}{\varphi_\infty}-1\right)^2\right\}}{(1+6\gamma)M_\mathrm{P}^2} \\ & \times \Theta_{d_1}(\varphi_1-\varphi)\Theta_{d_2}(\varphi-\varphi_2) \\ & + \frac{\mu_1}{4}(\varphi^2-\varphi_{01}^2)^2\,\Theta_{d_1}(\varphi-\varphi_1) \\ & + \frac{\mu_2}{4}(\varphi^2-\varphi_{02}^2)^2\,\Theta_{d_1}(\varphi_2-\varphi)\,, \end{aligned} \tag{4.3.2}$$

where each stage is connected to the subsequent one through the tanh-type "step" function (3.2.29). We define the first potential term as V_IG and the two Landau-Ginzburg terms as V_SR1 and V_SR2 correspondigly. We can see a possible realization in Fig. 4.1. The field values φ_1 and φ_2 represent the transition value, with $\varphi_1 < \varphi_2$, and together with d_1 and d_2, they determine both the position

and the duration of the transition between each stage of inflation. All the parameters are set in order to have a sufficiently smooth potential. The total normalization of the potential depends, in particular, on the parameters y_0, μ_1, μ_2, which can be related by imposing that at each transition the value of the potential varies smoothly: $V_{\rm IG}(\varphi_1) = V_{\rm SR1}(\varphi_1)$ and $V_{\rm IG}(\varphi_2) = V_{\rm SR2}(\varphi_2)$, in analogy with relations (3.2.31, 3.2.32), which we do not present due to the cumbersome expression for $V_{\rm IG}$. However, it is important to notice that the normalization factor is dependent also on the value of γ, which directly determines the structure of potential $V_{\rm IG}$ (4.2.25).

The power spectrum is obtained by solving the Mukhanov-Sasaki Eq. (4.1.21), for the variable v_k. In order to do so we need the time evolution for the slow-roll parameters δ_i, ϵ_i, which can be obtained by solving the following Klein-Gordon equation for the scalar inflaton φ, obtained by using the number of e-folds N as a time variable

$$\varphi_{,NN} = \frac{12\gamma\,\varphi}{1+6\gamma} + \frac{\varphi_{,N}^3(1+2\gamma)}{2\gamma\,\varphi^2(1+6\gamma)} + \frac{3\varphi_{,N}(-1+6\gamma)}{1+6\gamma} - \frac{\varphi_{,N}^2(7+6\gamma)}{\varphi(1+6\gamma)} + \frac{V_{,\varphi}(\varphi_{,N}+\varphi)(\varphi_{,N}^2 - 12\gamma\,\varphi_{,N}\varphi - 6\gamma\varphi^2)}{2\varphi\,V(1+6\gamma)}\,. \quad (4.3.3)$$

The evolution of the Hubble parameter is given by

$$H^2 = \frac{V/M_{\rm P}^2}{3\varphi^2\gamma}\left(1 + 2\delta_1 - \frac{1}{6\gamma}\delta_1^2\right)^{-1}\,. \quad (4.3.4)$$

The numerical evaluation of the time evolution of φ requires prescriptions similar to the minimal-coupling case. Indeed, the potential is tuned in order to induce a transient evolution of the field with an attractor value determined by the parameter φ_∞, which enters directly inside the form of the potential. However, the presence of the non-minimal coupling γ determines more possible solutions and has consequences on the dynamics of the scalar field φ. In the following, we consider two regimes of γ, in particular we work our numerical analysis for $\gamma = 10^{-2}$ and $\gamma = 10^{-4}$.

As we have already mentioned in Eq. (4.1.2), the non-minimal coupling is directly related to the vacuum expectation value of the inflaton and then to the evaluation of Newton's constant G_N. Thus, we set the minimum of our potential (4.3.2) at

$$\varphi_{02} = \frac{M_{\rm P}}{\sqrt{\gamma}}\,. \quad (4.3.5)$$

The initial value of our inflaton field $\varphi_i = \varphi(N=0)$ depends on the value of the minimum, and in order to have a large-field evolution $\varphi_i \gg \varphi_{02}$. The initial time $N = 0$ corresponds to the horizon exit of the pivot mode $k_0 = 0.002\,{\rm Mpc}^{-1}$.

In the following, we perform a study of the stability of our solutions, in analogy to the procedure followed in Section 3.2.3.

4.3.1 Stability analysis for the transient evolution

We clearly note that for the potential (4.2.25) it is extremely difficult to obtain an analytical description of the evolution of the scalar field φ. Even inverting the relation (4.2.6) does not

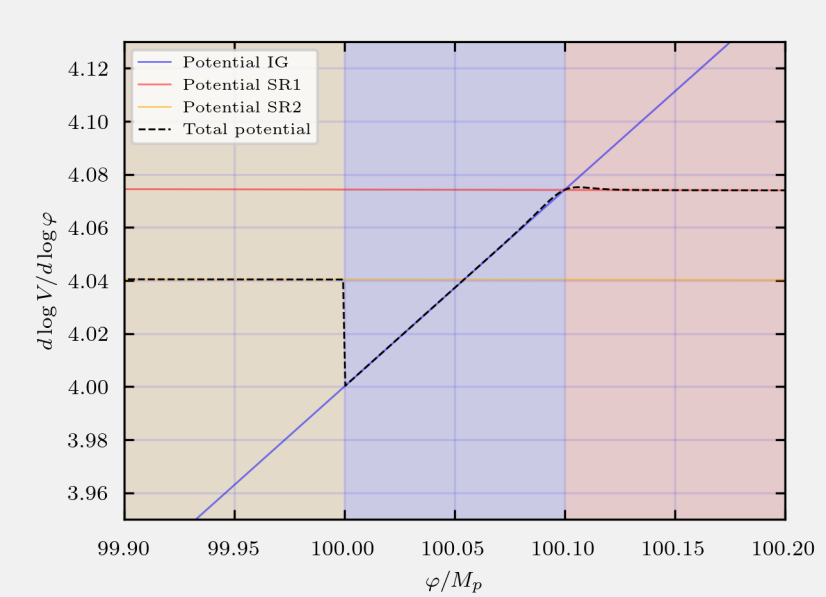

Figure 4.1: Logarithmic derivative of the total potential presented in Eq. (4.3.2). We considered as a working example the parameters in Tab. 4.1, with $n = 2$ and $\gamma = 10^{-2}$. We have highlighted the three regimes with different colours: red (SR1), blue (IG) and orange (SR2). We represent only a small interval around the field value $\varphi \sim \varphi_\infty = 100$ and notice how $\mathrm{d}\log V/\mathrm{d}\log\varphi \simeq 4$ at such value.

lead to a complete analytical description of the evolution of the field during the transient phase. Nevertheless, we can derive the main features of the homogeneous evolution restricting our analysis to the evolution of the field close to the attractor point φ_∞.

In particular, the solutions in the large time limit introduced in (4.2.29), (4.2.30) and (4.2.31) suggest that it is possible to study the properties of final power spectrum analyzing the time dependence of the slow-roll parameter δ_2 in such regime. We check the stability exploring the possible behaviour of such a parameter and verifying if the results are compatible with the analytical estimates for a potential (4.2.25).

Therefore, we obtain a differential equation for δ_2. We start considering Eqs. (4.1.10) and (4.1.13), and solving for δ_2 to derive

$$\delta_2 = \frac{\mathrm{d}\log V}{\mathrm{d}\log\varphi}\frac{(1+\delta_1)\left(\delta_1^2 - 6\gamma(1+2\delta_1)\right)}{2\delta_1(1+6\gamma)} - \frac{(2\gamma(\delta_1-2)+\delta_1)\left(-\delta_1^2+6\gamma(1+2\delta_1)\right)}{2\gamma\delta_1(1+6\gamma)}\,. \tag{4.3.6}$$

Before differentiating Eq. (4.3.6), we must consider that in the limit $\varphi \to \varphi_\infty$, we expect that $\delta_1 \sim 0$ and $\delta_2 \sim$ constant. Therefore, we have $\delta_{1,NN}$, $\delta_{1,N} \sim \mathcal{O}(\delta_1)$, due to the iterative definition of the hierarchy δ_i. Thus, substituting the definition $\delta_2 = \delta_{1,N}/\delta_1$ inside (4.3.6), and differentiating with respect to N, we obtain the second order differential equation

$$\begin{aligned}\delta_{1,NN}\delta_{1,N} - (\delta_{1,N})^2 \simeq -\frac{12\gamma\delta_{1,N}}{1+6\gamma} + 3\,\frac{\mathrm{d}\log V}{\mathrm{d}\log\varphi}\,\frac{\gamma\delta_{1,N}}{1+6\gamma} \\ \underbrace{-\,3\left[\frac{\mathrm{d}\log V}{\mathrm{d}\log\varphi} + \frac{\mathrm{d}^2V}{\mathrm{d}\varphi^2}\frac{\varphi^2}{V} - \left(\frac{\mathrm{d}\log V}{\mathrm{d}\log\varphi}\right)^2\right]\delta_1}_{\frac{\mathrm{d}}{\mathrm{d}N}\frac{\mathrm{d}\log V}{\mathrm{d}\log\varphi}}\,\frac{\gamma\delta_1}{1+6\gamma} + O(\delta_1^3)\,,\end{aligned} \tag{4.3.7}$$

where we have neglected any cubic terms in δ_1. We observe that for $\varphi \to \varphi_\infty$, in order to obtain a general relation between the slow-roll parameter and the logarithmic derivative of V, one has

$$\begin{aligned}\frac{\mathrm{d}\log V}{\mathrm{d}\log\varphi} &= \frac{1}{\delta_1}\frac{\mathrm{d}\log V}{\mathrm{d}N} = 2 - \frac{2\epsilon_1}{\delta_1} + \frac{2\delta_{1,N}/\delta_1 - \delta_{1,N}/3\gamma}{1 + 2\delta_1 - \delta_1^2/6\gamma} \\ &\simeq 4 - \frac{1+6\gamma}{\gamma}\delta_1 - \frac{1+6\gamma}{3\gamma}\delta_{1,N}\,,\end{aligned} \tag{4.3.8}$$

where we have used Eq. (4.2.11) for the potential, Eq. (4.1.10) for ϵ_1 and we expanded the final expression in δ_1 and $\delta_{1,N}$.

We can estimate the second order derivative term $\frac{V_{,\varphi\varphi}}{V}\varphi^2$ substituting the potential (4.2.25) and, Taylor expanding the relation around the attractor point φ_∞. We then obtain the leading term

$$\begin{aligned}\frac{\mathrm{d}^2V}{\mathrm{d}\varphi^2}\frac{\varphi^2}{V} &\simeq -\frac{4}{3(1+6\gamma)}\left[-3\left(3+\frac{y_2}{y_0}\right) + 2\gamma\left(-27+\left(-9+2\frac{y_2}{y_0}\right)\right)\right] + O(\varphi-\varphi_\infty) \\ &\simeq 12 + \frac{n(6-n)(1+6\gamma)}{12\gamma}\,,\end{aligned} \tag{4.3.9}$$

where we have used Eq. (4.2.28) for n.

Finally, we can insert each term inside Eq. (4.3.7), and, simplifying to the leading order in the slow-roll parameter δ_1, we obtain the first order linear differential equation

$$\delta_{1,NN} + 3\delta_{1,N} + \frac{n(6-n)}{4}\delta_1 = 0\,, \tag{4.3.10}$$

which admits the simple general solution

$$\delta_1(N) = C_1 e^{-\frac{n}{2}N} + C_2 e^{\frac{n-6}{2}N}\,, \tag{4.3.11}$$

where C_1 and C_2 are simple integration constants different from zero. Thus, we can directly obtain the approximate time dependence of δ_2 by a differentiation w.r.t. N of (4.3.11)

$$\delta_2(N) = \frac{1}{2}\frac{(n-6)e^{(n-3)N} - K\,n}{K + e^{(n-3)N}}\,, \tag{4.3.12}$$

where the integration constant $K \equiv C_1/C_2$ is introduced. In the large a limit we then have:

$$\delta_2 \xrightarrow{N\to\infty} \begin{cases} -\frac{n}{2}\,, & \text{if } n < 3\,, \\ \frac{n-6}{2}\,, & \text{if } n > 3\,, \end{cases} \tag{4.3.13}$$

that is, the solution is stable for $n < 3$, while for $n > 3$ the solution is unstable. This result is formally identical to the one obtained for the slow-roll parameter ϵ_2 in the late time regime for the evolution driven by the potential (3.2.22). Considering Eqs. (4.2.30) and (4.2.31), we can see that for $n < 3$ the power spectrum is blue tilted and a decreasing solution is present for the curvature modes. In the case $n > 3$ instead, the late time evolution described by the inflaton potential (4.2.25) is unstable and the late time behaviour of δ_2 is determined by $\delta_2 \simeq (n-6)/2 > -3/2$. In what

γ	n	φ_i	φ_2	d_1	d_2	φ_{01}
10^{-2}	1	$\varphi_\infty + \frac{21}{20}$	$\varphi_\infty + 10^{-5}$	10^{-2}	10^{-5}	10.84
	2	$\varphi_\infty + \frac{41}{20}$	$\varphi_\infty + 9 \times 10^{-6}$	10^{-2}	9×10^{-6}	13.50
	4	$\varphi_\infty + \frac{14}{5}$	$\varphi_\infty + 3 \times 10^{-5}$	10^{-2}	3×10^{-5}	21.78
	5	$\varphi_\infty + \frac{75}{20}$	$\varphi_\infty + 25 \times 10^{-6}$	10^{-2}	25×10^{-6}	24.68
10^{-4}	1	$\varphi_\infty + 1$	$\varphi_\infty + 10^{-5}$	10^{-2}	3×10^{-5}	71.50
	2	$\varphi_\infty + 2$	$\varphi_\infty + 10^{-5}$	10^{-2}	10^{-5}	79.15
	4	$\varphi_\infty + 3$	$\varphi_\infty + 16 \times 10^{-6}$	10^{-2}	16×10^{-6}	236.9
	5	$\varphi_\infty + \frac{19}{5}$	$\varphi_\infty + 5 \times 10^{-5}$	10^{-2}	5×10^{-5}	248.0

Table 4.1: Parameters considered for our working models. Each field value is normalized in $M_{\rm P}$, and it is taken with respect to the attractor point: $\varphi_\infty = 100$ for $\gamma = 10^{-2}$, and $\varphi_\infty = 300$ for $\gamma = 10^{-4}$. The first transition is considered to occur in all cases at $\varphi_1 = \varphi_\infty + 1/10$.

follows, we analyze different cases of evolutions, determined by the parameters n and γ, studying the amplification of the spectrum and comparing it with the numerical results.

4.3.2 Numerical results

In the following analysis, we shall consider two distinct cases of induced gravity inflation, corresponding to the value of the non-minimal coupling $\gamma = \{10^{-2}, 10^{-4}\}$.

The numerical simulations and their outcomes are discussed for the parameters listed in Tab. 4.1. We consider different values n to study a wide range of possible behaviours including decaying and enhanced perturbation solutions of the Mukhanov-Sasaki equations (4.1.21). In particular, we considered four different models of inflation with the parameter n having values $(1, 2, 4, 5)$. As in the previous Section 3.2.4, we set the initial conditions and adjust the transition periods properly to ensure that the scalar and tensor spectral power produced during the first phase of SR is within observational limits. In the following, we present field values in Planck units. From a model-building perspective, it was most convenient to express each parameter in terms of the attractor point φ_∞. In particular, we considered the first transition to occur at the field value $\varphi_1 = \varphi_\infty + \frac{1}{10}$ for each value of n and redefined the initial value of the evolution $\varphi_i = \varphi(N = 0)$.

Let us note that the parameter φ_{01} enters the total potential (4.3.2) as the minimum value of the Landau-Ginzburg potential for the first slow-roll phase (SR1). Ideally, the transition between the first slow-roll phase and the intermediate regime must be sufficiently smooth and the transition should occur at the value φ_1. In order to do so we constrain the value of the parameter φ_{01} in order to satisfy $V_{\rm IG,\varphi}(\varphi_1) = V_{\rm SR1,\varphi}(\varphi_1)$. However, for the cases with $n > 3$, we are interested in reproducing the growing solution of the fluctuation mode $\mathcal{R}_k$, which is unstable. In order to do that we need to impose some constraints on the transition between the first slow-roll phase and the intermediate phase, in a similar fashion to what we have done in Section 3.2.3. In contrast to this case, we did not calculate an exact analytical form for the field evolution during the transient stage and we found numerically the conditions required. Constraining the value of the free parameter φ_{01}

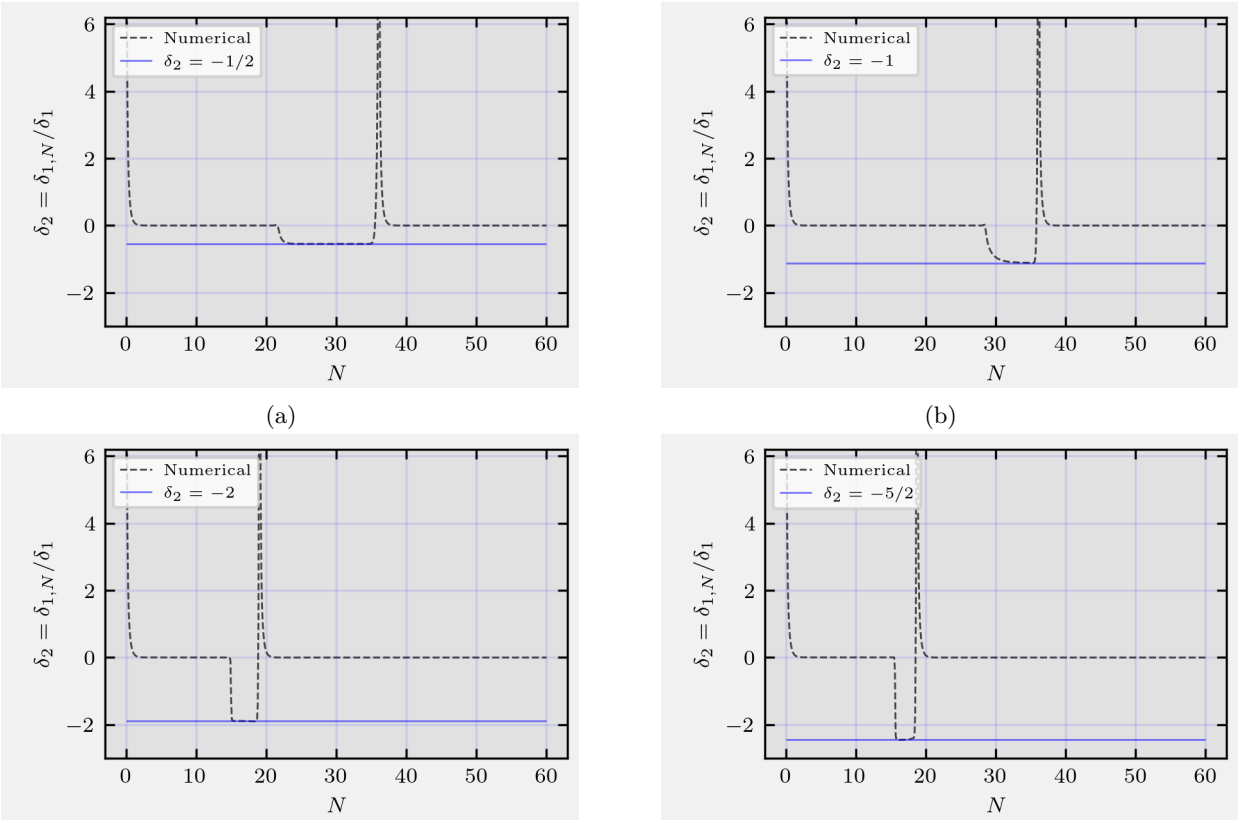

Figure 4.2: Time evolution of the slow-roll parameter δ_2 in the case $\gamma = 10^{-2}$ for different values of the parameter $n = \{1, 2, 4, 5\}$, correspondingly with subfigures (a), (b), (c), (d).

was possible through an iterative procedure to find the right value. The solutions of this procedure are shown in Fig. 4.2 (c), (d) and Fig. 4.3 (c), (d), for the cases $n = \{4, 5\}$. We can notice that during the transient phase we have a numerical evolution sufficiently compatible with the expected solution $\delta_2 \simeq -n/2$.

Thus, with the solutions for the homogeneous variables, we solved numerically the Mukhanov-Sasaki equation (3.1.17) with Bunch-Davies initial conditions and derive the power spectrum for the curvature perturbation $\mathcal{R}_k$ (App. A). We showed our results in four different plots, in Fig. 4.4, to highlight the differences between the models. We notice that the shapes of the spectra share many common features with the ones presented for the minimally-coupled inflaton, presented in Section 3.2.4. In particular, for the cases $n = 1, 2$, we have power-law growth of the spectrum compatible with the analytical estimate $n_s - 1 = n$, while in the case $n > 3$, the power spectrum grows initially as k^4 towards its peak and is characterized by a dip preceding the phase of steady growth. The peak region, in particular, is determined by the attractor solution (4.3.13), with a growth proportional to k^{6-n}, with $n > 3$.

We present in Tab. 4.2, the estimated result for the mass and abundance of PBH, derived from the simulations for each choice of n and γ. We have estimated the mass of the PBH both using Eqs. (2.2.4) and (2.2.5), choosing as interesting range of masses $M_{\rm PBH} \in [10^{-16}, 10]\, M_\odot$.

Finally, we present the analysis of the scalar power spectrum in relation to the production of

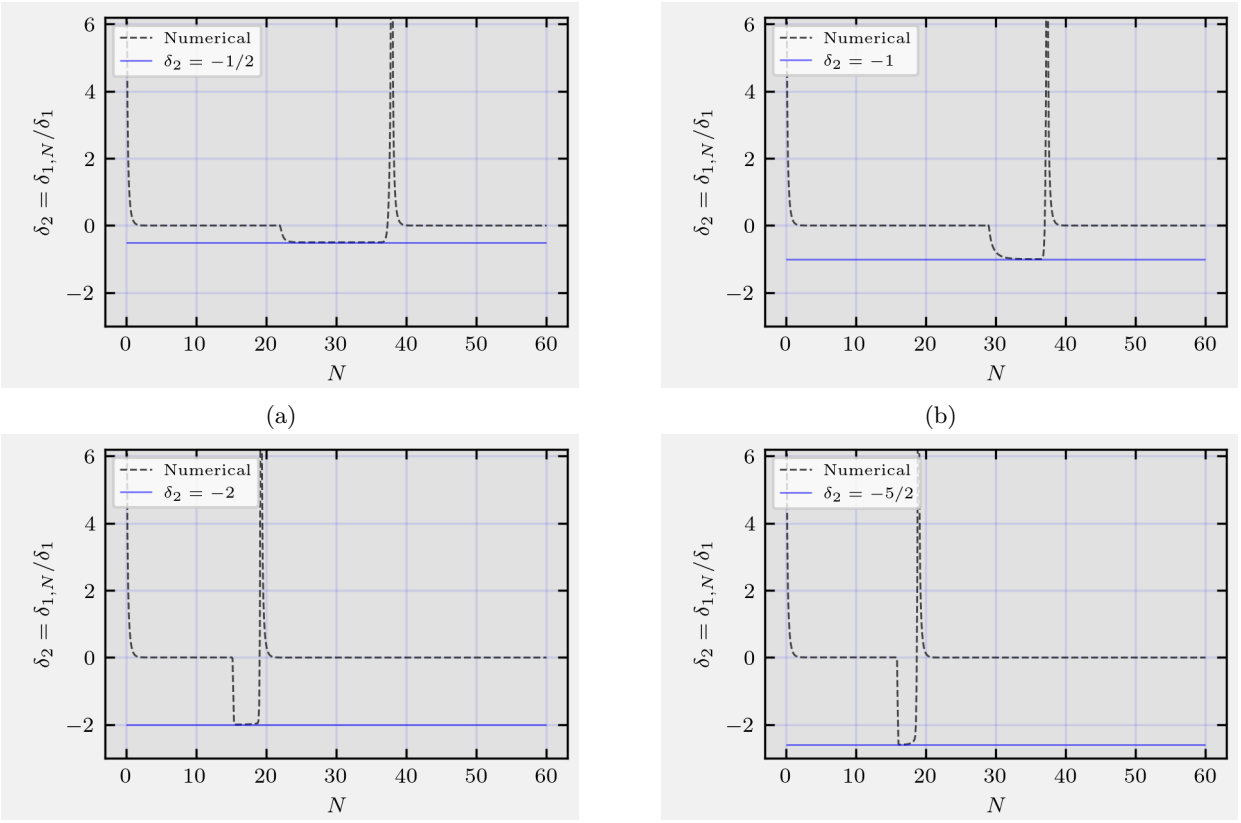

Figure 4.3: Time evolution of the slow-roll parameter δ_2 in the case $\gamma = 10^{-4}$ for different values of the parameter $n = \{1, 2, 4, 5\}$, correspondingly with subfigures (a), (b), (c), (d).

scalar-induced gravitational waves as did at the end of the previous Chapter. We follow the same procedure discussed in Section 3.3. In Tab. 4.3 we present the best-fit parameters for both the cases $\gamma = 10^{-2}$ and $\gamma = 10^{-4}$. In Figs. (4.5, 4.6) instead, we show the marginal distribution of the parameter α. We clearly notice, in analogy with Fig. 3.8 for the minimally coupled case that the values that best represent the growth of the spectrum are given by $n = 1$ and $n = 5$, where we have initial growth of the spectrum proportional to k^4 and secondary slope dependent on the attractor solution for the transient phase (4.3.13). We note that for the larger value of γ, $n = 1$ seems to be slightly favoured by observations. Indeed for smaller values of γ one should recover the behaviour of GR and $n = 1$ is shifted to the right w.r.t. the $\gamma = 10^{-2}$ case.

γ	n	ΔN	$M_{\rm pbh}^{(\Delta N)}/M_\odot$	$k_{\rm pbh}/{\rm Mpc}^{-1}$	$M_{\rm pbh}/M_\odot$	$f_{\rm pbh}$
10^{-2}	1	36.5	1.38×10^{-14}	1.48×10^{13}	1.41×10^{-14}	4.67×10^{-1}
	2	36.8	8.64×10^{-15}	1.87×10^{13}	8.81×10^{-15}	1.00×10^{-1}
	4	19.8	5.05	7.74×10^{5}	5.12	5.65×10^{-4}
	5	20.2	2.41	1.08×10^{6}	2.62	1.06×10^{-3}
10^{-4}	1	29.1	6.44×10^{-11}	2.18×10^{11}	6.45×10^{-11}	1.63×10^{-2}
	2	38.0	8.38×10^{-16}	5.99×10^{13}	8.55×10^{-16}	5.3×10^{-1}
	4	20.0	3.59	9.18×10^{5}	3.64	1.45×10^{-3}
	5	19.5	8.42	5.99×10^{5}	8.55	7.20×10^{-4}

Table 4.2: Estimate of the mass of the PBH, both using the time duration ΔN between the exit of PBH-forming modes and the exit of CMB modes, through Eq. (2.2.5), and identifying the peak mode $k_{\rm pbh}$ of the spectrum Eq. (2.2.4).

γ	n	$\log_{10} A$	α	β	$\log_{10} k_p/{\rm Mpc}^{-1}$
10^{-2}	1	-1.880 ± 0.005	1.29 ± 0.03	3.6 ± 0.2	13.18 ± 0.03
	2	-1.927 ± 0.009	1.90 ± 0.03	3.3 ± 0.2	13.23 ± 0.03
	4	-1.74 ± 0.02	1.96 ± 0.03	3.2 ± 0.2	5.86 ± 0.05
	5	-1.749 ± 0.006	1.33 ± 0.05	3.6 ± 0.4	6.03 ± 0.03
10^{-4}	1	-1.81 ± 0.01	1.09 ± 0.04	3.8 ± 0.2	13.97 ± 0.03
	2	-1.88 ± 0.02	1.88 ± 0.02	3.1 ± 0.2	13.75 ± 0.04
	4	-1.748 ± 0.008	1.80 ± 0.03	3.3 ± 0.2	5.96 ± 0.03
	5	-1.74 ± 0.02	1.30 ± 0.06	3.3 ± 0.8	5.76 ± 0.08

Table 4.3: Fit of the power spectrum for a BPL form for models presented in Fig. 4.4.

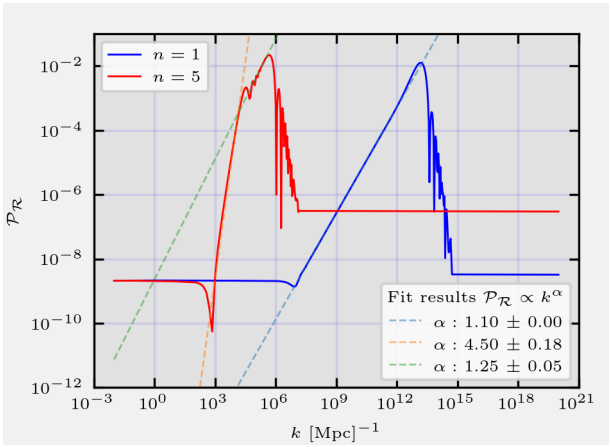

(a)

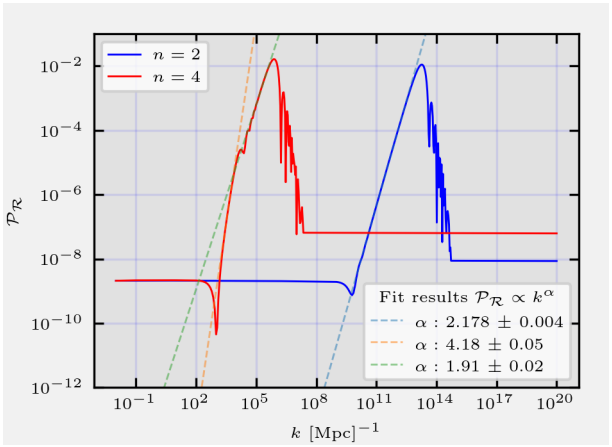

(b)

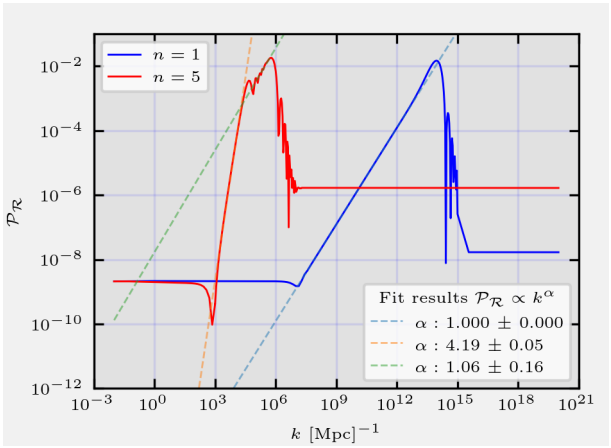

(c)

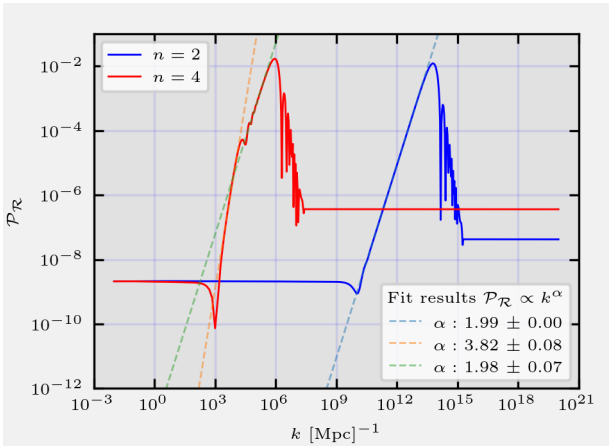

(d)

Figure 4.4: Power spectra of the comoving curvature perturbation for the cases $n = \{1, 5\}$ and $n = \{2, 4\}$. The first two subfigures (a) and (b) refer to $\gamma = 10^{-2}$ and the last two (c), (d) to $\gamma = 10^{-4}$. We can notice a relative spectrum enhancement, $\Delta\mathcal{P}_\mathcal{R} \sim 10^7$, between large CMB and small PBH-formation scales. For both the cases $n = \{1, 2\}$, the power index satisfies the relation (3.2.25). For $n = \{4, 5\}$ instead, we have an initial maximum growth proportional to k^4.

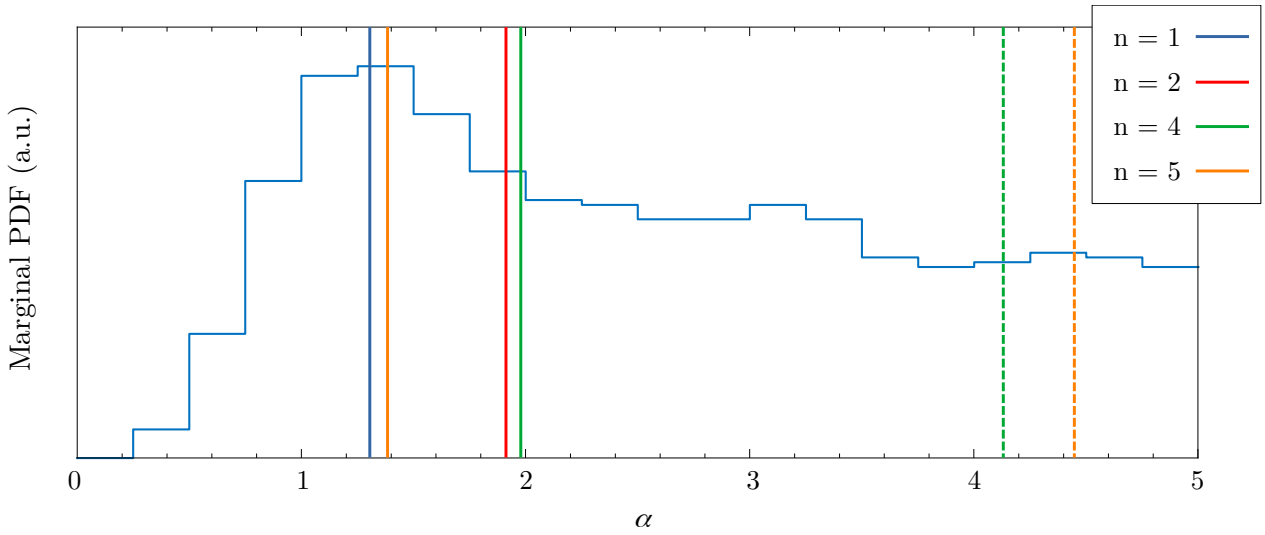

Figure 4.5: Marginal distribution of the parameter α obtained from the Bayesan analysis performed in [95]. We superimpose the results obtained from the fit of the growth of the power spectra for our inflationary models. The solid lines reproduce the best-fit values of α listed in Tab. 4.3, for $\gamma = 10^{-2}$, while the dashed ones correspond to the estimated values of α, assuming that the peak is reached with the maximum possible steep of the growth proportional to k^4, presented in Fig. 4.4 for $\gamma = 10^{-2}$.

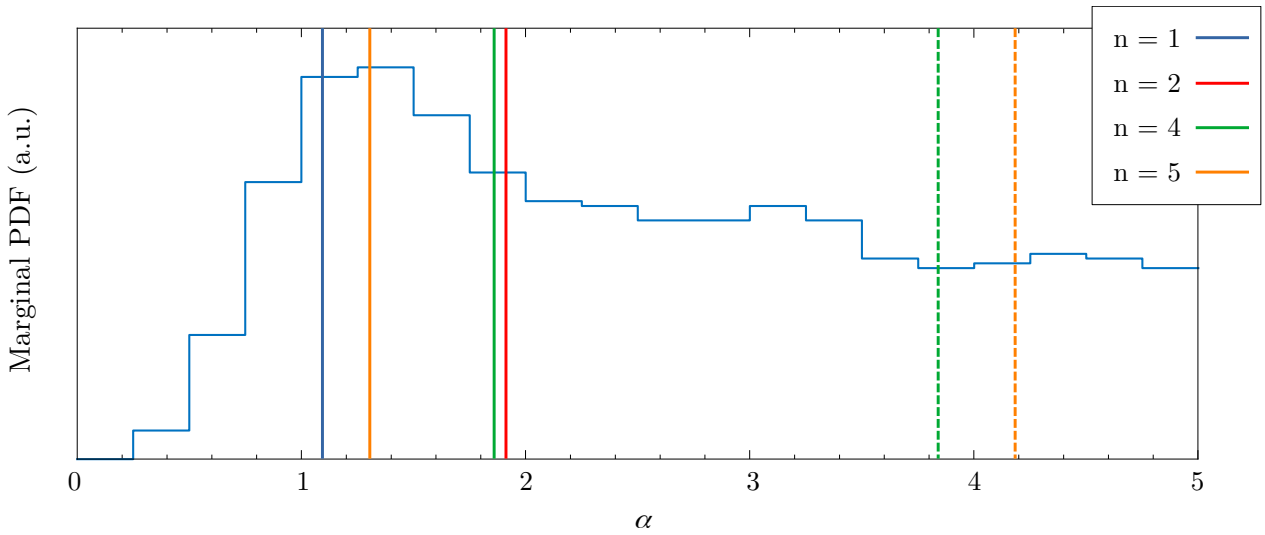

Figure 4.6: Marginal distribution of the parameter α obtained from the Bayesan analysis performed in [95]. We superimpose the results obtained from the fit of the growth of the power spectra for our inflationary models. The solid lines reproduce the best-fit values of α listed in Tab. 4.3, for $\gamma = 10^{-4}$, while the dashed ones correspond to the estimated values of α, assuming that the peak is reached with the maximum possible steep of the growth proportional to k^4, presented in Fig. 4.4 for $\gamma = 10^{-4}$.

Conclusions

In this thesis, we analyzed two different inflationary scenarios which investigate the consequences of a transient phase in the inflaton evolution and its effect on the primordial inflationary spectrum of scalar perturbations. These transients have been studied in recent years as a possible source for the amplification of the curvature power spectrum. We notice that if the amplitude of scalar perturbations grows large enough at small energy scales, it may induce gravitational collapse and seed the formation of compact astrophysical objects, such as primordial black holes (PBHs) after inflation ends. Since the first detection of gravitational waves in 2015, PBHs have attracted much interest. Indeed, PBHs could explain some of the LIGO/Virgo/Kagra collaboration black hole mergers and they could also have an important role in understanding inflationary cosmology. They could significantly contribute to or even entirely constitute dark matter, they may be related to baryogenesis, seeded supermassive black holes at the center of galaxies, and may as well have significantly modified the formation and growth of structures through the universe's history.

In Chapter 1, we introduced the shortcomings of the standard Hot Big Bang model, starting with a brief introduction of the FLRW metric for the description of a homogeneous and isotropic universe. We discussed how an early period of inflation could solve the "flatness" and "horizon" problems and how to realize a simple model of inflation by introducing a scalar field, the inflaton, minimally coupled to gravity. Using as a simple example the fluctuations of a generic massless scalar field, we showed how to perform their quantization on a curved spacetime. Subsequently, we studied how scalar and tensor fluctuations evolved during this early stage of the universe. We dealt with the problem of gauge invariance and derived the evolution equations for the gauge-invariant quantities in the context of inflation, in particular, the Mukhanov-Sasaki equation. We defined some fundamental quantities such as the power spectrum $\mathcal{P}$ for both scalar and tensorial perturbations, used for studying their statistical properties and comparing them with CMB observations.

Then, we gave an overview of the principal features of PBHs in Chapter 2. We discussed their production mechanism in the standard scenario. Using the definition of the comoving curvature perturbations $\mathcal{R}_k$, we showed how formation requires they exit the observable horizon during inflation undergoing an amplification. Once they re-enter the horizon, possibly after re-heating, as density perturbations δ, gravitational forces activate and PBHs may be created through collapse. We reviewed the principal assumptions of this collapse procedure, estimating the requirements necessary for it to occur and we estimated the threshold for collapse δ_c. Then, we examined other important properties of PBHs, like their mass at formation time. This quantity can be related to the characteristic size of perturbations leaving the horizon during inflation. We obtained the density fraction of PBH at the epoch of formation and its dependence on the distribution of density perturbations.

The Press-Schechter formalism was also illustrated. Finally, we analyzed the principal constraints on PBHs abundance, coming from different astrophysical sources and recent experimental activities. These limits allow an interesting mass window for PBHs that could explain all the dark matter of the universe: $\left[10^{-16} - 10^{-10}\right] M_{\odot}$

In Chapter 3 we illustrated the mechanism for the amplification of fluctuations in the context of inflation driven by a minimally coupled inflaton. We performed a model-independent analysis, reviewing different possible realizations considered by the literature. Two are the possible realizations considered: indeed the amplification may be due to the existence of a growing solution to the Mukhanov-Sasaki equation for the curvature perturbations, or simply a consequence of a blue-tilted spectrum in the absence of the growing solution. We reviewed a reconstruction method for the inflaton potential to obtain the amplification starting from a general form of the Hubble parameter $H = H(a)$. We studied in detail the transient evolution induced by such a potential, focusing on the stability of the solutions for different values of the parameter n. In particular, we found that solutions with $n > 3$ are not stable and in order to have the growing solution we need to impose some constraints on the initial condition of the amplification phase. We applied these results to the construction of complete models of inflation that take into account the constraints at large length scale, coming from the CMB observations, and lead to the production of PBHs at smaller scales, with an amplification of $\Delta\mathcal{P}_{\mathcal{R}} \sim 10^7$. We evaluated the abundances of PBHs from our numerical simulations. Finally, we compared these models to some of the recent PTA datasets analysis. Fitting the resulting power spectra with a broken power law form we obtained that inflationary models described by $n = 1$ and $n = 5$, if the latter evolves on the stable attractor close to the peak of maximum amplitude, seem to be mildly favoured in fitting the constraints for the production of SIGW.

Finally, in Chapter 4, we generalize the problem of the enhancement of the primordial spectrum in the context of inflation with a non-minimally coupled scalar field. We take the Induced-Gravity model as a working example, describing the homogenous dynamics in terms of the more general Hubble and scalar field flow functions hierarchies. We reviewed the reconstruction method for the inflaton potential, following the "superpotential" mechanism. In this way, we were able to determine a transient stage of evolution for the scalar field that has a de Sitter universe as the limit. We then chose a simple description of the potential by truncating the Taylor expansion of field function Y to the quadratic order and verified the late-time properties of the slow-roll parameters, in order to have an analytical estimate for the power spectrum amplification. Then, we verified the stability of the transient evolution for the scalar field in the reconstructed models on varying the parameter of the inflaton potential. We found a result analogous to Chapter 3. Indeed, solutions with $n > 3$ are not stable. This fact should be considered to reproduce the desired inflaton evolution. In order to study complete models of inflation in the IG context, we considered two different values for the non-minimal coupling γ. By describing the slow-roll phases with a Landau-Ginzburg potential we satisfied CMB constraints. By numerically solving the homogeneous dynamics and the Mukhanov-Sasaki equation we finally evaluated the power spectrum for different cases of interest, calculating also the corresponding estimates for the PBH mass and abundance. Finally, employing the PTAs analysis in [95], we fitted and compared our spectra with the marginal distribution of the growth

steepness parameter α. For both values of the non-minimal coupling, and similarly to the results obtained in the context of the minimal coupling scenario, potentials described by $n = 1$ and $n = 5$ are mildly favoured compared with experimental data.

The procedure discussed in this thesis can be certainly adapted to study the evolution of inflationary models in different scenarios such as $f(R)$ gravity theories and non-canonical models, where the inflaton's kinetic term has a non-standard form. These applications are left for future work. Moreover, a more refined reconstruction of the complete inflaton potential should be certainly performed as a next step. Let us note that the numerical analysis complements the analytical reconstruction of potentials leading to an amplification. Indeed, in the presence of a growing solution of the Mukhanov-Sasaki equation, an analytic approximate estimate of the primordial spectra cannot be fulfilled as is commonly done in the case of SR.

Appendix A

Solving the Mukhanov-Sasaki equation: Numerical procedure

We briefly discuss the algorithm used to numerically solve the Mukhanov-Sasaki (MS) equation, and obtain the comoving curvature perturbation $\mathcal{R}_k$. The final goal is to obtain the scalar power spectrum in the inflationary scenarios described in Chapters 3 and 4.

We start then from Eq. (1.4.94) for the field variable v_k, defined as $v_k = \mathcal{R}_k/z$. In the minimally coupled case we have $z \propto a\sqrt{\epsilon_1}$ while in the IG scenario

$$z \propto a\varphi\,\delta_1\sqrt{\frac{1+6\gamma}{(1+\delta_1)^2}}\,. \tag{A.0.1}$$

We then solve numerically the equation mode by mode, to obtain the evolution in time of v_k, through which we evaluate the power spectrum, using the general formula

$$\mathcal{P}_{\mathcal{R}}(k) = \frac{k^3}{2\pi^2}\left|\frac{v_k}{z}\right|^2\,. \tag{A.0.2}$$

We start by simplifying the highly oscillatory behaviour of the Bunch-Davies vacuum initial conditions (1.4.28)

$$\lim_{\eta\to-\infty} v_k = \frac{1}{\sqrt{2k}}\,e^{ik\eta}\,, \qquad \lim_{\eta\to-\infty} v_k' = i\sqrt{\frac{k}{2}}\,e^{ik\eta}\,. \tag{A.0.3}$$

For this purpose, we define a new dimensionless function $\bar{v}_k$ through the relation

$$v_k(\eta) = \frac{\bar{v}_k(\eta)}{\sqrt{2k}}\,e^{-ik\eta}\,, \tag{A.0.4}$$

and we rewrite the MS equation as

$$\bar{v}_k''(\eta) - 2ik\,v_k'(\eta) - \frac{z''}{z}\,\bar{v}_k(\eta) = 0\,. \tag{A.0.5}$$

We shall use the number of *e-folds* N as a the "time" variable for our integration, and then rewrite

conformal-time derivative in terms of the number of e-folds using $\mathrm{d}N = aH\,\mathrm{d}\eta$. Doing so we obtain

$$\frac{\mathrm{d}^2\bar{v}_k}{\mathrm{d}N^2} + \left[(1-\epsilon_1) - 2i\frac{k}{aH}\right]\frac{\mathrm{d}v_k}{\mathrm{d}N} - f_{\mathrm{MS}}\,\bar{v}_k = 0\,. \tag{A.0.6}$$

The function f_{MS} depends on the slow-roll paramters in both GR and IG, in particular we have

$$f_{\mathrm{MS}}^{(\mathrm{GR})} = 2 - \epsilon_1 + \epsilon_2\left(\frac{3}{2} + \frac{\epsilon_2}{4} - \frac{\epsilon_1}{2} + \frac{\epsilon_3}{2}\right) \tag{A.0.7}$$

in the GR case and

$$f_{\mathrm{MS}}^{(\mathrm{IG})} = \delta_1^2 + \delta_2^2 + (3-\epsilon_1)(\delta_1+\delta_2+1)\delta_2\delta_3 + \frac{\delta_1\delta_2}{1+\delta_1}\left(\epsilon_1 + \delta_1 - 3\delta_2 - \delta_3 + \frac{2\delta_1\delta_2}{1+\delta_1} - 2\right) - 1 \tag{A.0.8}$$

in the IG one. In terms of N the scale factor is $a(N) = a_0\,e^N$. The Hubble rate is obtained inverting respectively (3.2.12) and (4.1.3) and obtaining

$$H^{(\mathrm{GR})} = H_0\sqrt{\frac{V}{M_{\mathrm{P}}^2\,(3-\epsilon_1)}}\,, \tag{A.0.9}$$

$$H^{(\mathrm{IG})} = \sqrt{\frac{V}{3M_{\mathrm{P}}^2\,\varphi^2\,\gamma}\left(1 + 2\delta_1 - \frac{1}{6\gamma}\delta_1^2\right)^{-1}}\,, \tag{A.0.10}$$

which both depend on the time evolution of the scalar field φ. The evolution of the scalar field is obtained by solving the Klein-Gordon equations (3.2.34) and (4.3.3) respectively for the cases of GR and IG.

Our initial conditions for the function v_k and v_k', considered to be the Bunch-Davies conditions, are now

$$\bar{v}_k(N)|_{\mathrm{in}} = 1\,, \qquad \bar{v}_k'(N)|_{\mathrm{in}} = aH\frac{\mathrm{d}\bar{v}_k}{\mathrm{d}N}(N)\bigg|_{\mathrm{in}} = 0\,. \tag{A.0.11}$$

Once the background evolution is calculated numerically in terms of e-folds number N, the MS equation can be solved numerically as well for each k mode, in terms of the rescaled variable (A.0.4), using the initial conditions (A.0.11). Each mode starts its evolution deep inside the horizon $k^2 \gg z''/z$, where the solution to (A.0.6) is highly oscillatory and numerical computation are costly. Typically, however, it is enough to initialize the modes at some time such that they are sufficiently inside the horizon, where, the BD condition is still valid[1] to a very good approximation.For this purpose, we choose to evolve each mode by setting the initial time as

$$N_{\mathrm{in}}^{(k)} = N_0^{(k)} - 5\,, \tag{A.0.12}$$

where the "k" super-script indicates the intrinsic mode dependence for the choice of N_{in}^k and $N_0^{(k)}$ denotes the horizon crossing time $k = a(N_0^{(k)})\,H(N_0^{(k)})$. Having then obtained the individual mode

[1] Unless modes undergo resonance and get excited deep inside the horizon, the choice of initial condition in Eqs. (A.0.11) and (A.0.12) provide an accurate prescription for the initialization of the numerical evaluation.

evolution from $N_{\rm in}^{(k)}$ to $N_{\rm end} = 60$, the power spectrum can be described as

$$\mathcal{P}_{\mathcal{R}}(k) = \frac{k^2}{4\pi^2\, M_{\rm p}^2\, a^2(N_{\rm end})\, \epsilon_1(N_{\rm end})}\, |\bar{v}_k(N_{\rm end})|^2 \ . \tag{A.0.13}$$

In order to set the overall normalization of the power spectrum we need to determine a_0 w.r.t $M_{\rm p}$. We do so by requiring the normalization of the power spectrum indicated by Planck at the pivot scale $k_{\rm CMB} = 0.05\,{\rm Mpc}^{-1}$ using $\mathcal{P}_{\mathcal{R}}(k_{\rm CMB}) \simeq 2.1 \times 10^{-9}$.

Appendix B

Analytic estimate for the threshold of collapse

In this short appendix, we provide an analytic estimate of the characteristic value of the collapse threshold for PBH formation during RDU, closely following [31]. For this purpose, we take the background space-time after inflation to have the spatially flat FLRW form (1.1.1) and so the evolution of the scale factor is described by the Friedmann equation (1.1.5): $3H^2M_{\rm P}^2 = \rho(t)$. It follows from the theory of peaks of random fields in the Gaussian approximation [113] that extreme peaks tend to be spherical. Therefore, it is reasonable to consider a locally perturbated, spherical symmetric region in the universe that is initially outside the horizon and will later collapse to form a PBH upon horizon re-entry. The metric describing such a region can be written as

$$\mathrm{d}s^2 = \mathrm{d}t^2 - a^2(t)\, e^{-2\mathcal{R}(\hat{r})} \left[\mathrm{d}\hat{r}^2 + \hat{r}^2 \left(\mathrm{d}\theta^2 + \sin^2\theta \mathrm{d}\varphi^2\right)\right] \tag{B.0.1}$$

where now $\mathcal{R} < 0$ is the non-linear generalization of the conserved comoving perturbation defined on a super-Hubble scales [114]. At large distances $\hat{r} \to \infty$, curvature perturbation is assumed to vanish ($\mathcal{R} \to 0$) so that the universe is described by a spatially flat FLRW metric. By making the coordinate redefinition, $r = \hat{r}\, e^{-\mathcal{R}(\hat{r})}$, the metric describing the spherical perturbed region (B.0.1) can be transformed into that of a closed universe with positive spatial curvature

$$\mathrm{d}s^2 = \mathrm{d}t^2 - a^2(t) \left[\frac{\mathrm{d}r^2}{1 - K(r)\, r^2} - r^2 \left(\mathrm{d}^2\theta + \sin^2\theta \mathrm{d}^2\varphi\right)\right] \tag{B.0.2}$$

where we used K to identify the curvature and the relation between perturbations of the two metrics is given by $K(r)r^2 = \hat{r}\, \mathcal{R}'(\hat{r})\ (2 - \hat{r}\mathcal{R}'(\hat{r}))$, showing that the local spatial curvature is related to the first order derivatives of the curvature perturbation $\mathcal{R}(\hat{r})$. Ignoring higher order spatial derivatives of K, the evolution of the spherical region is given by the 00 component of the Einstein equations (1.1.3)

$$H^2 \equiv \frac{\rho_{\rm tot}}{3\, M_{\rm P}^2} = \frac{\rho(t)}{3\, M_{\rm P}^2} - \frac{K(r)}{a} \tag{B.0.3}$$

which is equivalent to the evolution of a closed universe (1.1.18) with a small perturbation $\delta\rho$ induced by the spatial curvature $K(r)$:

$$\delta \equiv \frac{\rho_{\rm tot} - \rho}{\rho} = \frac{\delta\rho}{\rho} = \frac{K(r)}{a^2\, H^2}\,, \tag{B.0.4}$$

where $\rho(t) = 3H^2\, M_{\rm P}^2$. Considering (B.0.3), since radiation density dilutes faster than $\rho \propto a^{-4}$, a local spherical region with $K > 0$ will eventually stop expanding and begin collapsing to form a PBH. This leads to a breakdown of the separate universe approximation, precisely when the right-hand-side of Eq. (B.0.3) becomes negative, *i.e.* when $3K = a^2 = \frac{\rho}{M_{\rm P}^2}$ or $\delta = 1$ at the time called $t = t_c$. Since only the modes corresponding to scales larger than the Jeans length ($k_J = aH/c_s$) can collapse, we identify $k^2 = a^2H^2/c_s^2$. Therefore, we have

$$\delta(t_c) = \frac{K}{k^2}\,\frac{k^2}{a^2H^2} = \frac{K}{c_s^2k^2} = 1\,, \tag{B.0.5}$$

which leads to $K = c_s^2k^2$. This means that at the horizon crossing time of the relevant perturbation (i.e. when $k^2 = a_f^2H_f^2$), the only perturbations which can collapse must have a density contrast larger than

$$\delta_c = \frac{K}{(a_f\, H_f)^2} = c_s^2\left(\frac{k}{a_f\, H_f}\right)^2 = c_s^2\,. \tag{B.0.6}$$

Bibliography

[1] N. Aghanim *et al.* (Planck Collaboration). "Plack 2018 results, VI. Cosmological parameters". In: *Astron. Astrphys* 641.A6 (2020). DOI: https://doi.org/10.1051/0004-6361/201833910 (cit. on pp. 4, 10, 35, 41, 42).

[2] Ya. B. Zel'dovich and I. D. Novikov. "The hypothesis of cores retarded during expansion and the hot cosmological model". In: *Soviet Astronomy (English Translation)* 10 (1967) (cit. on p. 4).

[3] S. Hawking. "Gravitationally collapsed objects of very low mass". In: *Monthly Notices of the Royal Astronomical Society* 152.1 (1971). DOI: https://doi.org/10.1093/mnras/152.1.75 (cit. on p. 4).

[4] B. J. Carr and S. Hawking. "Black Holes in the early Universe". In: *Monthly Notices of the Royal Astronomical Society* 168.2 (1974). DOI: https://doi.org/10.1093/mnras/168.2.399 (cit. on p. 4).

[5] G. F. Chapline. "Cosmological effects of primordial black holes". In: *Nature* (5489 1975). DOI: 10.1038/253251a0 (cit. on p. 4).

[6] E. Aubourg et al. "Evidence for gravitational microlensig by dark objects in the Galactic halo". In: *Nature* (Oct. 1993). DOI: 10.1038/365623a0 (cit. on p. 5).

[7] P. Tisserand et al. "Limits on the Macho Content of the Galactic Halo from the EROS-2 Survey of the Magellanic Clouds". In: *Astron. Astrophys.* 469 (2007), pp. 387–404. DOI: 10.1051/0004-6361:20066017. arXiv: astro-ph/0607207 (cit. on p. 5).

[8] Ł. Wyrzykowski et al. "The OGLE view of microlensing towards the Magellanic Clouds – III. Ruling out subsolar MACHOs with the OGLE-III LMC data*". In: *Monthly Notices of the Royal Astronomical Society* 413.1 (Apr. 2011), pp. 493–508. ISSN: 0035-8711. DOI: 10.1111/j.1365-2966.2010.18150.x. URL: https://doi.org/10.1111/j.1365-2966.2010.18150.x (cit. on p. 5).

[9] L. Wyrzykowski et al. "The OGLE view of microlensing towards the Magellanic Clouds – IV. OGLE-III SMC data and final conclusions on MACHOs*". In: *Monthly Notices of the Royal Astronomical Society* 416.4 (Sept. 2011), pp. 2949–2961. ISSN: 0035-8711. DOI: 10.1111/j.1365-2966.2011.19243.x. URL: https://doi.org/10.1111/j.1365-2966.2011.19243.x (cit. on p. 5).

[10] B. P. Abbot *et al.* (LIGO Scientific Collaboration and Virgo Collaboration). "Observation of Gravitational Waves from a Binary Black Hole Merger". In: *Phys. Rev. D* 116.061102 (). DOI: https://doi.org/10.1103/PhysRevLett.116.061102 (cit. on pp. 5, 41).

[11] J. Garcia-Bellido and E. Ruiz Morales. "Primordial black holes from singe-field models of inflation". In: *Phys. Dark Univ.* 17 (2017), pp. 47–54. DOI: https://doi.org/10.1016/j.dark.2017.09.007 (cit. on pp. 5, 51).

[12] Leonardo Chataignier et al. "Reconstruction methods and the amplification of the inflationary spectrum". In: *Physical Review D* 107.8 (Apr. 2023). ISSN: 2470-0029. DOI: 10.1103/physrevd.107.083506. URL: http://dx.doi.org/10.1103/PhysRevD.107.083506 (cit. on pp. 5, 82, 83).

[13] Alexander Y. Kamenshchik, Alessandro Tronconi, and Giovanni Venturi. "DBI inflation and warped black holes". In: *Journal of Cosmology and Astroparticle Physics* 2022.01 (Jan. 2022), p. 051. ISSN: 1475-7516. DOI: 10.1088/1475-7516/2022/01/051. URL: http://dx.doi.org/10.1088/1475-7516/2022/01/051 (cit. on p. 5).

[14] Alexander Y. Kamenshchik et al. "Non-canonical inflation and primordial black holes production". In: *Physics Letters B* 791 (Apr. 2019), pp. 201–205. ISSN: 0370-2693. DOI: 10.1016/j.physletb.2019.02.036. URL: http://dx.doi.org/10.1016/j.physletb.2019.02.036 (cit. on p. 5).

[15] Gabriella Agazie et al. "The NANOGrav 15 yr Data Set: Observations and Timing of 68 Millisecond Pulsars". In: *Astrophys. J. Lett.* 951.1 (2023), p. L9. DOI: 10.3847/2041-8213/acda9a. arXiv: 2306.16217 [astro-ph.HE] (cit. on pp. 5, 71).

[16] Gabriella Agazie et al. "The NANOGrav 15 yr Data Set: Evidence for a Gravitational-wave Background". In: *Astrophys. J. Lett.* 951.1 (2023), p. L8. DOI: 10.3847/2041-8213/acdac6. arXiv: 2306.16213 [astro-ph.HE] (cit. on pp. 5, 71).

[17] Andrew Zic et al. "The Parkes Pulsar Timing Array Third Data Release". In: (June 2023). arXiv: 2306.16230 [astro-ph.HE] (cit. on pp. 5, 71).

[18] Daniel J. Reardon et al. "Search for an Isotropic Gravitational-wave Background with the Parkes Pulsar Timing Array". In: *Astrophys. J. Lett.* 951.1 (2023), p. L6. DOI: 10.3847/2041-8213/acdd02. arXiv: 2306.16215 [astro-ph.HE] (cit. on pp. 5, 71).

[19] J. Antoniadis et al. "The second data release from the European Pulsar Timing Array - I. The dataset and timing analysis". In: *Astron. Astrophys.* 678 (2023), A48. DOI: 10.1051/0004-6361/202346841. arXiv: 2306.16224 [astro-ph.HE] (cit. on pp. 5, 71).

[20] J. Antoniadis et al. "The second data release from the European Pulsar Timing Array - III. Search for gravitational wave signals". In: *Astron. Astrophys.* 678 (2023), A50. DOI: 10.1051/0004-6361/202346844. arXiv: 2306.16214 [astro-ph.HE] (cit. on pp. 5, 71).

[21] Heng Xu et al. "Searching for the Nano-Hertz Stochastic Gravitational Wave Background with the Chinese Pulsar Timing Array Data Release I". In: *Res. Astron. Astrophys.* 23.7 (2023), p. 075024. DOI: 10.1088/1674-4527/acdfa5. arXiv: 2306.16216 [astro-ph.HE] (cit. on pp. 5, 71).

[22] Georges Aad et al. “Observation of a new particle in the search for the Standard Model Higgs boson with the ATLAS detector at the LHC”. In: *Phys. Lett. B* 716 (2012), pp. 1–29. DOI: 10.1016/j.physletb.2012.08.020. arXiv: 1207.7214 [hep-ex] (cit. on p. 6).

[23] Fedor L. Bezrukov and Mikhail Shaposhnikov. “The Standard Model Higgs boson as the inflaton”. In: *Phys. Lett. B* 659 (2008), pp. 703–706. DOI: 10.1016/j.physletb.2007.11.072. arXiv: 0710.3755 [hep-th] (cit. on p. 6).

[24] Y. Akrami *et al.* Planck Collaboration. “Plack 2018 results, X. Constraints on inflation”. In: *Astron. Astrphys* 641.A10 (2020). DOI: https://doi.org/10.1051/0004-6361/201833887 (cit. on pp. 6, 37, 39, 61, 62).

[25] Steven Weinberg. *Gravitation and Cosmology: Principles and Applications of the General Theory of Relativity*. New York: John Wiley and Sons, 1972 (cit. on pp. 7, 8, 16).

[26] D. Baumann. *Cosmology*. Cambridge University Press, July 2022 (cit. on pp. 12, 13, 29).

[27] N. Aghanim et al. “Planck 2018 results: V. CMB power spectra and likelihoods”. In: *Astronomy and Astrophysics* 641 (Sept. 2020), A5. ISSN: 1432-0746. DOI: 10.1051/0004-6361/201936386. URL: http://dx.doi.org/10.1051/0004-6361/201936386 (cit. on p. 13).

[28] Jerome Martin, Christophe Ringeval, and Vincent Vennin. “Encyclopædia Inflationaris”. In: *Phys. Dark Univ.* 5-6 (2014), pp. 75–235. DOI: 10.1016/j.dark.2014.01.003. arXiv: 1303.3787 [astro-ph.CO] (cit. on pp. 19, 20).

[29] V.F. Mukhanov, H.A. Feldman, and R.H. Brandenberger. “Theory of cosmological perturbations”. In: *Physics Reports* 215.5 (1992), pp. 203–333. ISSN: 0370-1573. DOI: https://doi.org/10.1016/0370-1573(92)90044-Z. URL: https://www.sciencedirect.com/science/article/pii/037015739290044Z (cit. on pp. 26, 31, 33).

[30] A. Riotto. *In ation and the Theory of Cosmological Perturbations*. June 2017. URL: arXiv:hep-ph/0210162v2 (cit. on pp. 34, 35).

[31] G. Franciolini. *Primordial Black Holes: from Theory to Gravitational Wave Observations*. 2021. arXiv: 2110.06815 [astro-ph.CO] (cit. on pp. 38, 43, 45, 103).

[32] B. J. Carr. “The Primordial black hole mass spectrum”. In: *Astrophys. J.* 201 (1975), pp. 1–19. DOI: 10.1086/153853 (cit. on p. 40).

[33] I. Musco. “Threshold for primordial black holes: Dependencies on the shape of the cosmological perturbations”. In: *Phys. Rev. D* 100.125324 (2019). DOI: https://doi.org/10.1103/PhysRevD.100.123524 (cit. on pp. 40, 43).

[34] Tomohiro Nakama, Joseph Silk, and Marc Kamionkowski. “Stochastic gravitational waves associated with the formation of primordial black holes”. In: *Physical Review D* 95.4 (Feb. 2017). ISSN: 2470-0029. DOI: 10.1103/physrevd.95.043511. URL: http://dx.doi.org/10.1103/PhysRevD.95.043511 (cit. on p. 40).

[35] O. Özsoy and G. Tasinato. *Inflation and Primordial Black Holes*. In: *Universe* vol. 9 (5 2023). DOI: https://doi.org/10.3390/universe9050203 (cit. on pp. 41, 42, 50, 52).

[36] Kazunori Akiyama et al. "First Sagittarius A* Event Horizon Telescope Results. I. The Shadow of the Supermassive Black Hole in the Center of the Milky Way". In: *Astrophys. J. Lett.* 930.2 (2022), p. L12. DOI: 10.3847/2041-8213/ac6674. arXiv: 2311.08680 [astro-ph.HE] (cit. on p. 41).

[37] W. H. Press and P. Schechter. "Formation of galaxies and clusters of galaxies by selfsimilar gravitational condensation". In: *Astrophys. J.* 187 (1974), pp. 425–438. DOI: 10.1086/152650 (cit. on p. 43).

[38] Albert Escrivà. "PBH Formation from Spherically Symmetric Hydrodynamical Perturbations: A Review". In: *Universe* 8.2 (Jan. 2022), p. 66. ISSN: 2218-1997. DOI: 10.3390/universe8020066. URL: http://dx.doi.org/10.3390/universe8020066 (cit. on p. 43).

[39] C. T. Brynes S. Young and M. Sasaki. "Calculating the mass fraction of primordial black holes". In: *JCAP* 07 (2014). DOI: 10.1088/1475-7516/2014/07/045 (cit. on p. 44).

[40] Bernard Carr et al. "Constraints on primordial black holes". In: *Reports on Progress in Physics* 84.11 (Nov. 2021), p. 116902. ISSN: 1361-6633. DOI: 10.1088/1361-6633/ac1e31. URL: http://dx.doi.org/1088/1361-6633/ac1e31 (cit. on pp. 45, 46).

[41] Eleni Bagui et al. "Primordial black holes and their gravitational-wave signatures". In: (Oct. 2023). arXiv: 2310.19857 [astro-ph.CO] (cit. on pp. 45, 46).

[42] Bernard Carr et al. "Primordial black hole constraints for extended mass functions". In: *Physical Review D* 96.2 (July 2017). ISSN: 2470-0029. DOI: 10.1103/physrevd.96.023514. URL: http://dx.doi.org/10.1103/PhysRevD.96.023514 (cit. on p. 45).

[43] V. De Luca et al. "Constraints on primordial black holes: The importance of accretion". In: *Physical Review D* 102.4 (Aug. 2020). ISSN: 2470-0029. DOI: 10.1103/physrevd.102.043505. URL: http://dx.doi.org/10.1103/PhysRevD.102.043505 (cit. on p. 45).

[44] B V Vainer and P D Nasel'skii. "Cosmological implications of the process of primordial black hole evaporation". In: *Sov. Astron. AJ (Engl. Transl.); (United States)* (Mar. 1978). URL: https://www.osti.gov/biblio/6638523 (cit. on p. 46).

[45] Patrick Stöcker et al. "Exotic energy injection with ExoCLASS: Application to the Higgs portal model and evaporating black holes". In: *JCAP* 03 (2018), p. 018. DOI: 10.1088/1475-7516/2018/03/018. arXiv: 1801.01871 [astro-ph.CO] (cit. on p. 46).

[46] Alexandre Arbey, Jérémy Auffinger, and Joseph Silk. "Constraining primordial black hole masses with the isotropic gamma ray background". In: *Physical Review D* 101.2 (Jan. 2020). ISSN: 2470-0029. DOI: 10.1103/physrevd.101.023010. URL: http://dx.doi.org/10.1103/PhysRevD.101.023010 (cit. on p. 46).

[47] Mathieu Boudaud and Marco Cirelli. "Voyager 1 $e^{\pm}$ Further Constrain Primordial Black Holes as Dark Matter". In: *Phys. Rev. Lett.* 122.4 (2019), p. 041104. DOI: 10.1103/PhysRevLett.122.041104. arXiv: 1807.03075 [astro-ph.HE] (cit. on p. 46).

[48] William DeRocco and Peter W. Graham. "Constraining Primordial Black Hole Abundance with the Galactic 511 keV Line". In: *Physical Review Letters* 123.25 (Dec. 2019). ISSN: 1079-7114. DOI: 10.1103/physrevlett.123.251102. URL: http://dx.doi.org/10.1103/PhysRevLett.123.251102 (cit. on p. 46).

[49] Ranjan Laha, Julian B. Muñoz, and Tracy R. Slatyer. "INTEGRAL constraints on primordial black holes and particle dark matter". In: *Phys. Rev. D* 101.12 (2020), p. 123514. DOI: 10.1103/PhysRevD.101.123514. arXiv: 2004.00627 [astro-ph.CO] (cit. on p. 46).

[50] Hiroko Niikura et al. "Microlensing constraints on primordial black holes with Subaru/HSC Andromeda observations". In: *Nature Astronomy* 3.6 (Apr. 2019), pp. 524–534. ISSN: 2397-3366. DOI: 10.1038/s41550-019-0723-1. URL: http://dx.doi.org/10.1038/s41550-019-0723-1 (cit. on pp. 47, 49).

[51] C. Alcock et al. "The MACHO Project: Microlensing Detection Efficiency". In: *The Astrophysical Journal Supplement Series* 136.2 (Oct. 2001), pp. 439–462. ISSN: 1538-4365. DOI: 10.1086/322529. URL: http://dx.doi.org/10.1086/322529 (cit. on p. 47).

[52] Masamune Oguri et al. "Understanding caustic crossings in giant arcs: Characteristic scales, event rates, and constraints on compact dark matter". In: *Physical Review D* 97.2 (Jan. 2018). ISSN: 2470-0029. DOI: 10.1103/physrevd.97.023518. URL: http://dx.doi.org/10.1103/PhysRevD.97.023518 (cit. on p. 47).

[53] Hiroko Niikura et al. "Constraints on Earth-mass primordial black holes from OGLE 5-year microlensing events". In: *Physical Review D* 99.8 (Apr. 2019). ISSN: 2470-0029. DOI: 10.1103/physrevd.99.083503. URL: http://dx.doi.org/10.1103/PhysRevD.99.083503 (cit. on p. 47).

[54] Miguel Zumalacarregui and Uros Seljak. "Limits on stellar-mass compact objects as dark matter from gravitational lensing of type Ia supernovae". In: *Phys. Rev. Lett.* 121.14 (2018), p. 141101. DOI: 10.1103/PhysRevLett.121.141101. arXiv: 1712.02240 [astro-ph.CO] (cit. on p. 47).

[55] Bernard Carr and Joseph Silk. "Primordial black holes as generators of cosmic structures". In: *Monthly Notices of the Royal Astronomical Society* 478.3 (May 2018), pp. 3756–3775. ISSN: 1365-2966. DOI: 10.1093/mnras/sty1204. URL: http://dx.doi.org/10.1093/mnras/sty1204 (cit. on p. 47).

[56] Savvas M. Koushiappas and Abraham Loeb. "Dynamics of Dwarf Galaxies Disfavor Stellar-Mass Black Holes as Dark Matter". In: *Physical Review Letters* 119.4 (July 2017). ISSN: 1079-7114. DOI: 10.1103/physrevlett.119.041102. URL: http://dx.doi.org/10.1103/PhysRevLett.119.041102 (cit. on p. 47).

[57] Timothy D. Brandt. "Constraints on MACHO Dark Matter from Compact Stellar Systems in Ultra-Faint Dwarf Galaxies". In: *Astrophys. J. Lett.* 824.2 (2016), p. L31. DOI: 10.3847/2041-8205/824/2/L31. arXiv: 1605.03665 [astro-ph.GA] (cit. on p. 47).

[58] Pasquale D. Serpico et al. "Cosmic microwave background bounds on primordial black holes including dark matter halo accretion". In: *Physical Review Research* 2.2 (May 2020). ISSN: 2643-1564. DOI: 10.1103/physrevresearch.2.023204. URL: http://dx.doi.org/10.1103/PhysRevResearch.2.023204 (cit. on p. 47).

[59] Daniele Gaggero et al. "Searching for Primordial Black Holes in the radio and X-ray sky". In: *Phys. Rev. Lett.* 118.24 (2017), p. 241101. DOI: 10.1103/PhysRevLett.118.241101. arXiv: 1612.00457 [astro-ph.HE] (cit. on p. 47).

[60] Yoshiyuki Inoue and Alexander Kusenko. "New X-ray bound on density of primordial black holes". In: *JCAP* 10 (2017), p. 034. DOI: 10.1088/1475-7516/2017/10/034. arXiv: 1705.00791 [astro-ph.CO] (cit. on p. 47).

[61] Philip Lu et al. "Constraining Primordial Black Holes with Dwarf Galaxy Heating". In: *Astrophys. J. Lett.* 908.2 (2021), p. L23. DOI: 10.3847/2041-8213/abdcb6. arXiv: 2007.02213 [astro-ph.CO] (cit. on p. 47).

[62] Volodymyr Takhistov et al. "Impacts of Jets and winds from primordial black holes". In: *Mon. Not. Roy. Astron. Soc.* 517.1 (2022), pp. L1–L4. DOI: 10.1093/mnrasl/slac097. arXiv: 2111.08699 [astro-ph.HE] (cit. on p. 47).

[63] Tomohiro Nakama, Bernard Carr, and Joseph Silk. "Limits on primordial black holes from μ distortions in cosmic microwave background". In: *Phys. Rev. D* 97.4 (2018), p. 043525. DOI: 10.1103/PhysRevD.97.043525. arXiv: 1710.06945 [astro-ph.CO] (cit. on p. 48).

[64] Keisuke Inomata, Masahiro Kawasaki, and Yuichiro Tada. "Revisiting constraints on small scale perturbations from big-bang nucleosynthesis". In: *Phys. Rev. D* 94.4 (2016), p. 043527. DOI: 10.1103/PhysRevD.94.043527. arXiv: 1605.04646 [astro-ph.CO] (cit. on p. 48).

[65] Yacine Ali-Haïmoud, Ely D. Kovetz, and Marc Kamionkowski. "Merger rate of primordial black-hole binaries". In: *Phys. Rev. D* 96.12 (2017), p. 123523. DOI: 10.1103/PhysRevD.96.123523. arXiv: 1709.06576 [astro-ph.CO] (cit. on p. 48).

[66] Ville Vaskonen and Hardi Veermäe. "Lower bound on the primordial black hole merger rate". In: *Phys. Rev. D* 101.4 (2020), p. 043015. DOI: 10.1103/PhysRevD.101.043015. arXiv: 1908.09752 [astro-ph.CO] (cit. on p. 48).

[67] V. De Luca et al. "The evolution of primordial black holes and their final observable spins". In: *Journal of Cosmology and Astroparticle Physics* 2020.04 (Apr. 2020), pp. 052–052. ISSN: 1475-7516. DOI: 10.1088/1475-7516/2020/04/052. URL: http://dx.doi.org/10.1088/1475-7516/2020/04/052 (cit. on p. 48).

[68] Zu-Cheng Chen, Chen Yuan, and Qing-Guo Huang. "Pulsar Timing Array Constraints on Primordial Black Holes with NANOGrav 11-Year Dataset". In: *Phys. Rev. Lett.* 124.25 (2020), p. 251101. DOI: 10.1103/PhysRevLett.124.251101. arXiv: 1910.12239 [astro-ph.CO] (cit. on p. 48).

[69] Juan Garcia-Bellido, Marco Peloso, and Caner Unal. "Gravitational Wave signatures of inflationary models from Primordial Black Hole Dark Matter". In: *JCAP* 09 (2017), p. 013. DOI: 10.1088/1475-7516/2017/09/013. arXiv: 1707.02441 [astro-ph.CO] (cit. on p. 48).

[70] Zaven Arzoumanian et al. "The NANOGrav 12.5 yr Data Set: Search for an Isotropic Stochastic Gravitational-wave Background". In: *Astrophys. J. Lett.* 905.2 (2020), p. L34. DOI: 10.3847/2041-8213/abd401. arXiv: 2009.04496 [astro-ph.HE] (cit. on p. 49).

[71] A. Barnacka, J.-F. Glicenstein, and R. Moderski. "New constraints on primordial black holes abundance from femtolensing of gamma-ray bursts". In: *Physical Review D* 86.4 (Aug. 2012). ISSN: 1550-2368. DOI: 10.1103/physrevd.86.043001. URL: http://dx.doi.org/10.1103/PhysRevD.86.043001 (cit. on p. 49).

[72] Peter W. Graham, Surjeet Rajendran, and Jaime Varela. "Dark Matter Triggers of Supernovae". In: *Phys. Rev. D* 92.6 (2015), p. 063007. DOI: 10.1103/PhysRevD.92.063007. arXiv: 1505.04444 [hep-ph] (cit. on p. 49).

[73] Fabio Capela, Maxim Pshirkov, and Peter Tinyakov. "Constraints on primordial black holes as dark matter candidates from capture by neutron stars". In: *Phys. Rev. D* 87.12 (2013), p. 123524. DOI: 10.1103/PhysRevD.87.123524. arXiv: 1301.4984 [astro-ph.CO] (cit. on p. 49).

[74] Nolan Smyth et al. "Updated Constraints on Asteroid-Mass Primordial Black Holes as Dark Matter". In: *Phys. Rev. D* 101.6 (2020), p. 063005. DOI: 10.1103/PhysRevD.101.063005. arXiv: 1910.01285 [astro-ph.CO] (cit. on p. 49).

[75] Andrey Katz et al. "Femtolensing by Dark Matter Revisited". In: *JCAP* 12 (2018), p. 005. DOI: 10.1088/1475-7516/2018/12/005. arXiv: 1807.11495 [astro-ph.CO] (cit. on p. 49).

[76] Paulo Montero-Camacho et al. "Revisiting constraints on asteroid-mass primordial black holes as dark matter candidates". In: *Journal of Cosmology and Astroparticle Physics* 2019.08 (Aug. 2019), pp. 031–031. ISSN: 1475-7516. DOI: 10.1088/1475-7516/2019/08/031. URL: http://dx.doi.org/10.1088/1475-7516/2019/08/031 (cit. on p. 49).

[77] Bernard Carr et al. "Observational Evidence for Primordial Black Holes: A Positivist Perspective". In: (June 2023). arXiv: 2306.03903 [astro-ph.CO] (cit. on p. 49).

[78] Hiromasa Nakatsuka Kenta Ando Masahiro Kawasaki. "Formation of primordial black holes in an axionlike curvaton model". In: *Phys. Rev. D* 98.1 (8 2018). DOI: 10.1103/PhysRevD.98.083508 (cit. on p. 50).

[79] Subodh P. Patil Christian T. Byrnes Philippa S. Cole. "Steepest growth of the power spectrum and primordial black holes". In: *Journal of Cosmology and Astroparticle Physics* 2019 (2019). DOI: 10.1088/1475-7516/2019/06/028 (cit. on pp. 50, 69).

[80] H. V. Ragavendra et al. "Primordial black holes and secondary gravitational waves from ultraslow roll and punctuated inflation". In: *Phys. Rev. D* 103 (8 Apr. 2021), p. 083510. DOI: 10.1103/PhysRevD.103.083510. URL: https://link.aps.org/doi/10.1103/PhysRevD.103.083510 (cit. on p. 50).

[81] Matteo Braglia et al. "Generating PBHs and small-scale GWs in two-field models of inflation". In: *Journal of Cosmology and Astroparticle Physics* (8 Aug. 2020), p. 083510. DOI: 10.1088/1475-7516/2020/08/001. URL: https://dx.doi.org/10.1088/1475-7516/2020/08/001 (cit. on p. 50).

[82] Konstantinos Dimopoulos. "Ultra slow-roll inflation demystified". In: *Physics Letters B* 775 (2017), pp. 262–265. DOI: https://doi.org/10.1016/j.physletb.2017.10.066. URL: https://www.sciencedirect.com/science/article/pii/S037026931730878X (cit. on p. 50).

[83] Hayato Motohashi, Alexei A. Starobinsky, and Jun'ichi Yokoyama. "Inflation with a constant rate of roll". In: 9 (Sept. 2015). DOI: 10.1088/1475-7516/2015/09/018. URL: https://dx.doi.org/10.1088/1475-7516/2015/09/018 (cit. on p. 50).

[84] Ogan Özsoy et al. "Mechanisms for primordial black hole production in string theory". In: *Journal of Cosmology and Astroparticle Physics* 07 (July 2018). DOI: 10.1088/1475-7516/2018/07/005. URL: https://dx.doi.org/10.1088/1475-7516/2018/07/005 (cit. on p. 50).

[85] J. Beltran Jimenez G. Ballesteros and M. Pieroni. "Black hole formation from a general quadratic action for inflationary primordial fluctuations". In: *JCAP* 06 (2019), p. 016. DOI: 10.1088/1475-7516/2019/06/016 (cit. on pp. 50, 51, 54, 55).

[86] Samuel M. Leach and Andrew R. Liddle. "Inflationary perturbations near horizon crossing". In: *Phys. Rev. D* 63 (4 Jan. 2001), p. 043508. DOI: 10.1103/PhysRevD.63.043508. URL: https://link.aps.org/doi/10.1103/PhysRevD.63.043508 (cit. on p. 50).

[87] Samuel M. Leach et al. "Enhancement of superhorizon scale inflationary curvature perturbations". In: *Phys. Rev. D* 64 (2 June 2001), p. 023512. DOI: 10.1103/PhysRevD.64.023512. URL: https://link.aps.org/doi/10.1103/PhysRevD.64.023512 (cit. on pp. 50, 52).

[88] Jose Maria Ezquiaga, Juan Garcia Bellido, and Ester Ruiz Morales. "Primordial black hole production in Critical Higgs Inflation". In: *Physics Letters B* 776 (2018). DOI: https://doi.org/10.1016/j.physletb.2017.11.039. URL: https://www.sciencedirect.com/science/article/pii/S0370269317309310 (cit. on p. 51).

[89] Ioannis Dalianis, Alex Kehagias, and George Tringas. "Primordial black holes from α-attractors". In: *Journal of Cosmology and Astroparticle Physics* 01 (Jan. 2019). DOI: 10.1088/1475-7516/2019/01/037. URL: https://dx.doi.org/10.1088/1475-7516/2019/01/037 (cit. on p. 51).

[90] Michele Cicoli, Victor A. Diaz, and Francisco G. Pedro. "Primordial black hles from string inflation". In: *Journal of Cosmology and Astrparticle Physcis* 06 (June 2018). DOI: 10.1088/1475-7516/2018/06/034. URL: https://dx.doi.org/10.1088/1475-7516/2018/06/034 (cit. on p. 51).

[91] M. Yamaguchi T. Kobayashi and J. Yokoyama. "Generalized G-Inflation: Inflation with the Most General Second-Order Field Equations". In: *Prog. Theor. Phys.* 126.3 (2011) (cit. on p. 51).

[92] Hayato Motohashi and Wayne Hu. "Primordial black holes and slow-roll violation". In: *Phys. Rev. D* 96 (6 Sept. 2017), p. 063503. DOI: 10.1103/PhysRevD.96.063503. URL: https://link.aps.org/doi/10.1103/PhysRevD.96.063503 (cit. on p. 53).

[93] Hayato Motohashi, Shinji Mukohyama, and Michele Oliosi. "Constant roll and primordial black holes". In: 03 (Mar. 2020). DOI: 10.1088/1475-7516/2020/03/002. URL: https://dx.doi.org/10.1088/1475-7516/2020/03/002 (cit. on pp. 61, 62).

[94] A. A. Starobinsky. "A new type of isotropic cosmological models". In: 91.1 (1980). DOI: https://doi.org/10.1016/0370-2693(80)90670-X. URL: https://www.sciencedirect.com/science/article/pii/037026938090670X (cit. on p. 61).

[95] Zhi-Qiang You, Zhu Yi, and You Wu. "Constraints on primordial curvature power spectrum with pulsar timing arrays". In: *Journal of Cosmology and Astroparticle Physics* 2023.11 (Nov. 2023), p. 065. ISSN: 1475-7516. DOI: 10.1088/1475-7516/2023/11/065. URL: http://dx.doi.org/10.1088/1475-7516/2023/11/065 (cit. on pp. 71–73, 75, 96, 98).

[96] Chengcheng Han et al. "Self-interacting dark matter implied by nano-Hertz gravitational waves". In: (June 2023). arXiv: 2306.16966 [hep-ph] (cit. on p. 71).

[97] John Ellis et al. "Cosmic superstrings revisited in light of NANOGrav 15-year data". In: *Phys. Rev. D* 108.10 (2023), p. 103511. DOI: 10.1103/PhysRevD.108.103511. arXiv: 2306.17147 [astro-ph.CO] (cit. on p. 72).

[98] Pau Amaro-Seoane et al. *Laser Interferometer Space Antenna*. 2017. arXiv: 1702.00786 [astro-ph.IM] (cit. on p. 72).

[99] Wen-Rui Hu and Yue-Liang Wu. "The Taiji Program in Space for gravitational wave physics and the nature of gravity". In: *National Science Review* 4.5 (Oct. 2017), pp. 685–686. ISSN: 2095-5138. DOI: 10.1093/nsr/nwx116. URL: https://doi.org/10.1093/nsr/nwx116 (cit. on p. 72).

[100] Yungui Gong, Jun Luo, and Bin Wang. "Concepts and status of Chinese space gravitational wave detection projects". In: *Nature Astron.* 5.9 (2021), pp. 881–889. DOI: 10.1038/s41550-021-01480-3. arXiv: 2109.07442 [astro-ph.IM] (cit. on p. 72).

[101] Seiji Kawamura et al. "Current status of space gravitational wave antenna DECIGO and B-DECIGO". In: *PTEP* 2021.5 (2021), 05A105. DOI: 10.1093/ptep/ptab019. arXiv: 2006.13545 [gr-qc] (cit. on p. 72).

[102] Stephen L. Adler. "Einstein gravity as a symmetry-breaking effect in quantum field theory". In: *Rev. Mod. Phys.* 54 (3 July 1982), pp. 729–766. DOI: 10.1103/RevModPhys.54.729. URL: https://link.aps.org/doi/10.1103/RevModPhys.54.729 (cit. on p. 76).

[103] Y. M. Cho. "Reinterpretation of Jordan-Brans-Dicke theory and Kaluza-Klein cosmology". In: *Phys. Rev. Lett.* 68 (21 May 1992), pp. 3133–3136. DOI: 10.1103/PhysRevLett.68.3133. URL: https://link.aps.org/doi/10.1103/PhysRevLett.68.3133 (cit. on p. 76).

[104] N. D. Birrell and P. C. W. Davies. *Quantum Fields in Curved Space*. Cambridge Monographs on Mathematical Physics. Cambridge University Press, 1982. DOI: 10.1017/CBO9780511622632 (cit. on p. 76).

[105] C. Brans and R. H. Dicke. "Mach's Principle and a Relativistic Theory of Gravitation". In: *Phys. Rev.* 124 (3 Nov. 1961), pp. 925–935. DOI: 10.1103/PhysRev.124.925. URL: https://link.aps.org/doi/10.1103/PhysRev.124.925 (cit. on p. 76).

[106] A. D. Sakharov. "Vacuum quantum fluctuations in curved space and the theory of gravitation". In: *Dokl. Akad. Nauk Ser. Fiz.* 177 (1967). Ed. by Yu. A. Trutnev, pp. 70–71. DOI: 10.1070/PU1991v034n05ABEH002498 (cit. on p. 76).

[107] A. Zee. "Broken-Symmetric Theory of Gravity". In: *Phys. Rev. Lett.* 42 (7 Feb. 1979), pp. 417–421. DOI: 10.1103/PhysRevLett.42.417. URL: https://link.aps.org/doi/10.1103/PhysRevLett.42.417 (cit. on pp. 76, 78, 87).

[108] A. Yu. Kamenshchik et al. "Reconstruction of scalar potentials in modified gravity models". In: *Physical Review D* 87.6 (Mar. 2013). DOI: 10.1103/physrevd.87.063503. URL: https://doi.org/10.1103%2Fphysrevd.87.063503 (cit. on pp. 77, 83).

[109] A. Cerioni et al. "Inflation and reheating in spontaneously generated gravity". In: *Physical Review D* 81.12 (June 2010). DOI: 10.1103/physrevd.81.123505. URL: https://doi.org/10.1103%2Fphysrevd.81.123505 (cit. on pp. 78, 80, 81, 87).

[110] Yasunori Fujii and Kei-ichi Maeda. *The Scalar-Tensor Theory of Gravitation*. Cambridge Monographs on Mathematical Physics. Cambridge University Press, 2003. DOI: 10.1017/CBO9780511535093 (cit. on p. 78).

[111] Jai-chan Hwang. "Quantum generations of cosmological perturbations in generalized gravity". In: *Classical and Quantum Gravity* 14.12 (Dec. 1997), pp. 3327–3336. DOI: 10.1088/0264-9381/14/12/016. URL: https://doi.org/10.1088%2F0264-9381%2F14%2F12%2F016 (cit. on pp. 80, 81).

[112] A. Cerioni et al. "Inflation and reheating in induced gravity". In: *Physics Letters B* 681.5 (Nov. 2009), pp. 383–386. DOI: 10.1016/j.physletb.2009.10.066. URL: https://doi.org/10.1016%2Fj.physletb.2009.10.066 (cit. on p. 87).

[113] James M. Bardeen et al. "The Statistics of Peaks of Gaussian Random Fields". In: *Astrophys. J.* 304 (1986), pp. 15–61. DOI: 10.1086/164143 (cit. on p. 103).

[114] David H Lyth, Karim A Malik, and Misao Sasaki. "A general proof of the conservation of the curvature perturbation". In: *Journal of Cosmology and Astroparticle Physics* 2005.05 (May 2005), pp. 004–004. ISSN: 1475-7516. DOI: 10.1088/1475-7516/2005/05/004. URL: http://dx.doi.org/10.1088/1475-7516/2005/05/004 (cit. on p. 103).